THERMIONIC ENERGY CONVERSION SYSTEM DESIGN

FINAL TECHNICAL REPORT

Prepared Under Contract No. 952781 by
Donald W. Douglas Laboratories
McDonnell Douglas Astronautics Company — West
Richland, Washington
for
JET PROPULSION LABORATORY

THERMIONIC ENERGY CONVERSION SYSTEM DESIGN

FINAL TECHNICAL REPORT

by
J. G. DeSteese

This work was performed for the Jet Propulsion Laboratory, California Institute of Technology, as sponsored by the National Aeronautics and Space Administration under Contract NAS7-100.

Prepared Under Contract No. 952781 by
Donald W. Douglas Laboratories
McDonnell Douglas Astronautics Company — West
Richland, Washington
for
JET PROPULSION LABORATORY

This report contains information prepared by the Donald W. Douglas Laboratories, a Subdivision of the McDonnell Douglas Astronautics Company-West, Richland, Washington, under JPL subcontract. Its content is not necessarily endorsed by the Jet Propulsion Laboratory, California Institute of Technology, or the National Aeronautics and Space Administration.

ABSTRACT

System-integrated performance characteristics are calculated for a new family of space power generators each consisting of a multicell array of low temperature, integrally-fueled radioisotope-thermionic converters operating in the quasi-vacuum mode. Dominant variables, including the choice and influence of thermionic surface parameters, emitter geometry, fuel form, helium management, array reliability, system integration, and nuclear safety requirements are considered.

Parametric study of plutonia-fueled multicell generators in the power range from 100 to 200 w_e shows that system-integrated specific power of approximately 4 w_e/lb and overall conversion efficiencies in excess of 7% are achievable. This performance level is substantiated by a detailed 100 w_e generator design.

Current fuel and materials technologies are adequate for the development of this concept. A brief review of future technology indicates substantial growth potential. Anticipated improvements in thermionic surfaces, fuel and fuel capsule fabrication, and aeroshell technology appear to permit system-integrated specific power in excess of 20 w_e/lb and efficiencies approaching 10%.

Modular construction results in additional nuclear safety, greatly reduced development costs, and a single basic converter "building-block" approach to generator design. A large range of configurations and power options provides compact, low-drag, and radiation-resistant power sources applicable to many aerospace missions.

CONTENTS

FIGURES

TABLES

SYMBOLS

A	=	Emitter area (cm^2)
d	=	Electrode spacing (mils)
e	=	Electronic charge (1.6×10^{-19} coulomb)
ℓ/a	=	Emitter lead length-to-area ratio
L/D	=	Cylindrical converter capsule length-to-diameter ratio
L_a/D_a	=	Aeroshell length-to-diameter ratio
P	=	Converter power (w_e)
$Parameter_o$	=	Optimum value of parameter (subscript)
P_g	=	Generator power (w_e)
P_{max}	=	Maximum converter power (w_e)
Q	=	Input thermal power (w_t)
Q_c	=	Sum of conduction components of thermal energy balance (w_t)
Q_e	=	Electron-cooling component of thermal energy balance (w_t)
Q_r	=	Radiation component of thermal energy balance (w_t)
R_L	=	Converter load resistance (Ω)
T	=	Surface temperature (°K)
T_c	=	Collector temperature (°K)
T_e	=	Emitter temperature (°K)
T_R	=	Temperature of liquid cesium reservoir (°K)
T_{rad}	=	Aeroshell heat rejection temperature (°K)
V	=	Converter electrode potential (v)
V_g	=	Generator voltage (v)
β	=	Aeroshell ballistic coefficient (lb/ft^2)
ε	=	Electrode emissivity
ϕ	=	Surface work function (ev)
ϕ_B	=	Electrode cesium-bare work function (ev)
ϕ_c	=	Collector work function (ev)
ϕ'_c	=	Collector emission barrier height (ev)
ϕ_e	=	Emitter work function (ev)
ϕ_{min}	=	Work function minimum on Rasor-Warner plot (ev)
ϕ_n	=	Neutralization work function (ev)

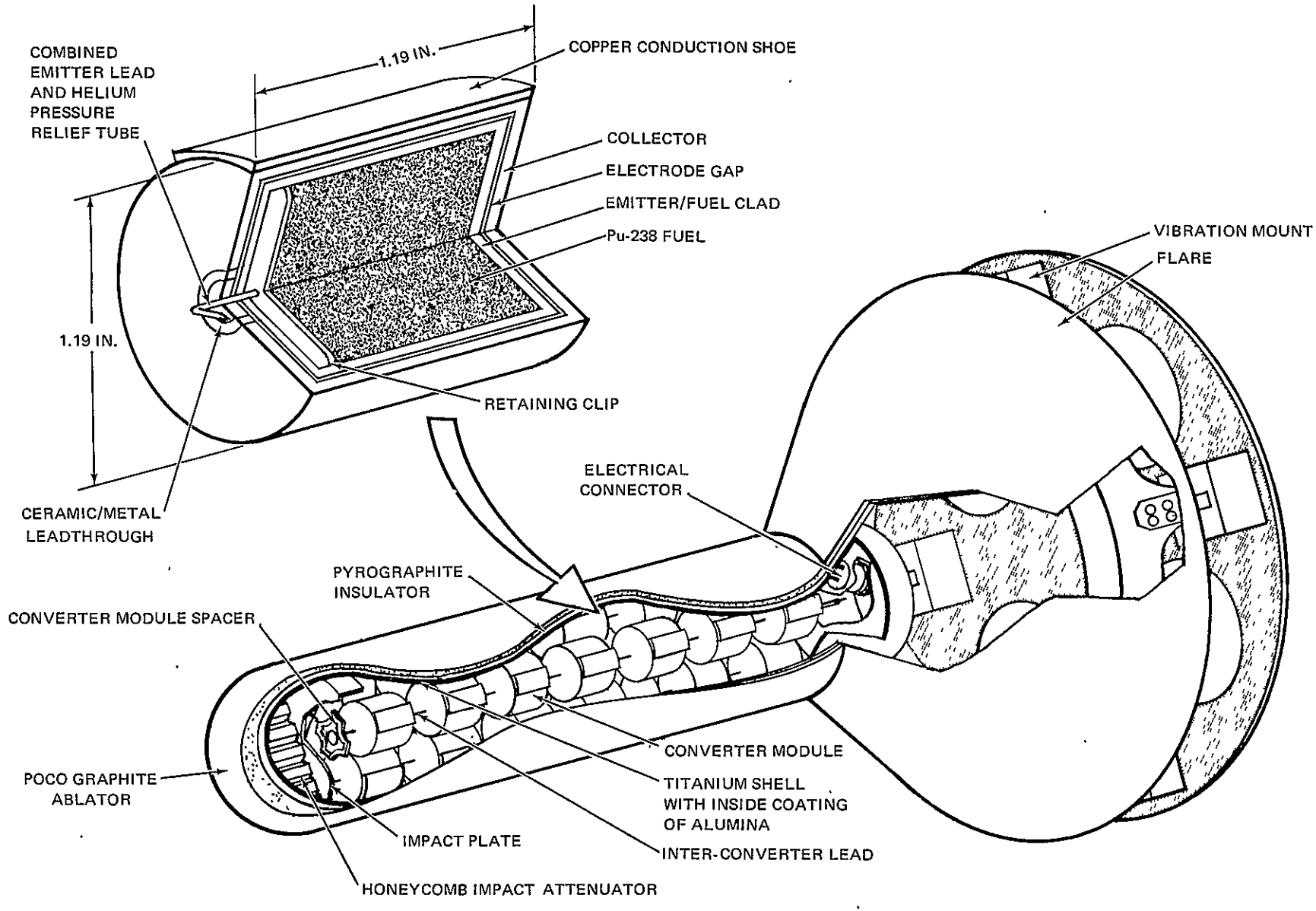

100 W_e Quasi-Vacuum Mode Multicell Radioisotope Thermionic Generator

SUMMARY

System-integrated performance and characteristics are calculated both parametrically and in detail for space power generators composed of low-temperature, integrally-fueled, radioisotope-thermionic converter arrays operating in a quasi-vacuum mode. A novel and attractive nuclear thermionic conversion system is identified which provides a highly flexible and redundant modular design approach to satisfy multihundred watt space power requirements. Dominant variables including the choice and influence of thermionic surface parameters, emitter geometry, fuel form, helium management, array reliability, system integration, and nuclear safety requirements are considered.

Plutonia-fueled Isomite* multicell generators in the 100- to 200-w_e power range achieve a fully system-integrated specific power of 4 w_e/lb and conversion efficiencies in excess of 7%; optimum module size is between 3 and 4 w_e. Growth potential of the system is associated principally with the use of high thermal power density heat sources (such as Cm-244 fuel forms). High thermal power density fuel and future thermionic surface, fuel capsule, and aeroshell development permit system specific power in excess of 20 w_e/lb and conversion efficiencies approaching 10%. The current competitive performance and future growth potential provide strong motivation for the development of the thermionic multicell generator, considering current and projected thermoelectric generator (RTG) performance.

Isomite converters are self-contained, radionuclide-fueled thermionic battery cells operating in a low-current density, quasi-vacuum mode with low emitter temperatures (<1400 °K) which permit the expectation of long life and reliability typical of RTG devices. The multicell Isomite array is not subject to application limitations imposed by the high temperature (>1600 °K) operational mode of conventional, high-current density thermionic devices (Section 1).

---

*ISOMITE is a registered trademark, the property of the McDonnell Douglas Corporation.

Modular construction and low emitter temperatures are compatible with current fuel technology and create an operational environment for the fuel and materials no more stringent than currently accepted RTG practice.

Isomite devices operate with about the same high heat rejection temperatures (700° to 900°K) characteristic of most thermionic systems. The multicell generator is therefore an attractive power source for long-duration space missions and is probably the only candidate for missions requiring operation in some high temperature environments. The modular "building-block" approach to generator design appears to be valid over a wide range of power with the advantage that a large number of generator configurations and power options are available at low cost following initial development and qualification of a single converter module (Section 7). Modular design results in a significant reduction in generator development cost.

To achieve generator reliability goals, reliability testing of individual converters is required. System development costs are, however, minimized by the potential long-life of the plutonia-fueled converter module. Converter modules undergoing reliability testing can be designed with excess BOL power to permit those which survive the test period to be incorporated in generators assigned to subsequent missions. Probabilistic reliability analysis of multicell converter arrays shows that two-column arrays of series/parallel-connected converters satisfy typical generator reliability goals in the power range from 50 to 200 w_e. This situation is promoted by the anticipation that converters will have an intrinsically lower open circuit than short circuit failure propensity (Section 5). Analysis shows that attractive current-technology multicell system performance is provided with plutonia-fueled arrays of nominally 3 to 4 w_e converter modules in aeroshell structures of conventional design (Section 7).

Off-optimum converter performance resulting from off-optimum values of converter parameters is estimated in this study (Section 3). From the standpoint of present experience, it can be shown that an acceptable off-design range of the most influential variables, collector temperature, collector work function, and reservoir temperature, can be achieved by system design and manufacturing quality control. The variability of other parameters is less influential on converter output and can be controlled by mechanical design and compensatory effects between competing parameter influences. DWDL experience suggests

that, in total, parameter variability adds an uncertainty of less than 10% to calculated parametric output characteristics.

A unique dependence of output characteristics on emitter thermal flux density (Q/A) is identified for the quasi-vacuum mode converter operating in aerospace environments. In a gravity field, a non-Q/A dependent term contributed by the electrode spacer conduction loss enters the thermal energy balance and degrades power with increasing effect as the module size is decreased (Section 2). The artificial or natural gravity experienced in a specific mission, therefore, influences the choice of converter power and the configuration of the generator.

The influence of fuel capsule geometry on converter specific power and helium containment is discussed (Section 4). Thin-shell vented capsules of spherical and cylindrical form are shown to contribute approximately the same specific power level as a thin-shell unvented spherical capsule which can make use of the collector reinforcement after yielding across the electrode gap. Unvented cylindrical capsules both with and without collector reinforcement are shown to be significantly inferior to vented capsules of all shapes and the unvented spherical capsule.

Future development of the multicell generator system assumes the availability of an integral helium-venting device as system components approach flight qualification status. The unvented spherical configuration, however, offers a backup configuration if the credibility or availability of the integral helium-venting device is considered questionable (Section 4).

The flared cone aeroshell design is selected as a representative and scalable current-technology structural component which provides the multicell generator concept with a high degree of nuclear safety credibility for all conditions of the space mission environment (Section 6). The aeroshell shares a common nuclear safety structure with all converters in the array and its shape provides passively oriented reentry, a predictable terminal velocity, and limited transmission of impact force to the converters. The aeroshell provides a fourth fuel containment structure complementing the cermet fuel matrix, emitter capsule, and collector structure.

The design flexibility of both aeroshell and converter array permits the accommodation of special mission requirements such as low orbital drag, small radar cross section, and resistance to environmental radiation.

A detailed study of a 100 w_e generator (Section 8) substantiates the performance trends identified in Sections 2 through 7. The detailed design includes the additional weight of system-integration components and shows that design refinements of all system components are possible when a specific generator configuration is considered. The constraint imposed by the assumed generator reliability goal strongly influences the choice of converter module power and array configuration. A three-way optimization occurs in the process of providing sufficient radiator area to maintain collector temperature near its optimum value. The provision of power redundancy reflects reliability criteria and the sensitivity of converter specific power and efficiency to off-optimum collector temperature and module size.

Current or near-term fuel and materials technology is shown to be adequate for development of a distinctly superior family of radioisotope power generators. However, the value of advanced technology is also estimated considering anticipated thermionic surface, fuel capsule, and aeroshell development. A principal component contributing growth potential is the development of the Langmuir W-O-Cs surface system (Section 2). Although, at present, uncertainties exist regarding the preparation and long-term stability of this surface, the intrinsically low-emissivity, low-work-function surface system theoretically permits an increase in quasi-vacuum mode conversion efficiency to approximately 10%.

Development of spherical emitter and collector capsules would allow slight gains in specific power (Section 4). The spherical structure is amenable to incorporation into advanced technology omnidirectional aeroshell structures of lighter weight than conventional flared cylinder configurations. In combination with this advanced technology, full system growth potential is achieved by using high power density fuel which, in the case of Cm-244, offers considerable potential for greatly reduced generator cost (Section 9). The increase in specific power more than offsets added shield weight which may be necessary to shield, for example, a curia-fueled system to provide dose rates equivalent to those of plutonia-fueled generators.

Technical Monitor on this program for the Jet Propulsion Laboratory was Peter Rouklove.

Section 1
INTRODUCTION

This Final Technical Report and appended Supplemental Data are deliverable under Article 1(a)3(D) and 1(a)3(E) of Contract 952781 and summarize a space power system study to establish parametric performance characteristics of three Isomite multicell generators in the power range from 50 to 200 w_e and a detailed design of a 100 w_e generator. This report describes Phase I and Phase II effort in detail.

CONVENTIONAL RADIONUCLIDE THERMIONIC GENERATOR DESIGN

In the early 1960s, before the Isomite concept evolved, thermionic research and development concentrated on cesium plasma devices operating with high emitter temperatures (>1600°K). Conventional radionuclide-thermionic electric power sources can be classified according to the mode of heat transfer between heat source and converter. Typical configurations involve thermal coupling by direct conduction (Reference 1), fluid-metal loops (Reference 2), and radiant energy (Reference 3). Although components of several thermionic space power generator concepts have been developed using conventional converters powered by radionuclide thermal sources, the thermoelectric generator (RTG) is still favored for most applications to date, despite the high heat rejection temperatures, projected superior specific power, and competitive efficiency of thermionic systems. The reasons for this preference and consequent low level of interest in thermionic generators have been the relatively short demonstrated life, stringent requirements for high temperature fuel and materials technology, and low reliability which are inherent characteristics of high temperature thermionic devices.

ISOMITE CONCEPT

In the last three years, the McDonnell Douglas Astronautics Company-West has developed a novel, quasi-vacuum mode radionuclide thermionic battery cell operating at low emitter temperatures (<1400°K). Attractive features resulting from low temperature operation include reliable and efficient small module design, direct

thermal coupling to fuels of any practical thermal power density, inherently compatible materials; and long life. The quasi-vacuum mode thermionic converter retains the high temperature heat rejection capability (700°to 900°K) and hence the compact radiator characteristics of conventional thermionic converters.

Although RTGs have an established position in space power applications, based on their current level of development and demonstrated reliability, their characteristically low heat rejection temperatures are unsuitable for high-temperature operational environments (for example: Venus Lander Vehicle, near-sun, and Mercury missions). The performance of other interplanetary vehicles might also be penalized by RTGs requiring larger radiators than those of equivalent thermionic systems.

A modular space power generator composed of series/parallel connected Isomite converter arrays offers a highly redundant, integrated system of competitive efficiency which is superior to the RTG in specific power. Modular construction, involving a relatively large number of separately fueled and completely independent power cells, permits rapid development of generators "tailored" to an optimum size and configuration for specific mission requirements. The development costs of a family of generators covering a wide range of power, therefore, tend to be modest, compared to the investment required for development and qualification of a single module. Generator performance and life characteristics can be demonstrated by testing a relatively small number of fueled converters.

PROGRAM OBJECTIVES

Primary objectives of this effort are:

1. To establish parametric performance characteristics of three thermionic multicell generators with respective outputs of 50, 100, and 200 w_e.
2. To design a 100 w_e multicell generator in sufficient detail to identify materials and critical dimensions.

To satisfy Objective 1, output characteristics, efficiency, specific power, and weight were evaluated for practical ranges of dominant system variables. The influence of thermionic parameters, emitter geometry, fuel form, helium management, array reliability, system integration, and nuclear safety requirements were considered. Objective 2 was achieved by a 100 w_e generator

design based on results of the parametric study (Objective 1). Both primary objectives are based on current or near-term technology. A secondary goal of the program was to indicate the growth potential of the multicell generator concept, considering long term technology developments. These objectives have been achieved.

PROGRAM APPROACH

To achieve the primary and secondary objectives of this program the following eight objectives were identified:

1. To identify the influence of electrode surface parameters on the performance characteristics and growth potential of individual converters.
2. To evaluate off-optimum performance of converters in the module power range of interest.
3. To define constraints imposed by choice of fuel form, emitter geometry, and helium management technique.
4. To optimize converter selection and interconnection based on requirements for generator reliability and voltage.
5. To optimize converter array stacking configuration in the aeroshell.
6. To determine the weight and other parametric characteristics of a 50, 100, and 200 w_e generator based on the design inputs from Objective 1 through 5.
7. To design a 100 w_e generator based on Objective 6, in sufficient detail to identify materials and critical dimensions.
8. To review briefly, the credible growth potential of the multicell concept.

ASSUMPTIONS OF AVAILABLE TECHNOLOGY

The parametric performance study, generator design, and material selections reflect current and/or anticipated near-future technology, available within a reasonable development period. Table 1-1 summarizes the technology assumed for the baseline generator configuration studied in this program.

A brief survey of advanced concepts based on credible long-term technology illustrates the growth potential of the multicell generator. Advanced technology components are summarized in Table 1-2.

Table 1-1

BASELINE GENERATOR DESIGN

Component	Description
Radionuclide Fuel and Fuel Capsule(1)	Plutonia Solid Solution Cermet (SSC) and/or Plutonia Molybdenum Cermet (PMC). Vented cylinder, composed of platinum-rhodium oxidation barrier and tungsten fuel clad.
Emitter Surface	Tantalum applied as thin coating to fuel capsule surface and treated with oxygen to form Ta-O-Cs surface system in converter.
Collector Surface	Tantalum applied to collector substrate and treated as described for emitter surface.
Collector Substrate	T-111 or equivalent refractory alloy.
Electrode Spacing	Provided by 1-mil diameter ceramic spacers distributed over electrode surfaces (or equivalent using non-distributed support technique).
Effective Weight of Emitter and Collector Structure	2.15 g/cm^2 based on total thickness of 50 mils.
Helium Management(1)	Selective venting under reentry conditions to titanium vessel containing converter array.
Aeroshell Form	Flared-cylinder.

(1) Alternate design: unvented spherical capsule of same composition as vented cylindrical capsule.

Table 1-2

COMPONENTS OF ADVANCED GENERATOR DESIGN (1)

Component	Description
Radionuclide Fuel	Curia Cermet(2) (or fuel of equivalent thermal power density).
Fuel Capsule	Vented sphere with same composition as shown in Table 1-1.
Emitter and Collector Surface	Tungsten applied as described for tantalum in Table 1-1 and treated to form Langmuir W-O-Cs surface system in converter.
Aeroshell Form	Cubic shell and ablator for omnidirectional reentry trajectory.

(1) No improvement over that indicated in Table 1-1 is assumed for effective weight of emitter and collector, collector substrate, electrode spacing, and helium management technique.

(2) A curia cermet fuel form may, in fact, be considered credible near-term technology. It was however, excluded from consideration in the parametric study by the contractual scope of the program.

SYSTEM OPERATIONAL CONSTRAINTS

A large number of variables are involved in a parametric thermionic generator study. Variation in some mission requirements (such as life and reliability goals) have considerable influence on design recommendations. The parametric calculations and generator design of this program are based on system requirements summarized in Table 1-3. These requirements define the contractual scope of this study as provided by JPL direction.

Table 1-3

SYSTEM REQUIREMENTS GOVERNING MULTICELL GENERATOR DESIGN

Requirement	Description
Generator Power	50 to 200 w_e
Generator Voltage	3 to 10 v input to power conditioning equipment(1)
Generator Reliability Goal	(1) 0.98 at end of 5.5 years (5 year mission, half year shelf life).
	(2) No single converter failure results in catastrophic generator failure.
Failure Statement	(1) Power <70% of rated power at 5.5 years.
	(2) Voltage < 3 v.
Mission Conditions	(1) Zero-gravity operational environment.
	(2) No requirements of a specific future mission are considered.
Generator Survival	(1) Typical launch pad, reentry and impact hazards (Table 6-1).
	(2) Shocks of 100 g with 0.5 msec duration.
	(3) Vibration and acceleration up to 20 g in frequency range 0-2 kHz
	(4) Vibration and acceleration of 4.5 g peak superimposed white noise.
Helium Management	Considered for 10.5 year mission (10 year mission, half year shelf life).

(1) The characteristics and weight of power conditioning equipment are not included in estimations of multicell generator performance or characteristics.

BASIC QUASI-VACUUM MODE CONVERTER MODULE

The modular "building-block" of the multicell generator is the Isomite power cell shown typically in Figure 1-1. Detail variations from the configuration shown in Figure 1-1 accommodate specific constraints of each application, which may influence the choice of fuel, capsule design, thermionic surfaces, electrode spacing, spacing technique, and collector structural design. The converter is powered by direct thermal conduction from a radionuclide fuel contained in the emitter capsule. A second capsule completely surrounds the thermionic emitter and functions as the collector substrate. Both electrode surfaces may be formed as treated surfaces of the substrate materials or by applied surface coatings. The electrode gap is maintained by spacing elements, which provide both thermal and electrical isolation of the emitter. A wire lead from the emitter passes through an insulating sleeve in the collector and is attached to a terminal forming part of a ceramic/metal collector seal. A helium pressure relief tube could be substituted for the wire to form a combined emitter lead and venting device. The integral cesium reservoir is maintained at collector temperature and contained in the void region of the lead-through assembly. Low cesium vapor pressure (10^{-3} to 10^{-1} torr) establishes favorable emitter and collector work functions without introducing appreciable electron scattering effects in the electrode gap.

The Isomite cell combines design features which are impractical under the operating conditions of conventional converters. In the Isomite design, structural components can be optimally designed to perform single or non-compromise functions. For example, the collector body forms a rugged secondary enclosure around the emitter and the lead can be sized separately to have an optimum aspect ratio. In contrast, the emitter lead in a conventional converter also forms part of the vacuum enclosure and its design therefore, is non-ideal in either function.

The basic configuration scales nearly geometrically from 100 μw_e to several watts electrical output. Total enclosure of the emitter minimizes the relatively unscalable thermal leakage contributed by lead conduction and radiation, which limits the minimum size of an efficient conventional converter module to approximately 20 w_e. Thermal flux concentration to match the fuel thermal

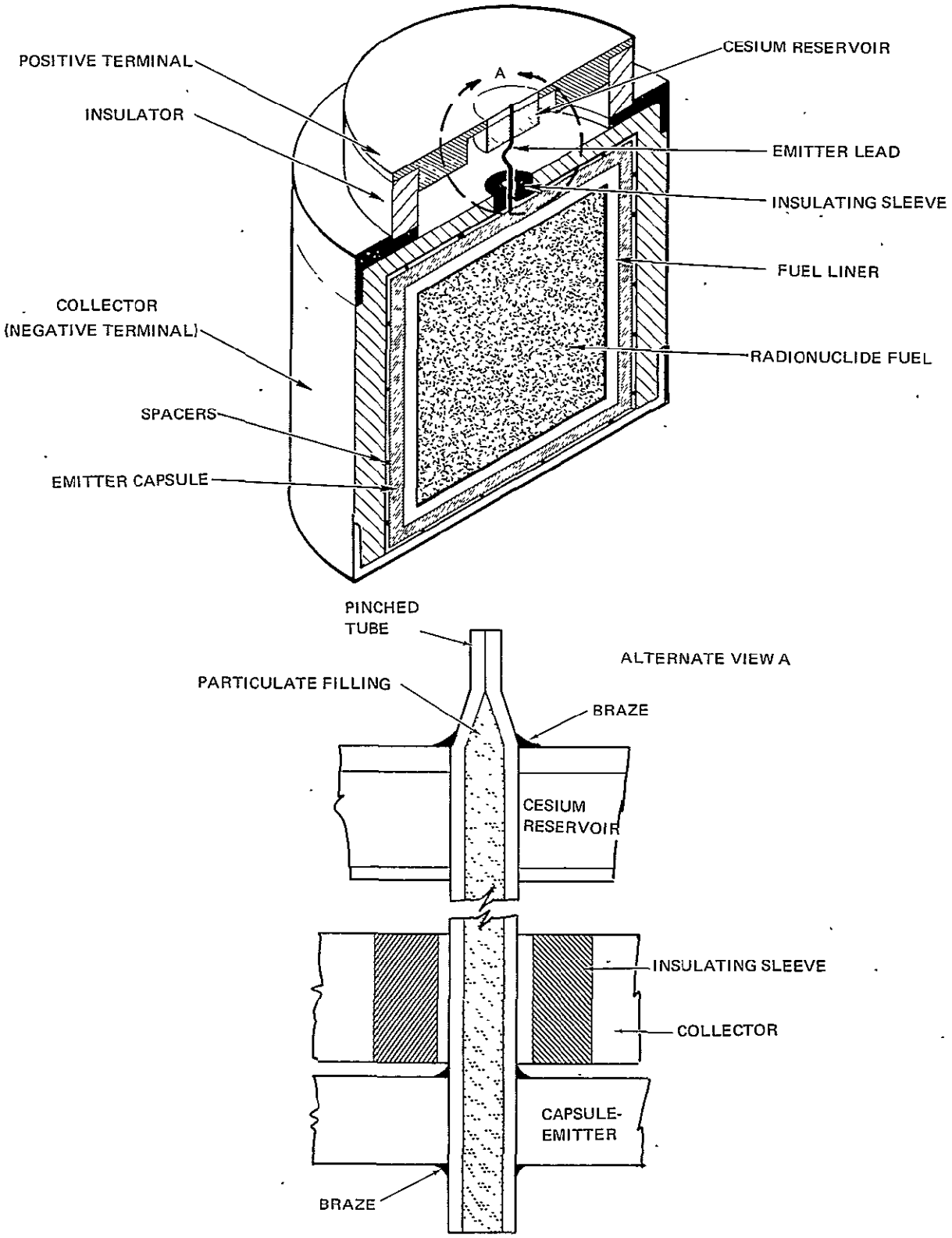

Figure 1-1. Isomite Power Cell

power and thermionic surface flux density is not a fundamental requirement in the vacuum mode converter. Optimum cells can be designed to accommodate all practical fuel power densities above approximately 1 w_t/cm^3.

GENERATOR AEROSHELL AND REENTRY VEHICLE SYSTEM

The Isomite cells which comprise the generator are considered to be arranged within a structure which provides an operational housing during mission life, launch pad abort debris protection, and intact reentry disposal. Reentry vehicle concepts which could be applied include the blunt cone (used in Isotope/Brayton power systems), flared-cylinders, high-drag cubes, rectangular parallelepipeds, and flat plates (References 4, 5, and 6). For the purpose of this design study, the flared-cylinder concept is selected as a characteristically low-weight (not necessarily minimum weight) housing/reentry vehicle system which is scalable to accommodate Isomite cell arrangement patterns. This concept is also considered to require a minimum of development to provide an acceptable level of safety. A basic attribute of the flared-cylinder is a configuration with four levels of fuel containment provided, in turn, by the fuel form, emitter and collector structures of the converters, and the aeroshell. The flared-cylinder has undergone development in ICBM programs as the shape of Mark 3 and 4 warheads and, for this reason, has been selected as a typical model.

MULTICELL GENERATOR CONFIGURATION

The flared-cylinder concept is illustrated in the frontispiece. A multicell converter array, series/parallel connected for maximum electrical reliability, is arranged within an ellipsoidal-ended cylinder with a ribbed impact plate and crush-up in the nose section. To protect the generator against reentry heating, a POCO graphite ablator covers the whole aeroshell exterior except in the region of the mounting ring. A metal shell provides a chamber for vented helium and additional structural protection against debris and over-pressure in launch pad explosions. The conical flare supplies aerodynamic drag to limit terminal impact velocities and earth burial. The aspect ratio and weight distribution of the aeroshell is designed to ensure that the center of pressure is on the axis of symmetry between the center of mass and the cone. This ensures proper orientation of the aeroshell during reentry.

PARAMETRIC DESIGN APPROACH

The characterization of multicell generators is established by the parametric design approach shown in Figure 1-2. Two major subsystems, the converter array and aeroshell, and their interactions are identified. Generator design and optimization requires consideration of basic converter design and performance optimization constrained by mission requirements and aeroshell characteristics. Converter performance is established by choice of fuel, electrode materials, electrode geometry, and helium management techniques. Selection of the multicell array is constrained by the available range of converter module power, credible current-technology components, and system design goals for reliability and generator voltage.

Aeroshell design involves identification of nuclear safety requirements for normal mission operation and accident conditions. Typical mission constraints and environments govern materials selection and structural design to survive abort, reentry disposal, impact, and post-impact conditions. The design of the aeroshell also reflects the requirement to match thermal characteristics of the converter array.

System integration of the generator is provided by electrical connections and components which isolate the aeroshell from mechanical shock and vibration transmitted from the space vehicle. The system-integrated generator is characterized by its weight, specific power, reliability, output voltage, and BOL thermal source. Characteristics of the converter array, aeroshell, and minimum-penalty system-integration components are considered. The aeroshell design establishes the safety characterization of the system and the extent of nuclear risk during its deployment.

DETAILED GENERATOR DESIGN

The detailed generator design is derived from the parametric study. Fine structure in optimization procedures is considered by tradeoffs between converter module power, off-optimum converter operation, converter decay characteristics, converter array/aeroshell thermal balance, and array redundancy. The consequent selection of optimum converter power, array size, and aeroshell stacking configuration permits reevaluation of structural

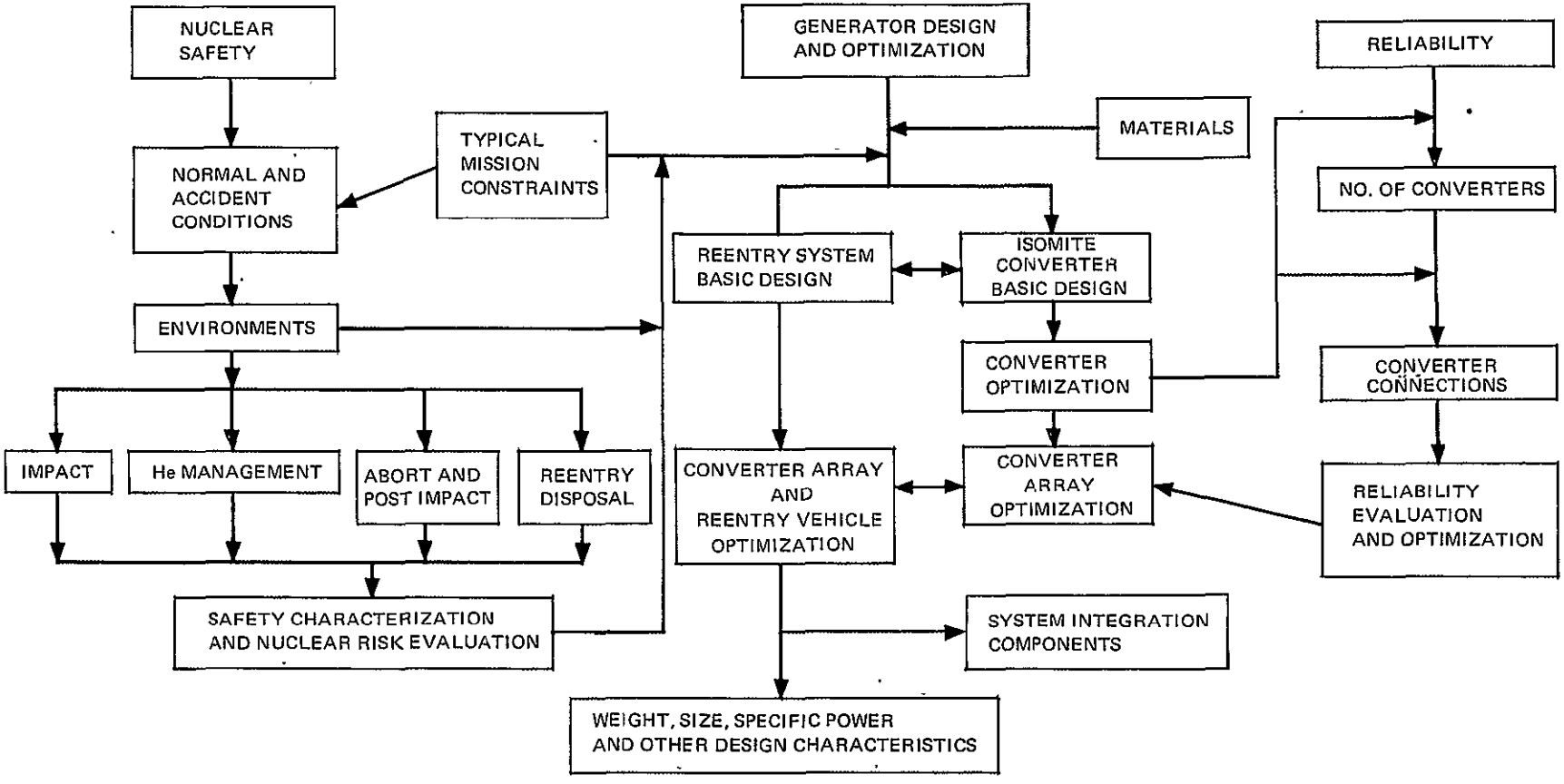

Figure 1-2. Flow-Diagram for Parametric Design Approach

components which provide an acceptable nuclear safety design. Finally, identification of a generator design leads to minimizing weight and other system penalties associated with system-integration components.

EVOLUTION OF TECHNOLOGY AND ANALYSIS

During the course of this program, new technical information and analytical techniques have become available from related effort conducted under DWDL Independent Research and Development (IRAD) programs. Incorporation and use of the most recent insight in this study as noted in subsequent sections provides the most up-to-date review of anticipated multicell generator characteristics. The contents of this report, therefore, render obsolete some portions of previous reports describing elements of this effort.

REPORT ORGANIZATION

The balance of this report is arranged as follows:

Section 2	Influence of electrode surface parameters.
Section 3	Off-optimum converter performance.
Section 4	Constraints imposed by choice of fuel form, emitter geometry, and helium management technique.
Section 5	Converter array selection and interconnection based on generator reliability and voltage.
Section 6	Aeroshell design and converter stacking optimization.
Section 7	Parametric generator characterization.
Section 8	Design and layout of a 100 w_e generator.
Section 9	Supporting experimental evidence of quasi-vacuum mode converter performance.
Section 10	Advanced technology and concept growth potential review.
Section 11	Conclusions and recommendations.
Section 12	New technology contractual statement.
Section 13	References.
Appendix A	Quasi-vacuum mode thermionic converter theory and optimization codes.
Appendix B	Plutonia fuel forms.
Appendix C	Unvented fuel capsule load limit optimization.
Appendix D	Converter array reliability.
Appendix E	Aeroshell calculations.
Appendix F	Detail design aeroheating analysis, aeroshell helium pressure effects, and busbar optimization.

Section 2
ELECTRODE SURFACE PARAMETER INFLUENCE

The Isomite converter behaves thermionically as a space-charge limited converter with a potential energy diagram as shown in Figure 2-1. Potential distribution in the electrode gap has been described in detail (References 7 and 8). For electrode spacing on the order of 1 mil, the converter operates with useful efficiencies at emitter temperatures below 1400°K, if the electrode work functions ϕ_e and ϕ_c are less than approximately 2.4 and 1.8 ev, respectively. Surface work functions of this magnitude or less are obtained by partial monolayer adsorption of cesium on refractory metal surfaces operating in the conventional collector regime of the Rasor-Warner (ϕ vs T/T_R) diagram (Reference 9). In the Isomite converter, cesium vapor pressures from 10^{-3} to 10^{-1} torr produce favorable work functions on the electrode surfaces without

70-2134

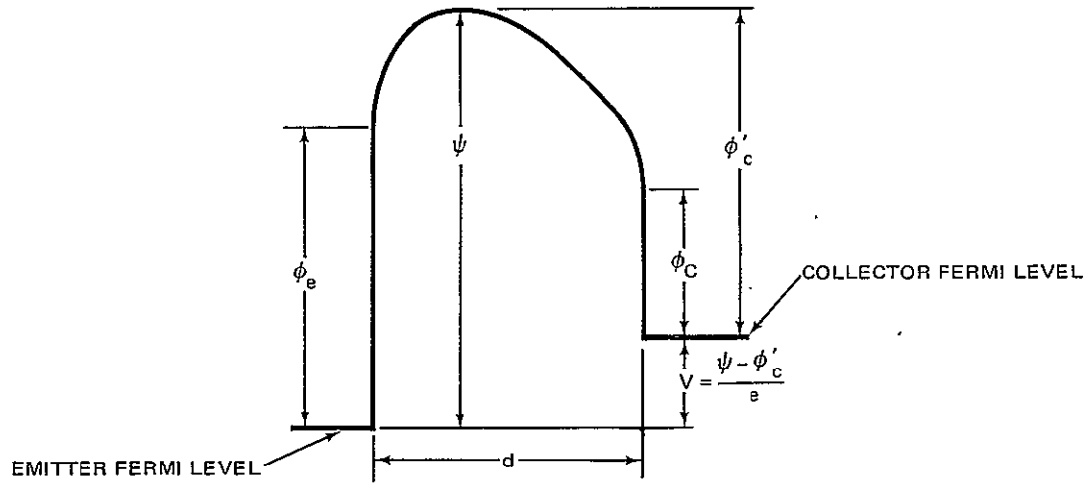

Figure 2-1. Space-Charge Limited, Vacuum-Mode Converter Potential Diagram

contributing electron scattering effects in the converter. Appendix A contains a detailed summary of quasi-vacuum mode operation.

Converter efficiency is defined by the ratio of useful power at the converter terminals to the sum of the components of the thermal energy balance. Figure 2-2 shows the apportionment of thermal losses for a typical converter. The dominance of radiation and electron cooling indicates the value in selecting electrode surfaces with low thermal emissivities and low ϕ_{min}.

AVAILABLE ELECTRODE SURFACES

Three electrode surface systems are currently under investigation at DWDL.

1. DWDL-developed Ta-O-Cs emitter and collector.
2. W-Cs emitter and Ta-O-Cs collector.
3. Langmuir W-O-Cs emitter and collector.

70-895

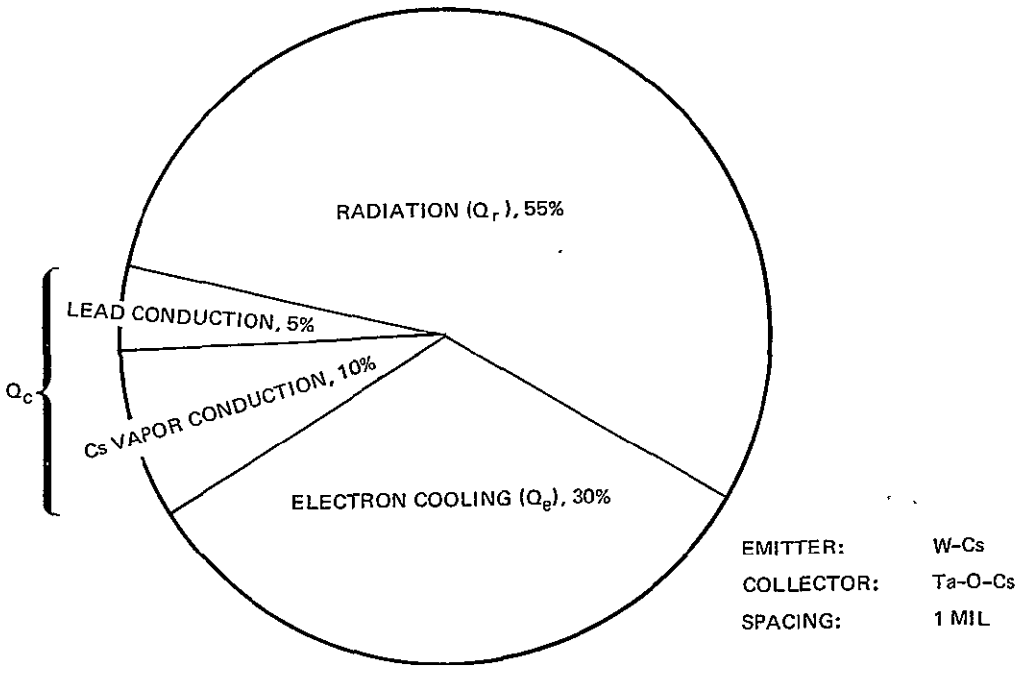

Figure 2-2. Apportionment of Thermal Losses for an Optimized 5 w_e Space Power Converter

Ta-O-Cs surface systems have been reduced to practice in over 50 radionuclide-fueled and electrically-heated converters and have accumulated over 150,000 hr of operation. Surfaces can be prepared reproducibly to achieve ϕ_{min} between 1.34 and 1.64 ev over the range of collector temperatures usually required in the Isomite converter. The Ta-O-Cs surface also provides acceptable values of ϕ_e (1.7 to 2.3 ev) over a range of T_e from 900° to 1400°K.

Characteristics of the Ta-O-Cs surface system are not totally understood in the ϕ_{min} region. Laboratory experience with the DWDL-proprietary surface shows a general temperature dependence of ϕ_{min}; however, the exact nature of this dependence is still under investigation in Independent Research and Development (IRAD) programs. For computational purposes in this study, recent laboratory data have been correlated by straightline approximations to describe the temperature dependence of ϕ_{min} to first order accuracy (Figure 2-3). Data which permit this refinement have been generated concurrently with the progress of this design study. Therefore, converter performance summarized in this report supersedes characteristics in previous monthly summaries which did not take this temperature dependence into account.

The W-Cs emitter is of interest because of its relatively lower emissivity than that of the Ta surface (Reference 10 and 11). The work function of the W-Cs surface (Reference 12) is not significantly higher than that of the Ta-O-Cs surface in the emitter region. The surface combination W-Cs emitter and Ta-O-Cs collector offers a lower Q_r loss component in some regions of the optimized converter power range.

The Langmuir W-O-Cs system (Reference 13), when plotted on the ϕ vs T/T_R plane (Figure 2-4) has rather remarkable characteristics, and three significant potential advantages compared with the systems considered so far:

1. Electrode emissivity can be expected to approach that of clean tungsten.
2. Values of ϕ_{min} and its temperature dependence are comparable with those of the Ta-O-Cs surface.
3. ϕ_{min} occurs at significantly higher values of T/T_R.

The W-O-Cs surface offers an operational domain in the ϕ vs T/T_R plane far removed from the Rasor-Warner envelope for conventional refractory metals. A potential disadvantage (compared with the Ta-O-Cs system) may

70-2152

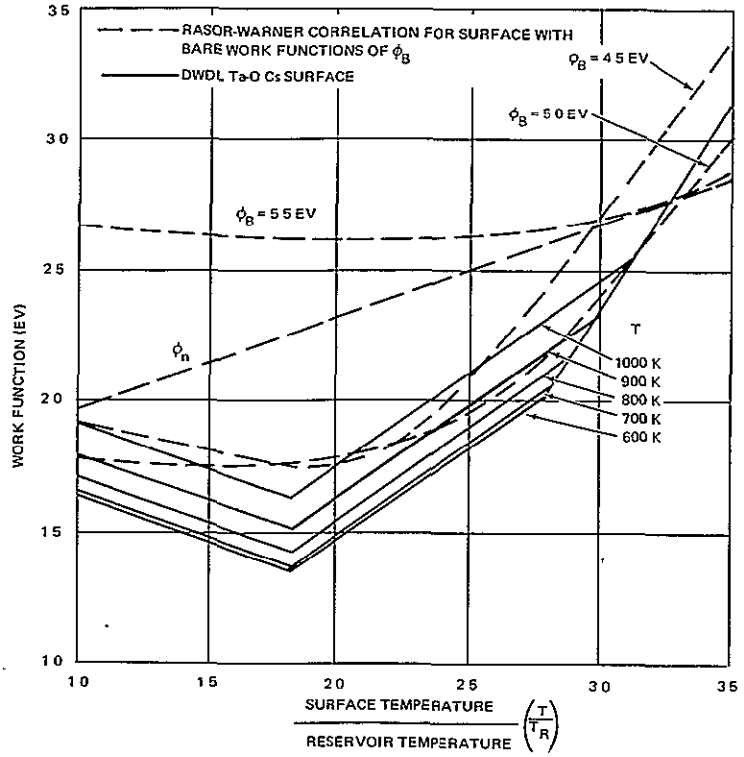

Figure 2-3. Work Function vs T/T_R Characteristics for the Ta-O-Cs Surface

70-2153

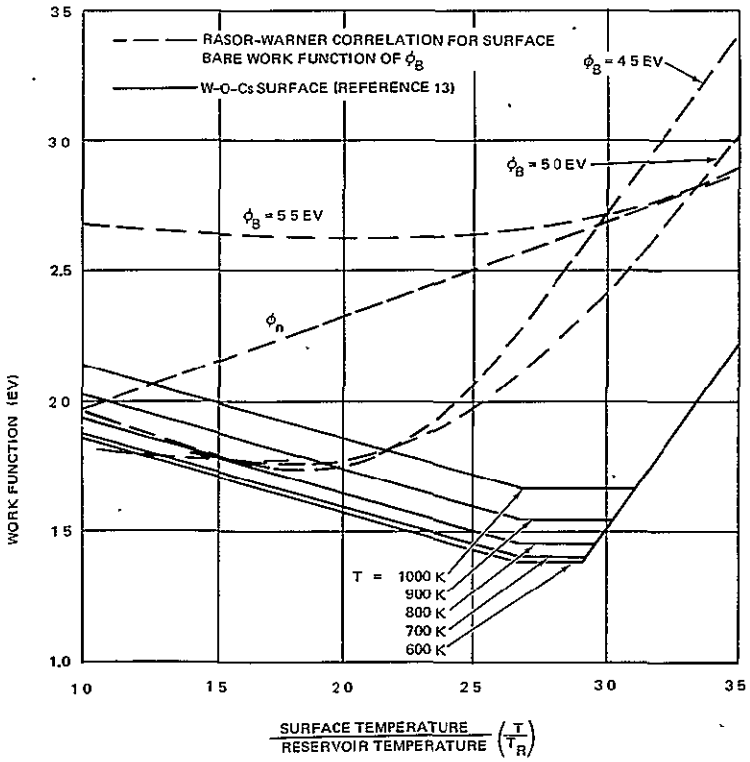

Figure 2-4. Work Function vs T/T_R For the W-O-Cs Surface

be that W-O-Cs surfaces depend apparently on the maintenance of an atomic oxygen monolayer, whereas oxygen in the Ta-O-Cs system appears to be contained in bulk solid solution. Corrosion of the Ta-O-Cs electrode surface may, therefore, tend to be repaired by a diffusion process in the substrate, in contrast with the tungsten-based surface, which may suffer irreparable degradation if the surface-active oxygen were removed by impurity reactions during the converter life.

COMPUTATIONAL APPROACH

The performance of optimized quasi-vacuum mode converters is surveyed in the range of Q and A from 10 to 100 w_t and 10 to 100 cm^2, respectively. With the surface systems under review, cell module power between 1 and 10 w_e is achieved for this range of Q and A. DWDL experience shows this range of converter power to be the general range of interest for multicell generator outputs between 50 and 200 w_e. DWDL-developed computer codes are used to calculate cell characteristics and describe converter performance parameters as functions of Q/A. In these calculations, all cell thermal loss mechanisms applicable to a general space mission environment are considered. The unique dependence of performance parameters on Q/A results from all components of the energy balance, with the exception of support conduction loss, being emitter area dependent. Laboratory measurement of emitter support loss (typically in the range 1 to 3 $mw_t/°K$ in a 1-g field) shows that it becomes negligible for the very small gravitational loads typical of most space missions. When support loading occurs (for instance, in spin-stabilized vehicles or planetary lander missions) it can be accounted for by adding an additional component to the input thermal inventory. In such instances however, the required thermal input power is increased typically less than 10% in the power range of interest. A parametric comparison of cell characteristics, ignoring the non-area-dependent thermal loss, is considered adequate for this study. The effect of gravity on the converter thermal balance is discussed again at the end of Section 2.

Three-Parameter Code

In the three-parameter code, the variables are ψ, T_c, and ℓ/a for the lead. The coding is arranged to cycle through a series of values of Q and A, but optimization with respect to these variables is not performed. A logic flow

diagram for the program is shown in Figure A-6, Appendix A. A nested stepping logic is used; with ℓ/a and T_c fixed, ψ is varied until the peak power is found. T_c is then changed and another ψ-loop performed. This continues until peak power for a particular ℓ/a has been located. Stepping ℓ/a then proceeds, followed by a double iteration on T_c and ψ. Eventually, a combination of ℓ/a, T_c, and ψ is found which leads to a maximum net electric power.

In this stepping technique, a parameter is varied monotonically with fixed-step size, until one step produces a lower power than the previous step. The penultimate step is taken as a new base, with the step size reduced by a factor of ten, and the process repeats. Termination occurs when either the peak has been found with steps 1/100 of the initial size, or, on the 1/10 and 1/100 size steps, a change in power of 0.01% or less occurs. Running time is minimized by using converged values from one iterative loop as starting information for the next loop.

Five-Parameter Code

The parameters available for optimization by the five-parameter code are Q, T_c, ℓ/a, ψ and collector-to-reservoir temperature ratio T_c/T_R. Parameterization using ψ is equivalent to using the load resistance and simpler to automate. Any or all of the parameters may be held constant and, if desired, a constant load resistance may be specified instead of a constant ψ.

Optimization starts with the selection of a set of initial parameter values. In the usual event of multiple calculations, the optimum configuration from one case is used as the initial value for the next. A pattern search is performed first, in which one parameter at a time is varied in an attempt to find a combination of parameter changes which produces a smaller objective function. Any improvement is accepted so long as it is greater than an input tolerance; steepest descent techniques are not used. At the completion of a pattern search, a base point is established, with an n-space vector specifying the direction from the initial value to the base point.

With the direction vector determined, a pattern move is made in which a new point is established by changing all parameters simultaneously to step along the vector. At the new base point a new search is made by varying one parameter at a time, thus modifying the direction vector. Stepping continues

from base point to base point until, eventually, a base point is reached at which the objective function is higher than at the previous base point even after all parameter variations have been tried. The search then reverts to the previous base point and a new pattern search occurs with a smaller step size.

The process continues, pattern moves interspersed by pattern searches, until a location is found in which a pattern search with all parameter step sizes at their minima does not produce any improvement. The search then terminates.

As part of the input to the search process, an upper and lower limit is required for each variable as well as an initial guess. Because of the nature of the search, different initial values or limits may cause termination at different combinations of parameters. This can be tolerated in parametric studies.

The two programs use the same subroutines to perform thermionic converter calculations and geometric calculations. The 3-parameter code is faster running but less flexible; a typical calculation will run in about 80 seconds on the IBM-1130, compared to 120 seconds for the same case on the 5-parameter code. However, the latter code is more flexible and has the option for searching for a specified power. A 4-parameter search for a predetermined power requires about 4 minutes, while using the 3-parameter code would require at least twice as long, and interpolation between results would be needed.

Converter optimizations are obtained in this manner, independent of emitter geometry. All characteristics, however, are strongly influenced by electrode spacing. A reference spacing of 1 mil has been chosen for the purposes of this study. This spacing represents developing technology in laboratory devices and is consistent with the credibility of building converters with thin-wall emitter and collector capsules several centimeters in diameter. The effect of off-design variation in electrode spacing is considered in Section 3.

PERFORMANCE COMPARISON

Parametric comparisons of optimum quasi-vacuum mode converter characteristics are presented in Figures 2-5, 2-6, and 2-7 showing the influence of three

electrode surface combinations. Two of the three combinations are worthy of consideration later in this study. The W-Cs emitter/Ta-O-Cs collector combination is only marginally more efficient (Figure 2-5) than the totally Ta-based surface system in the Q/A <1 range. It will become evident in Section 4 that fuel, geometry, and helium management choices can be arranged to exploit converter performance at higher values of Q/A, where Ta-O-Cs is the superior current technology electrode choice. Further consideration of the W-Cs emitter/Ta-O-Cs collector would apply only to lower module power than those of interest in a space power generator.

The W-O-Cs surface system has not yet been reduced to practice in a laboratory converter. The surface system provides, however, potentially superior conversion efficiency and higher cell output voltage (Figures 2-5 and 2-6). Potential disadvantages evident in Figure 2-7 are higher emitter and lower collector temperatures which might tend to prejudice materials compatibility and compact generator radiator sizing, respectively. The potential

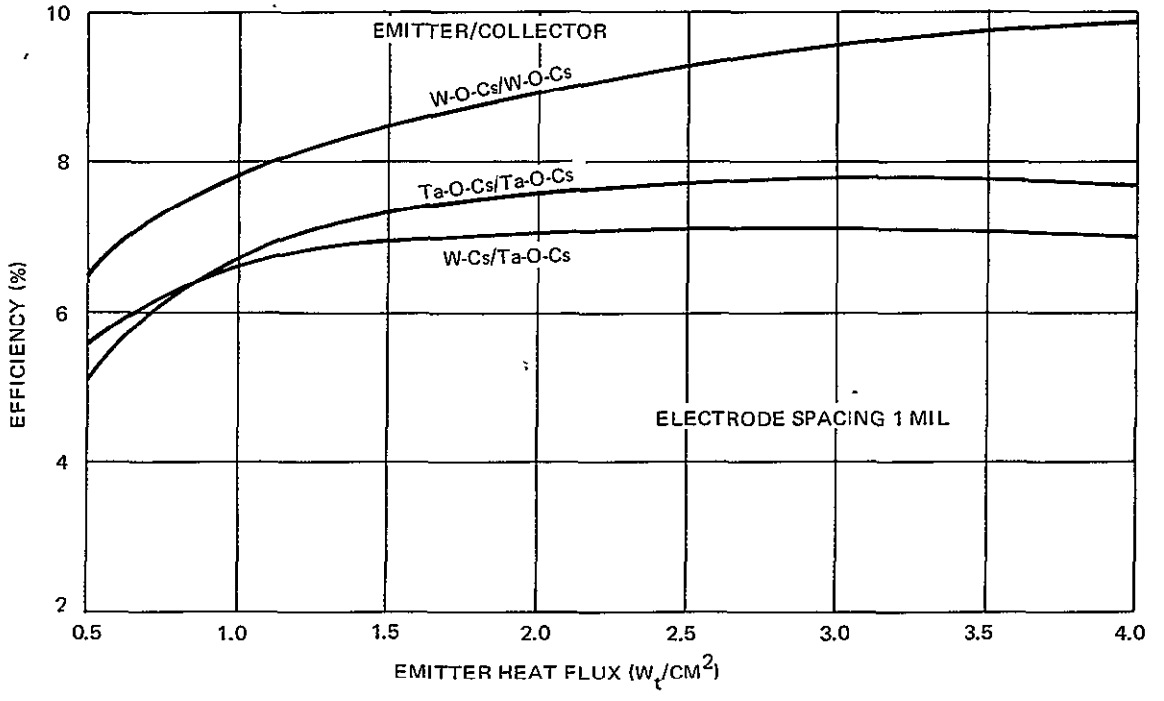

Figure 2-5. Efficiency vs Emitter Heat Flux

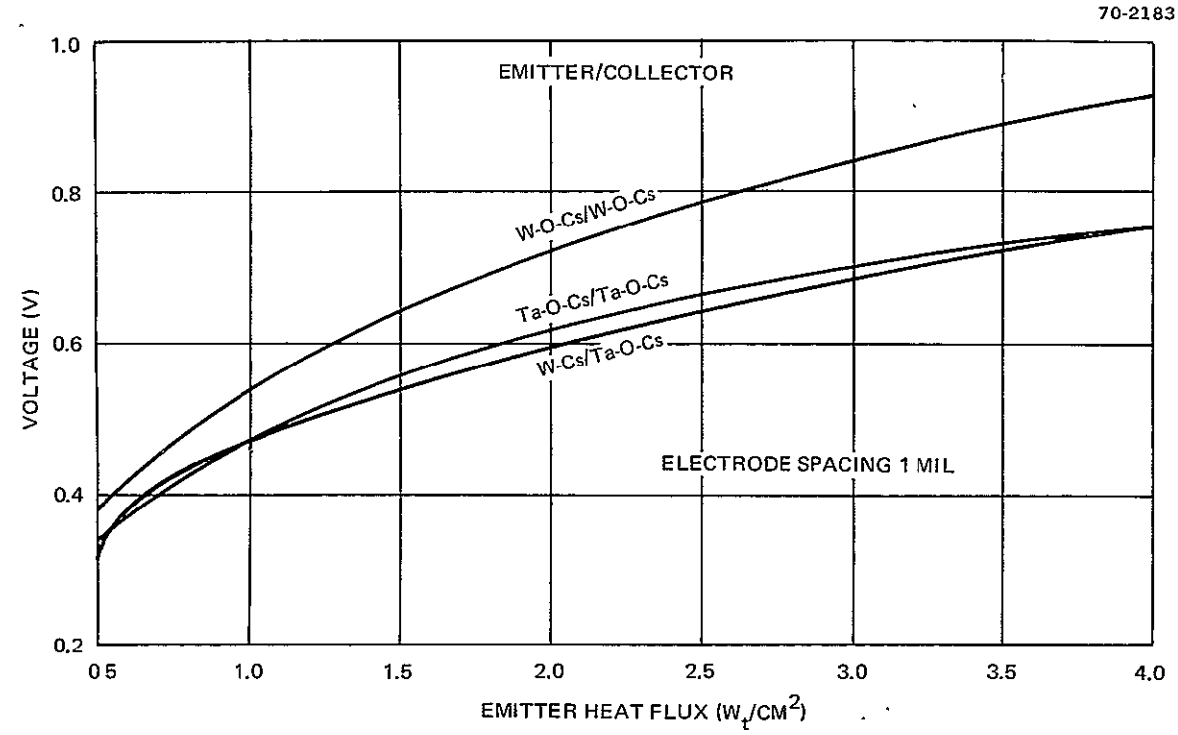

Figure 2-6. Net Converter Voltage vs Emitter Heat Flux

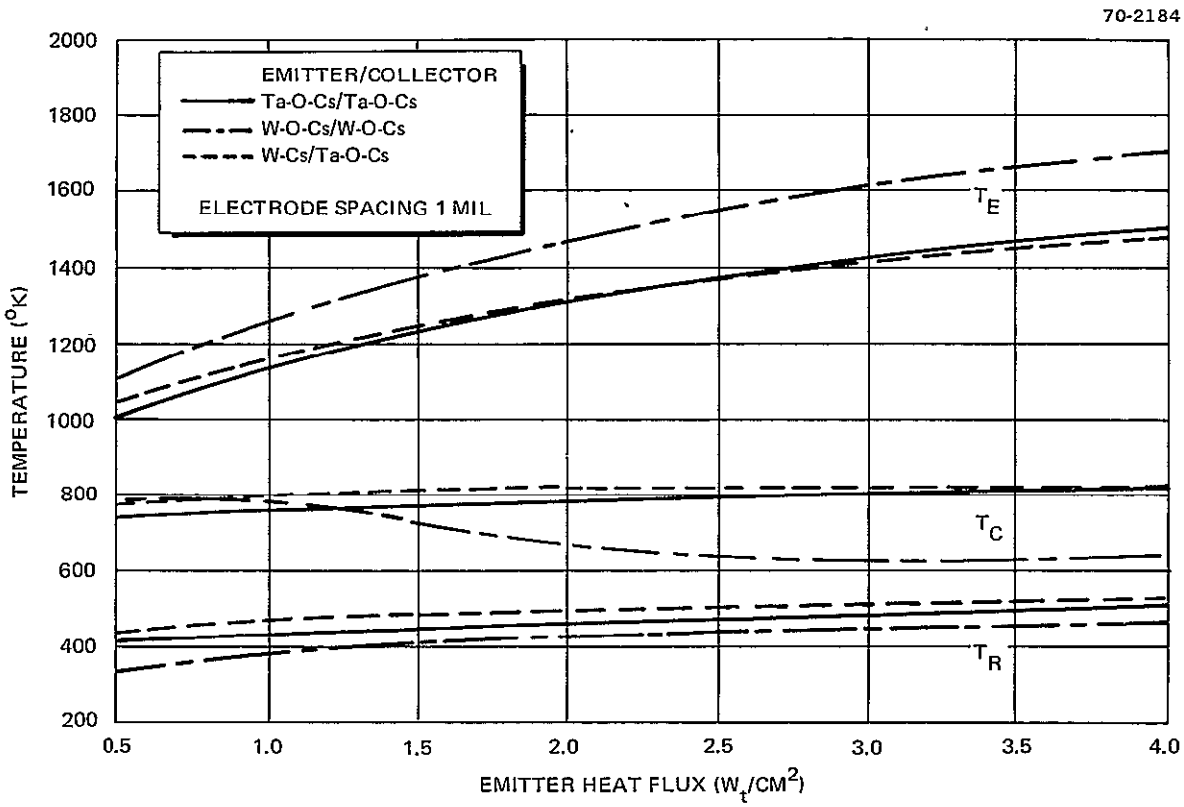

Figure 2-7. Surface and Reservoir Temperature vs Emitter Heat Flux at Optimum T_C/T_R

advantages appear to outweigh disadvantages and therefore the W-O-Cs surface is considered a component of advanced technology contributing a potential growth capability.

Mentioned previously, a non-Q/A dependent conduction loss is contributed by the electrode spacing and support mechanism, when subjected to a gravity field. This results from the dependence of thermal conduction on pressure at the electrode/spacer interfaces. The effect is shown in Figure 2-8 where converter efficiency is plotted against Q/A for various module powers for converters with Ta-O-Cs electrode surfaces. The support conduction in a 1-g field degrades efficiency with increasing influence as module power is reduced. The ∞ curve represents the zero-gravity (or infinite module power) condition. The Q/A range of interest for plutonia-fueled converters is between 1 and 2 w_t/cm^2. As shown in Figure 2-8, efficiency is penalized between 4% and 15% as module power decreases from 10 to 1 w_e. This effect is a significant tradeoff consideration in missions requiring operation in a gravity field.

The performance degradation shown in Figure 2-8 will be experienced during prelaunch converter and generator testing. Knowledge of the effect of a gravity field is, therefore, important as a basis of extrapolating generator behavior in the mission environment from data gained by terrestrial observation. This is discussed again in Section 9.

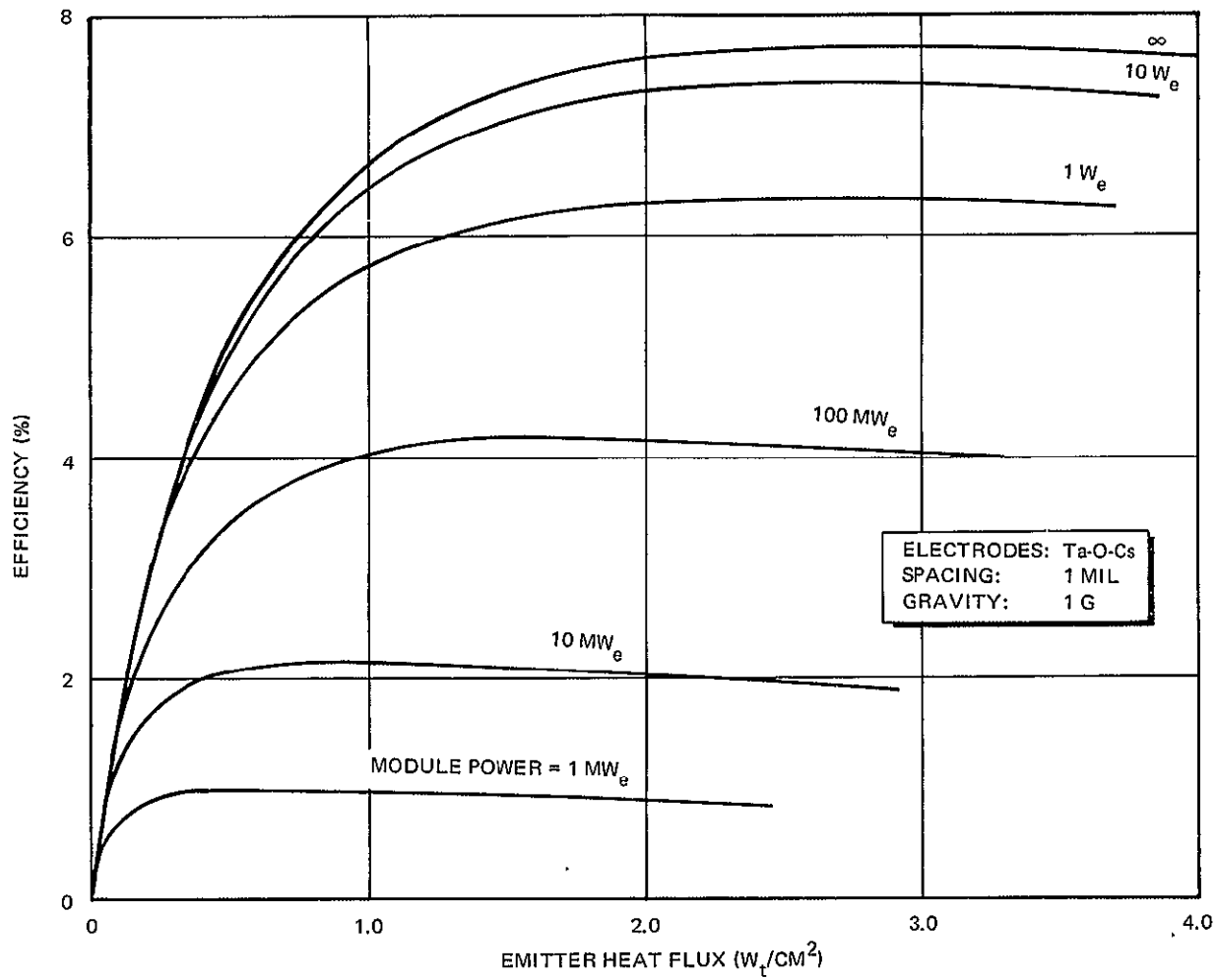

Figure 2-8. Efficiency vs Emitter Thermal Flux Showing Effect of Gravity-Dependent Conduction Loss

Section 3
OFF-OPTIMUM CONVERTER PERFORMANCE

The performance of converters in the multicell generator may be different from the optimum characteristics calculated in Section 2 as a result of materials variability, aeroshell-imposed effects, mission power profile, and fuel decay during mission life. The influence of variation in parameters which control converter output power can be calculated for suboptimum cases using the analytical codes of Section 2 with fixed-value parameter inputs. The power response to off-optimum and/or variations from reference design values of emitter and collector work function, surface thermal emissivity, collector and cesium reservoir temperature, electrode spacing and load resistance is shown in Figures 3-1 through 3-6, respectively.

Effects of parameter variation are shown by a plot of power degradation ratio P/Po vs the ratio of each parameter to its value if the converter were operating at optimum conditions. The ratio P/Po is shown as a function of parameter variability calculated for suboptimum cases of the subject parameter with all other independent parameters input at previous optimum values. This review of power response, therefore, does not necessarily account fully for converter output in the conditions of the total mission environment or allow re-optimization of independent variables. The summary is useful, however, in showing the generally worst-case bandwidths of allowable parameter deviation from optimum which maintain converter power within 10% of its maximum values. Figure 3-1 through 3-6 represent characteristics of converters with module power in the 1 to 7 w_e range to acceptable first-order accuracy.

A summary of the parameter variation producing ±10% change in P/Po is presented in Table 3-1. Parameters which have the greatest influence on power output are collector temperature, collector work function, and reservoir temperature, all of which require control to within about 6% for this power variation.

The influence of T_c is significant as a variable in the detailed generator design (Section 8). Because T_c is thermally coupled to the temperature of

70-2137

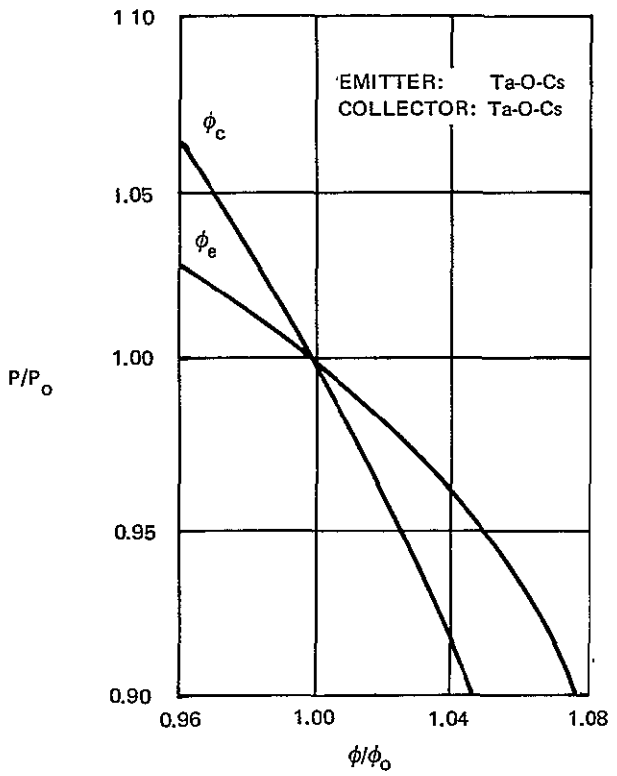

Figure 3-1. P/P$_o$ vs ϕ/ϕ_o with All Other Parameters Constant

70-2138

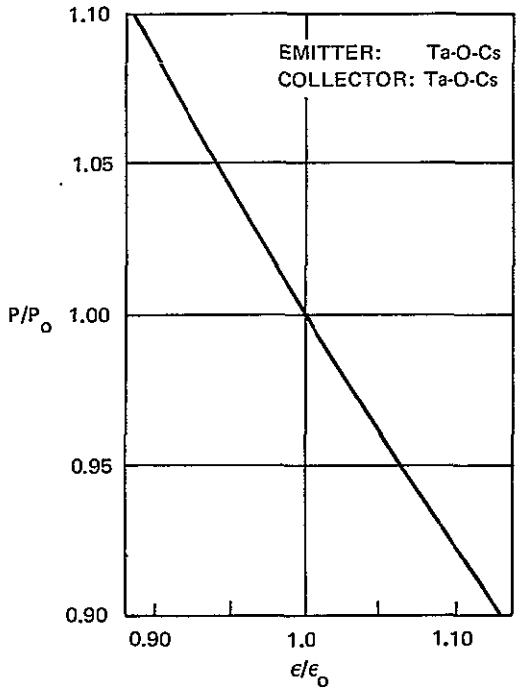

Figure 3-2. P/P$_o$ vs ϵ/ϵ_o with All Other Parameters Constant

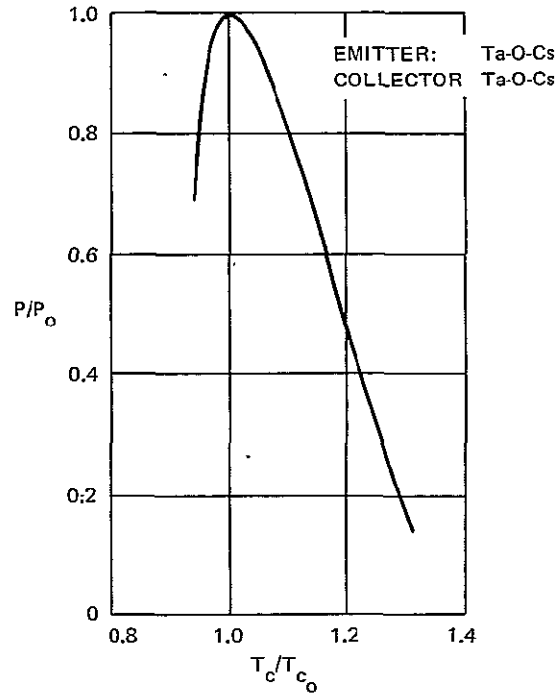

Figure 3-3. P/P_o vs T_c/T_{c_o} with All Other Parameters Constant

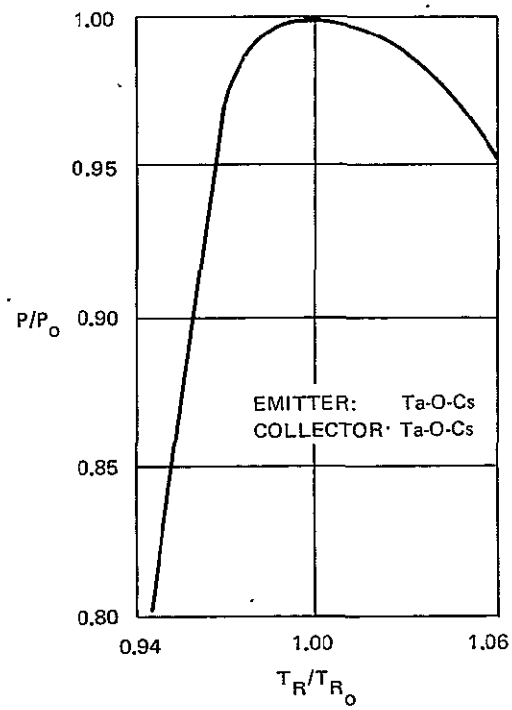

Figure 3-4. P/P_o vs T_R/T_{R_o} with All Other Parameters Constant

70-2142

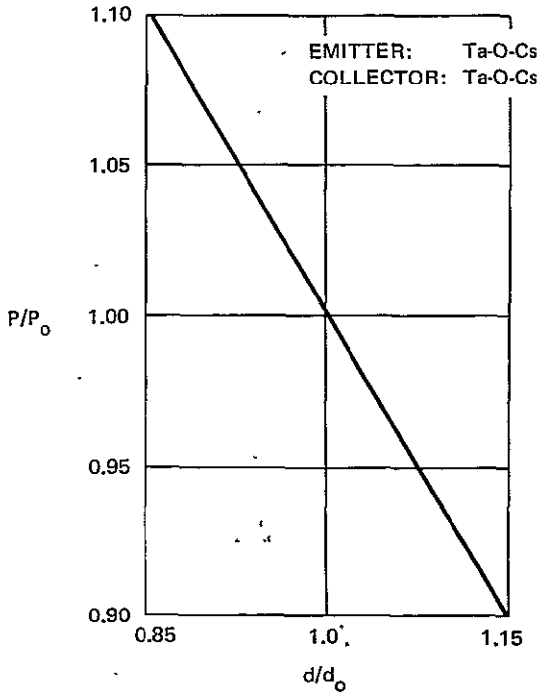

Figure 3-5. P/P_o vs d/d_o with All Other Parameters Constant

70-2143

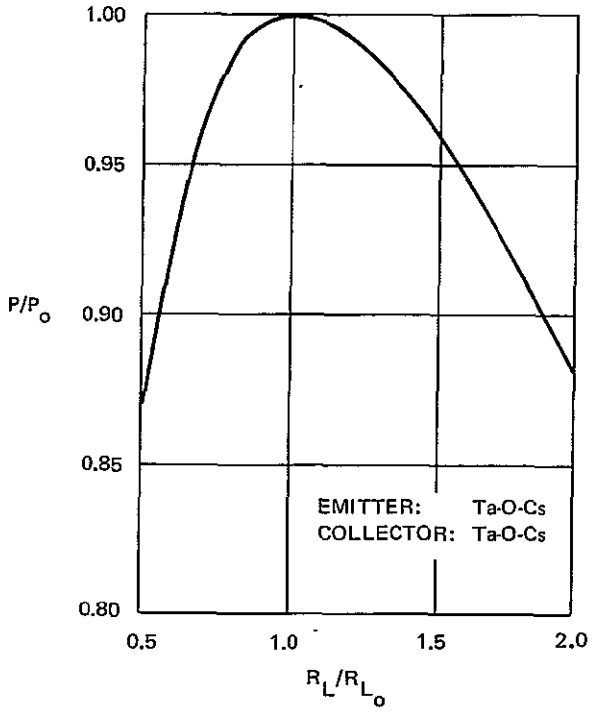

Figure 3-6. P/P_o vs R_L/R_{L_o} with All Other Parameters Constant

Table 3-1

PARAMETER VARIATION PRODUCING
±10% CHANGE IN P/Po

Parameter	Variation Above Optimization (%)	Variation Below Optimization (%)
ϕ_e	8	- (1)
ϕ_c	5	8
ε	13	12
T_C	4	7
R_L	85	44
d	15	15
T_R	4	9

(1) A 6% reduction in ϕ_e produces 4% increase in P. Further reduction in ϕ_e has negligible effect because energy balance at the emitter is controlled by the value of emission barrier ψ, which is independent of ϕ_e when $\phi_e << \psi_o - 2KT_e$.

the aeroshell radiator, variation in T_c after incorporation of converters in a generator should be predictable and dependent mainly on the decay characteristic of the fuel.

Collector work function is controlled by collector and reservoir temperature. The effect of T_R variation is minimized by use of an integral non-liquid cesium reservoir. By charging this reservoir with cesium, in a converter operating under simulated generator conditions, fine-tuning of the power output can be achieved. The effective reservoir temperature can, in this manner, be adjusted to compensate for some variation in ϕ_c and ϕ_e at the cost of creating an off-optimum cesium vapor conduction loss.

Output power is moderately sensitive to electrode spacing. However DWDL experience shows that, at 1 mil spacing, accumulated component tolerances can be held within ±0.1 mil. Power response to this variation in spacing is well within the ±10% band.

Change in surface thermal emissivity has a nearly linear influence on power output. Experience shows that control of construction and manufacturing processes produces electrode surfaces with reproducible surface characteristics. The monotonically varying relationships between power and ϕ_c, ϕ_e, ε, and d allows converter design in which variation in parameters may be compensated by controlled variation in other parameters. The influence of T_c, R_L, and T_R shows a maximum power with falling power on either side of optimum conditions. Use of these parameters as compensatory variable has limited applicability. However, the gross insensitivity of power to change in load resistance offers a very flexible device for adjusting the apportionment of the thermal balance to improve generator response to system-required conditions. It is assumed that this sensitivity to load resistance is reflected to the generator terminals and, therefore, describes an inherently small generator sensitivity to the load impedance.

In this review, emitter temperature does not appear as an independent variable because it is inherent in the choice of electrode materials, T_c, T_R, and d.

A detailed and quantitative evaluation of all consequences of off-optimum and/or off-design performance caused by random parameter variability is beyond the scope of this effort. However, based on component technology which is still quite early in its development cycle, it appears that variation of dominant parameters can be expected in total to cause no greater than a ±10% deviation from the parametric power optimization and generator design discussed in Sections 7 and 8 of this report.

Section 4

FUEL, EMITTER GEOMETRY, AND HELIUM MANAGEMENT CONSTRAINTS

The choice of radionuclide fuel, emitter geometry, and helium management techniques determines what fraction of the Q/A range is available in a practical converter design. It was established in Section 2 that most converter performance parameters increase monotonically with Q/A. Constraints which permit high Q/A designs are, therefore, to be desired.

FUEL CONSTRAINTS

For a given emitter capsule geometry and helium management choice (vented or unvented capsule), a fuel thermal inventory limit is established by the fuel form and its effective thermal power density. In vented capsules, this limit corresponds to the fuel inventory which fills a capsule of given surface area, thickness, and geometry with no void volume remaining. Figure 4-1 shows fuel load limits on a logarithmic Q vs A plane for three radionuclide fuels in vented spherical capsules with a 25-mil wall thickness. This wall thickness is used as a reference and represents a DWDL estimation of near-future practical vented capsule design in the configuration of the multicell generator. Fuel load limits in Figure 4-1 are calculated for EOL fuel thermal power at 10.5 years. Output isopower curves, derived from the analysis of Section 2, are plotted for optimum converters with Ta-O-Cs surfaces and 1-mil electrode spacing. The fuel forms considered are:

1. Plutonia Solid Solution Cermet (SSC)
2. Plutonia-Molybdenum Cermet (PMC)
3. Curia cermet

Plutonia fuel form properties (References 14 and 15) are summarized in Table 4-1 and discussed in Appendix B. The curia fuel limit shown in Figure 4-1 is the prediction (Reference 16) of a potentially feasible curia cermet with a density of 10.5 g/cm^3 and a power density of 19.1 w_t/cm^3. A curia ceramic fuel form has been developed for application in a conventional high-temperature thermionic

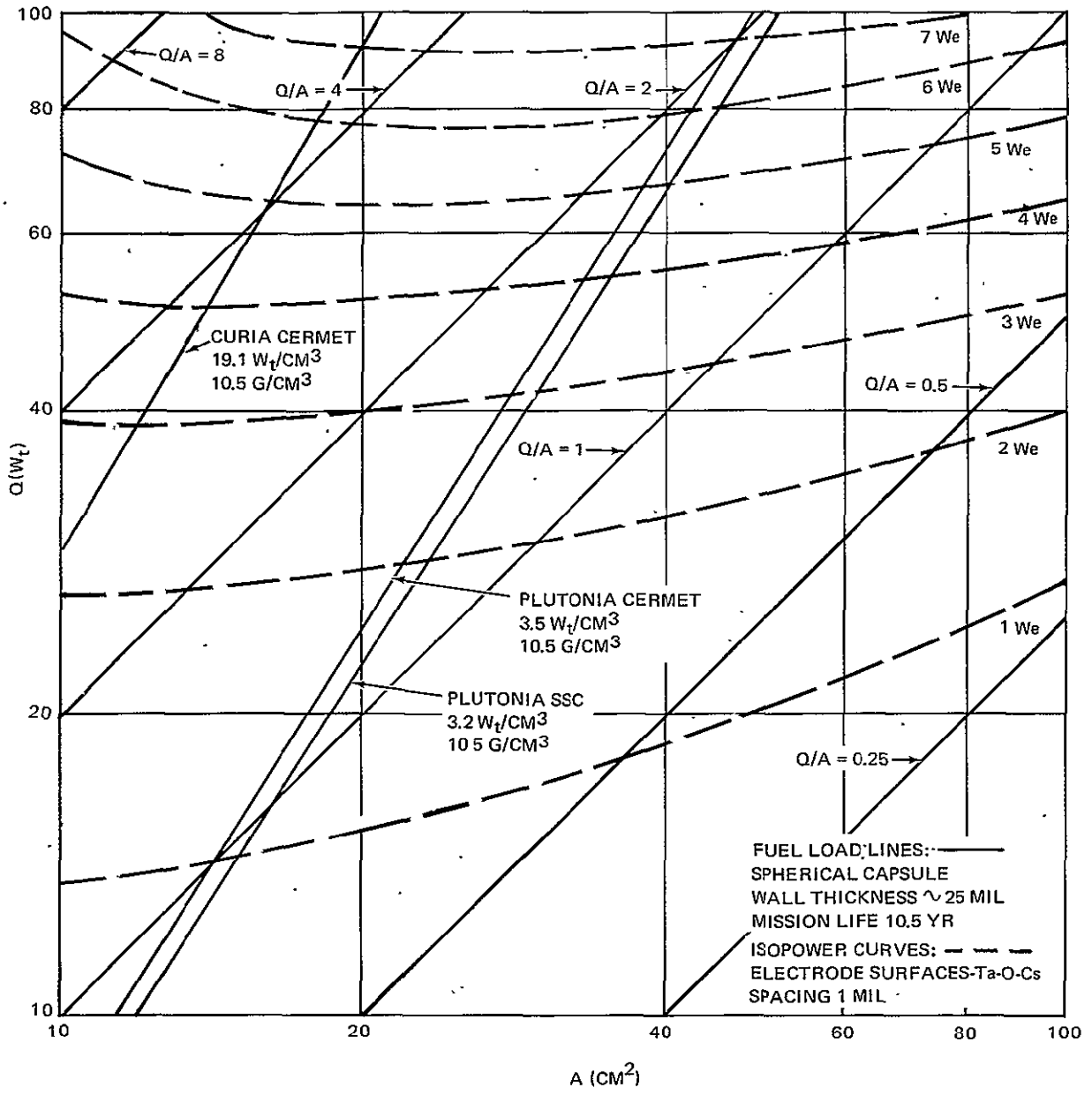

Figure 4-1. Fuel Load Limit for Three Fuel Forms on Q vs A Plane

Table 4-1

PLUTONIA FUEL FORM COMPARISON

Property	Plutonia Solid Solution Cermet	Plutonia Cermet
Density (g/cm^3)	10.5	10.7
Power Density (w_t/cm^3)	3.2	3.5
Thermal Conductivity (w_t/cm-°C):		
900°C	0.102	0.148
1200°C	0.098	0.146
Thermal Expansion (% $\Delta L/L$) (20° to 900°C)	0.53	0.85

generator concept (Reference 1) and therefore by analogy with plutonia development can be recognized as a basis for near-term technology. The scope of Objective 1 and 2 effort is restricted to plutonium fuel forms by contractual definition. As a result, consideration of curia cermet is contained in the advanced technology review, despite its near-term potential availability.

Figure 4-1 shows that, by increasing the effective thermal power density, the fuel load limit curve allows converter design at progressively higher and generally more favorable Q/A values. The region to the left of each load limit curve is unavailable for converter design in devices with all surfaces active. Operation to the left of the load limit line can be achieved by operating a fraction of the emitter thermionically and shielding other portions with insulating material. A similar plot is obtained with isopower curves for any other surface system by plotting P_{max} (derived from Figure 2-6) on the Q vs A plane.

The loci of best converter designs are intersection points of the fuel load and isopower curves in Figure 4-1. The fuel constraint imposed on converter specific power is compared in Figure 4-2 for several fuel and electrode surface combinations. Specific power rises with converter power and tends toward a plateau above 3-w_e module sizes. Increasing fuel thermal power density and improved electrode technology both allow higher specific converter power. However, fuel thermal power density is the dominant influence. Figure 4-2 shows that the relatively small improvement in power density provided by the

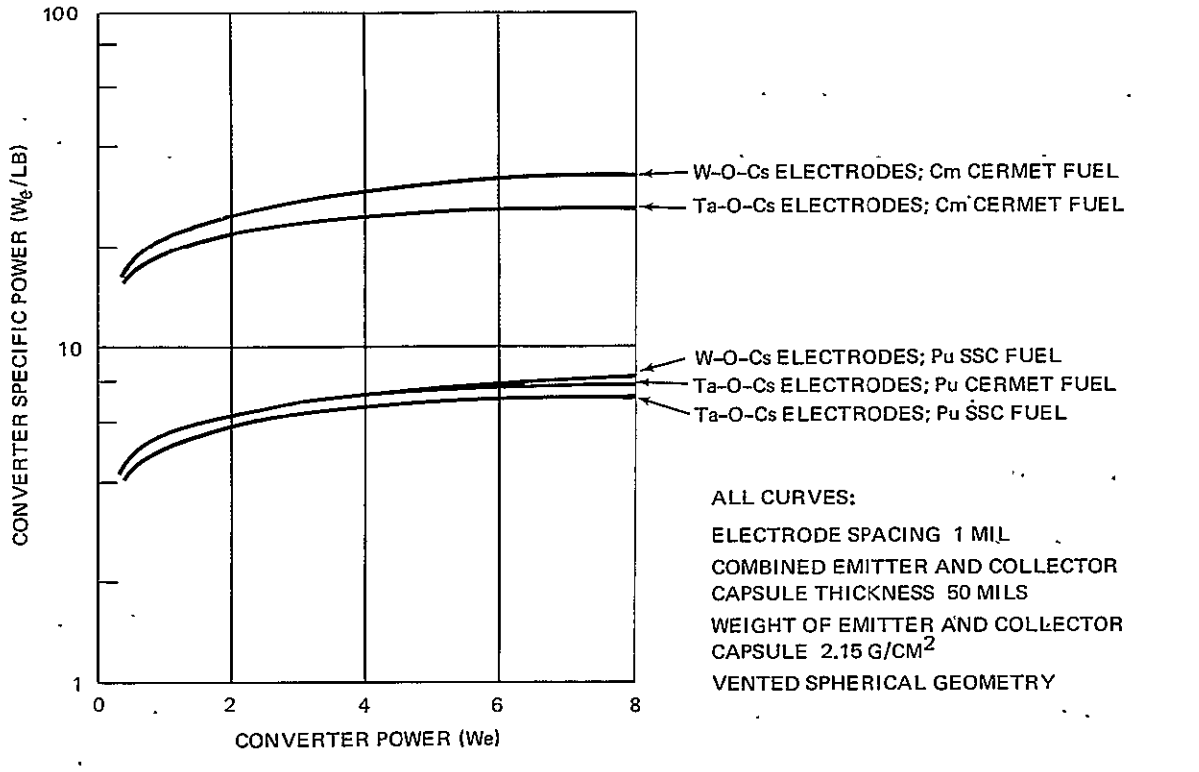

Figure 4-2. Converter Specific Power vs Cell Power Showing Fuel Load Constraint for Spherical Geometry

PMC over the SSC fuel form (3.5 and 3.2 w_t/cm^3, respectively) increases converter specific power approximately the same extent as that allowed by potential long-term thermionic surface development. The curia fuel, after allowing for its shorter half-life, provides up to a fourfold improvement in EOL converter specific power.

Figure 4-2 shows a slight advantage using PMC if theoretical power density is achieved. In current practice, the power density of this fuel form has been in the range 3.2 to 3.3 w_t/cm^3 and hence is little different from that calculated for plutonia SSC. The following sections of this report consider a plutonia fuel having a power density of 3.2 w_t/cm^3. The reported multicell generator performance will, therefore, be consistent with the eventual availability of plutonia SSC and slightly conservative for PMC.

EMITTER GEOMETRY CONSTRAINT

Emitter geometry has an influence on converter design analogous to that of the fuel load limit and is calculated in similar fashion. For a given fuel choice, helium management technique, and capsule wall thickness, the emitter geometry establishes a fuel load limit curve on the Q vs A plane (Figure 4-3). The Q/A region to the left of this curve is excluded from use in a practical converter except, as previously noted, when the emitter is partitioned into thermionically active and inactive areas.

For converters with all of the emitter surface thermionically active the progression from spheres to cylinders with increasing aspect ratios moves the design cut-off towards lower Q/A and a less favorable thermionic operational regime.

HELIUM MANAGEMENT

Figure 4-4 shows the fuel load limits imposed by vented and unvented capsules of spherical and cylindrical form, respectively. The vented capsule curves are those of Figure 4-3. The unvented spherical capsule curve represents the load limit associated with T-111 capsule required to contain the maximum plutonia SSC fuel inventory for a given emitter area and a mission life of 10.5 years. Helium containment was considered for temperatures 100°K above optimum emitter temperature at mission EOL. A minimum emitter capsule thickness of 25 mils was retained and in the low-Q region was found to be thicker than that required for safe helium containment. The strength of a 25-mil thick collector capsule was taken into account to establish a more favorable unvented capsule design of comparable specific power to that of vented devices. For this calculation, the emitter was considered to yield across the interelectrode gap and be reinforced by the collector. Calculation of the unvented cylindrical case was performed both with and without taking account of collector reinforcement. Details of these calculations are summarized in Appendix C.

Figure 4-5 summarizes the geometry effect (Figure 4-3) and helium management consideration (Figure 4-4) and shows converter specific power plotted

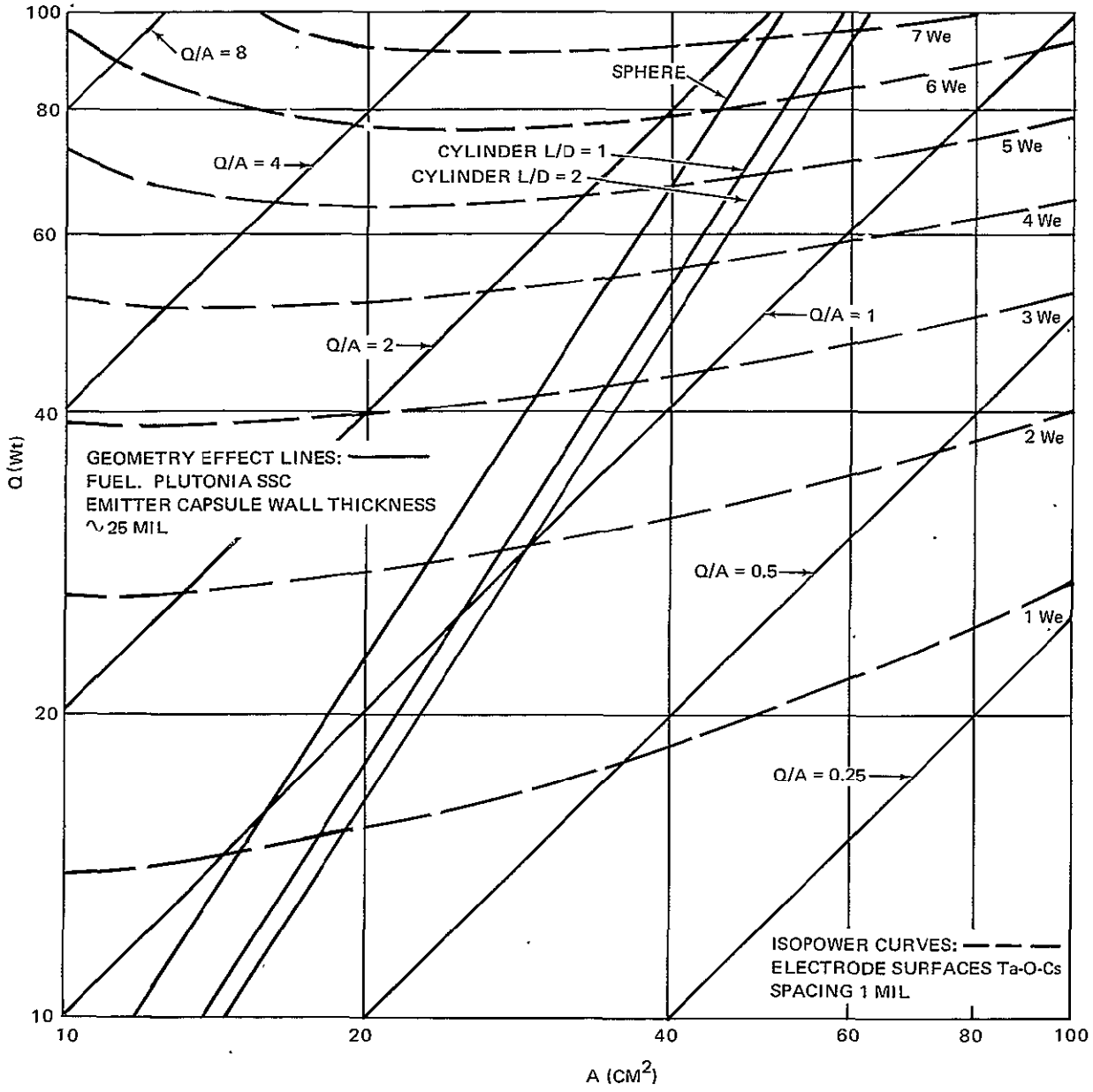

Figure 4-3. Geometry Effect Fuel Load Limit for Three Emitter Shapes on Q vs A Plane

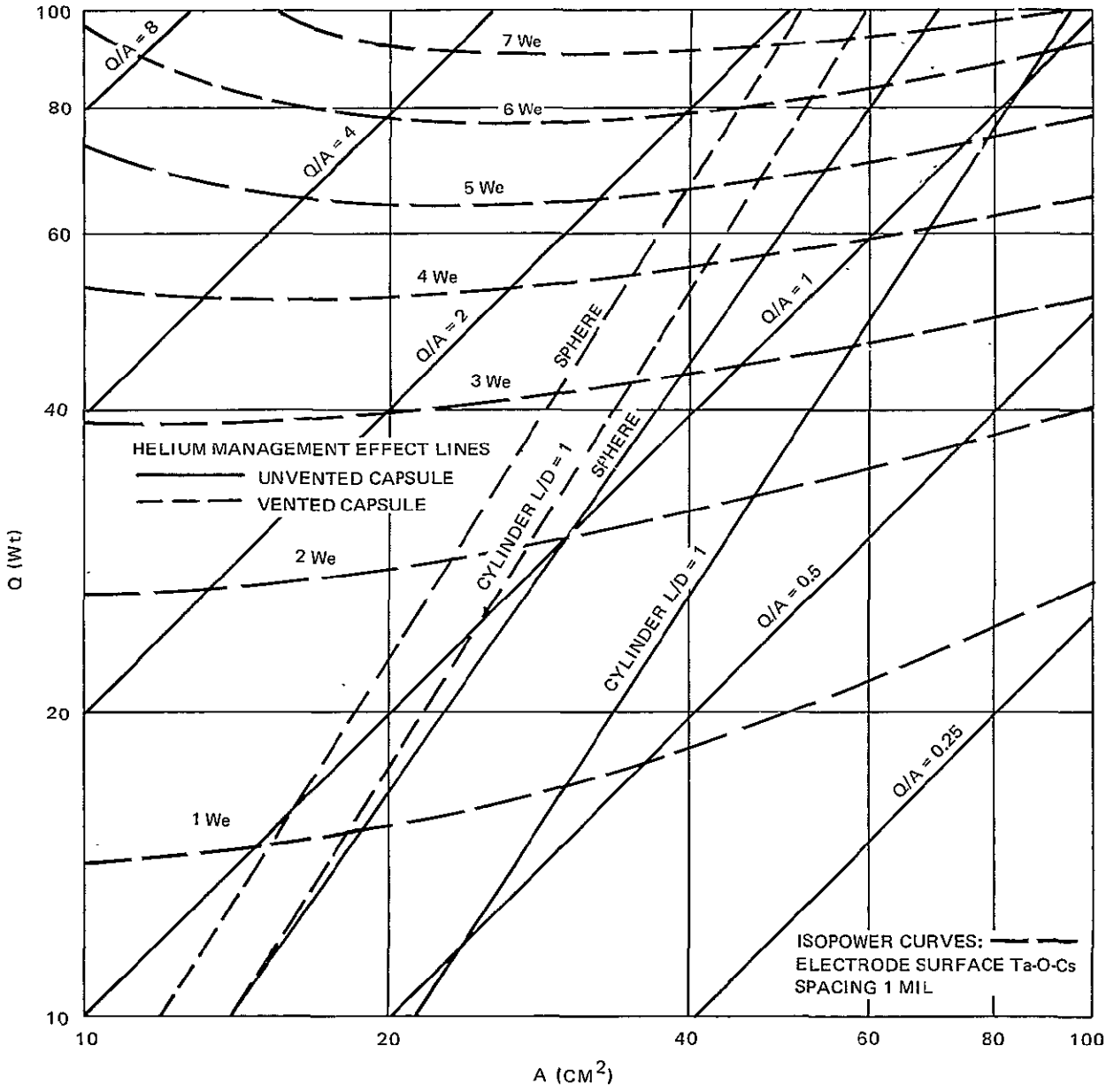

Figure 4-4. Effect of Helium Management on Fuel Load Limit Plotted on Q vs A Plane

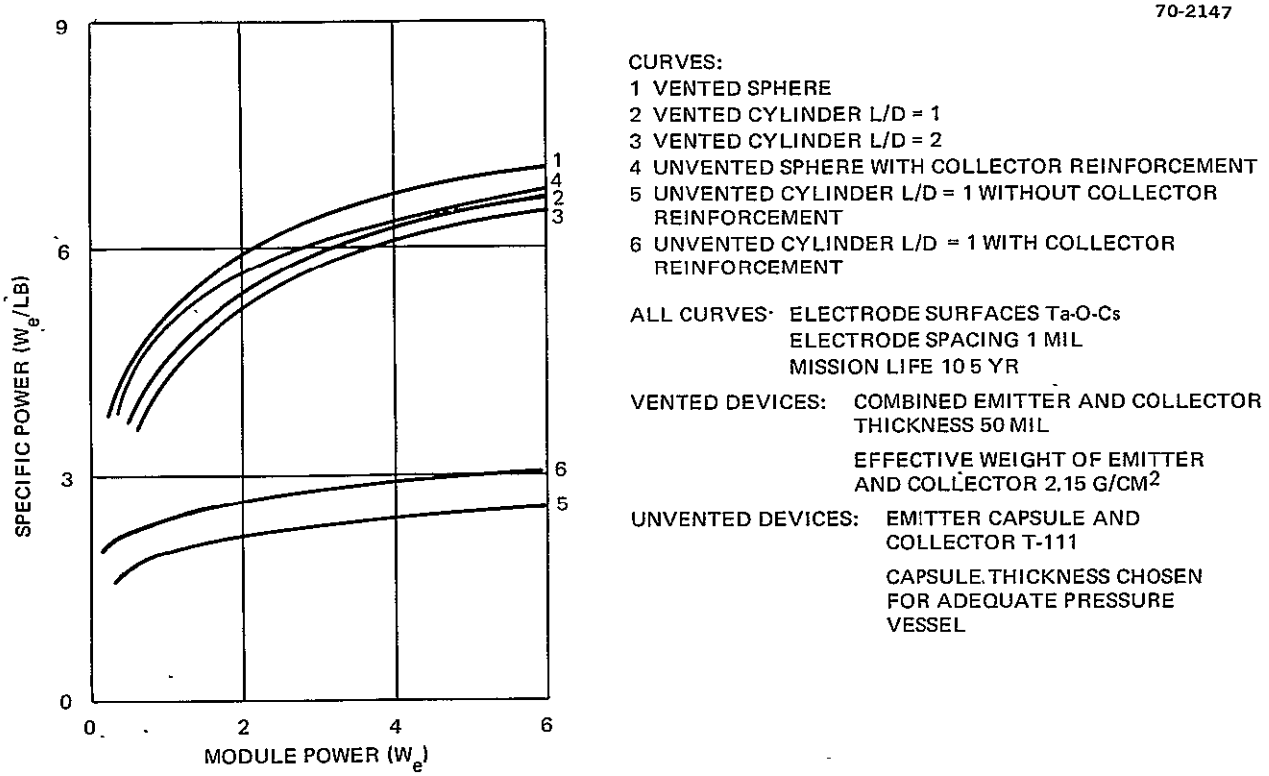

Figure 4-5. Converter Specific Power vs Module Power Showing Geometry and Helium Management Choices

against module power. The collector-reinforced unvented spherical capsule allows converter specific power of the same magnitude as that of vented capsule designs. In Figure 4-4, the unvented sphere operates at Q/A values close to those of the vented cylinder. In the event that an integral vent device requires longer development time than other generator components, the unvented sphere offers an alternate approach and an important secondary choice for the baseline converter design.

The vented spherical geometry permits specific power from 5% to 10% higher than that of the best vented cylinder. This difference is not sufficiently significant to warrant emphasis of spherical geometry (not yet fully reduced to practice) in place of the current-technology cylindrical configuration, as a component of the parametric generator study.

In general, unvented cylindrical emitter designs do not exploit the performance potential of the Isomite converter based on other elements of current technology. Unvented capsules also reflect weight penalties into the aeroshell design for structure to limit thermal exposure and impact of the pressure vessel. Because considerable effort is being invested in the development of reliable venting mechanisms, it is assumed that no significant loss of credibility results if the parametric system study is based on a vented cylindrical capsule design. The emitter and collector capsule thickness can be optimized in the tradeoff between achievement of high converter specific power and survival of accident conditions. This subject warrants further study.

Section 5
GENERATOR RELIABILITY AND VOLTAGE

The choice of converter module size for the multicell generator is influenced by system interface and reliability requirements. A detailed reliability study is inappropriate for this parametric review. This section, therefore, establishes converter selection and interconnection criteria based upon requirements for generator reliability, output voltage, and power. To accommodate converter failures, redundancy is introduced to provide a certain probability of achieving rated generator power and voltage.

To facilitate the reliability review within the resource level of this effort, analysis is based on series/parallel electrical interconnection of two- and three-column converter arrays. This limitation of scope is generally consistent with the expectation that Isomite converters will have a lower propensity to fail in the open-circuit than short-circuit condition, a situation promoted by the low temperature thermionic mode of operation in conjunction with close-spaced electrode systems. Because one purpose of series/parallel networks is to protect against catastrophic generator open-circuit failure by providing alternate paths for current in the event that converter open-circuit failures occur, two column arrays may be sufficiently reliable for devices with low open-circuit probability.

Figure D-1 shows a flat network array of converters composed of "c" columns and "r" rows. Three-dimensional networks have been reported (Reference 17 and 18) which suppress edge effects when failures occur. For the purposes of converter selection in this study, simple flat networks with zero impedance series and parallel connections are analyzed.

COMPUTATIONAL APPROACH

Analysis of converter array reliability in this report is generated by a probabilistic (Monte Carlo) technique. For complex networks, this is probably the only feasible approach. However, the technique is also valuable for analysis of the simple networks required for the multicell generator because

all statistical failure occurrences are counted if enough iterations are performed.

The reliability study reported previously was based on deterministic expansion of the failure trinomial (Appendix D). Using this method, analysis becomes rapidly cumbersome after more than two converter failures are considered. For this reason, the Monte Carlo technique was adopted as a more useful analytical tool. The results of the present analysis represent a refinement of the deterministic data reported previously.

The probabilistic analysis of converter arrays is based on generation of a random number for each module. The number is used to determine whether the converter is operating, open-circuited, or shorted out. After every device has been examined, the power and voltage of the array is determined and recorded. The process is repeated for up to several thousand cases, and the tabulated results are then interpreted to yield the probability of obtaining any given power or voltage.

This method has been computerized for use on the IBM 1130, using a pseudo-random number generator furnished by IBM. To minimize storage requirements, one row at a time is examined, and the equivalent resistance and voltage of the row calculated. These data are accumulated, row by row, until the entire array has been analyzed, following which the array power is calculated and the array statistics (power, voltage, number of open-circuit failures, number of short-circuit failures, and number of total failures) stored. After a preset number of array examinations, the cumulative results are output. Further details of this technique are presented in Appendix D.

The code was used to investigate parametrically the effect of changing the number of rows and columns and the reliability of individual converters. The results, after smoothing, are shown in Figures 5-1 through 5-3. All curves are presented as the probability of getting a specific fraction of the full array power vs the number of rows, with the fraction of full power as a parameter.

Figure 5-1 shows the results for 80% reliable converters, in which the ratio of short-circuit failures to open-circuit failures is 4:1. This is a reasonable

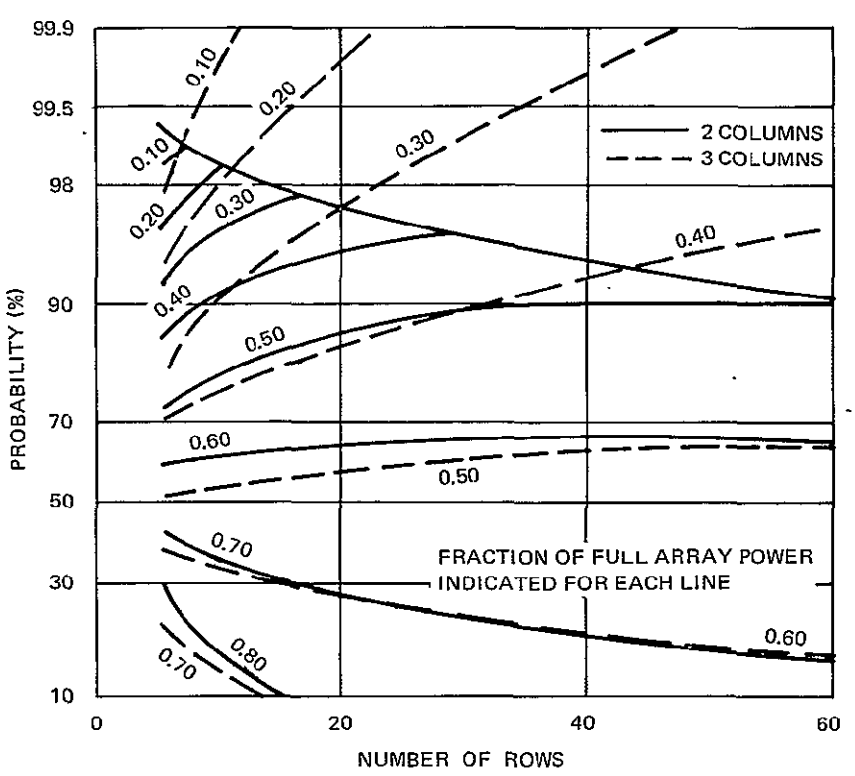

Figure 5-1. Probability of Obtaining a Given Fraction of Full Array Power vs Number of Rows for 80% Reliable Converters

ratio for Isomite converters with close spacing. Data for 2-column and 3-column arrays are plotted with solid lines and dashed lines, respectively. For any fraction of full power, the probability of achieving that fraction with a given number of rows is smaller with a 3-column array than with a 2-column array, except for a limited region in the upper portion of the graph.

This phenomenon occurs because the upper limit to the 2-column array data represents the probability of complete open-circuit failure. With 3 columns, the probability of complete open-circuit failure decreases drastically, which provides the primary incentive for going to a 3-column array. However, for any other condition, the effect on power of a single short-circuit failure is greater in a 3-column array than in a 2-column array. With short-circuits assumed to be 4 times as likely as open-circuit failures, the net effect is a reduction in probability of achieving any given fraction of full power in the 3-column array.

With 80% reliable converters, the probability of open-circuit failure is 4%, and an increase in converter reliability decreases the likelihood of open-circuit failure. It follows that, if a 2-column array is superior to a 3-column array with 4% open-circuit failure probability, there is little reason for further consideration of simple 3-column arrays at higher converter reliabilities. Figure 5-2 and 5-3 show the same information as in Figure 5-1 for 2-column arrays only, for 90 and 95 percent reliable converters, respectively. An increase in reliability increases both the probability of achieving any given fraction of full power and the probability of not having complete open circuit failure.

Figure 5-4 summarizes data from Figures 5-1 through 5-3. Here the fraction of full power which will be achieved with 98% probability is plotted vs number of rows for 80, 90, and 95% reliable diodes in 2-column arrays and for 80% reliable diodes in a 3-column array.

70-2148

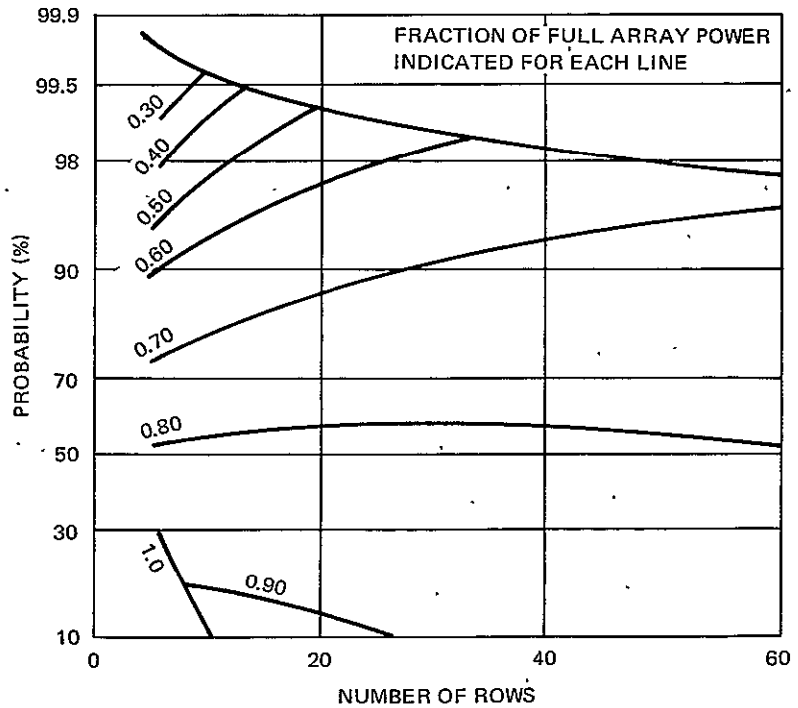

Figure 5-2. Probability of Obtaining a Given Fraction of Full Array Power vs Number of Rows for 90% Reliable Converters

70-2149

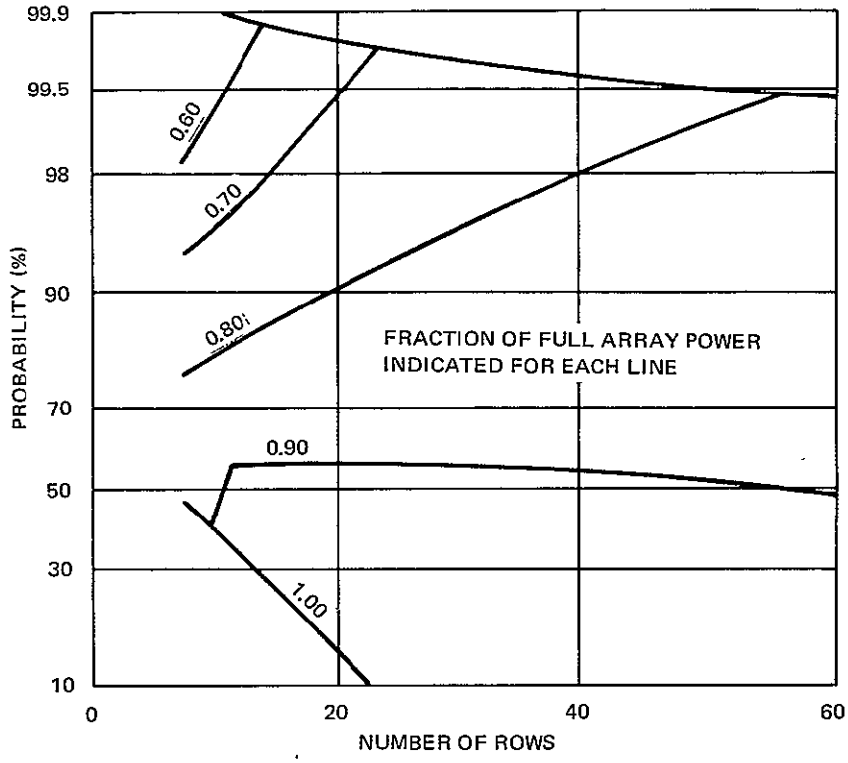

Figure 5-3. Probability of Obtaining a Given Fraction of Full Array Power vs Number of Rows for 95% Reliable Converters

70-2150

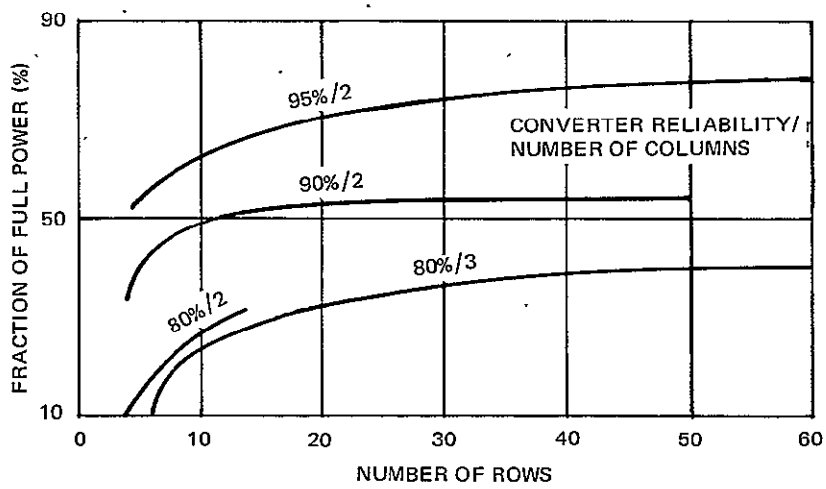

Figure 5-4. Fraction of Full Array Power Available with 98% Probability vs Number of Rows

Figure 5-3 shows that, in order to respond to the generator reliability goal of 0.98 at 5.5 years with not less than 70% of nominal power (Table 1-3), converter reliability approaching 95% is required to avoid very high redundancy. The failure statement relating to generator voltage ($V_g < 3$ v, Table 1-3) is most critical for the smallest number of rows which satisfy the generator power probability goal. Other than providing probabilistic assurance that minimum voltage requirements are observed in the array design, this analysis shows the absence of an optimum generator voltage based solely on array reliability. In general, probable generator voltage can be increased by increasing the number of series connected rows in the array. This is accomplished by decreasing module size for a given generator power, with resulting penalties in efficiency and specific power. The interaction of reliability criteria with other elements of parametric design is discussed in Section 7.

DIODE RELIABILITY DEMONSTRATION

In order to determine the reliability of a single diode over the required lifetime, life testing is necessary. Appendix D includes a discussion of the mathematics of life testing and associated confidence levels. Using the reliability equation and solving for the mean lifetime required for a specified reliability and operating life, Table 5-1 shows the test requirements to establish converter reliability for a 10.5 year mission with a 90% confidence level.

Table 5-1 shows that a relatively small number of converter life tests will be required to establish reliability if test time were accumulated over the period of a normal system development cycle. The reliability goal treated in this study is achieved by the number of tests required to indicate 90% reliability for 10.5 years (equivalent approximately to 5.5 year, 95% reliability). Over a 5-year development cycle, between approximately 50 and 100 converters will be needed to show required reliability. This number of converters will be required for generators assigned to missions requiring multihundred-watt power levels. With slight additional penalties in efficiency and specific power, test converters could be built oversize, for example, with BOL power providing 1 to 5 years decay life in excess of mission requirements. In this manner, most converters required for reliability testing will be available for incorporation in mission-assigned generators, reflecting a considerable cost reduction in the development program.

Table 5-1

TEST REQUIREMENTS FOR 10.5 YEAR CONVERTER LIFE

Reliability (%)	Mean Lifetime[1] (yr)	Test Time (yr)	Number of Failures 0	1	2
95	200	1	461	778	1065
		2	231	389	533
		5	93	156	213
		10	47	79	109
90[2]	100	1	231	390	533
		2	116	195	267
		5	47	79	109
		10	24	40	55
80	50	1	116	195	266
		2	58	98	133
		5	24	40	55
		10	12	20	28

(1) Mean lifetime calculated from reliability equation and rounded to nearest decade.

(2) Reliability of 90% after 10.5 years provides reliability approaching 95% for 5.5 year mission goal.

Section 6
PARAMETRIC AEROSHELL DESIGN

The aeroshell structure (Figure 6-1) provides an operational housing for the converter array throughout mission life. The weight and specific power of the entire generator are largely determined by intrinsic converter characteristics (module size and power) and the aeroshell structure. Electrical connections (busbars, leadthroughs, and connectors) and system integration hardware (shock mounts, mounting brackets, and attachment hardware) contribute generally small additional weight penalties. An important consideration is, therefore, optimum stacking of the converter array inside the aeroshell, which varies according to generator power and converter module selection. To facilitate this optimization, several aeroshell design constraints are assumed.

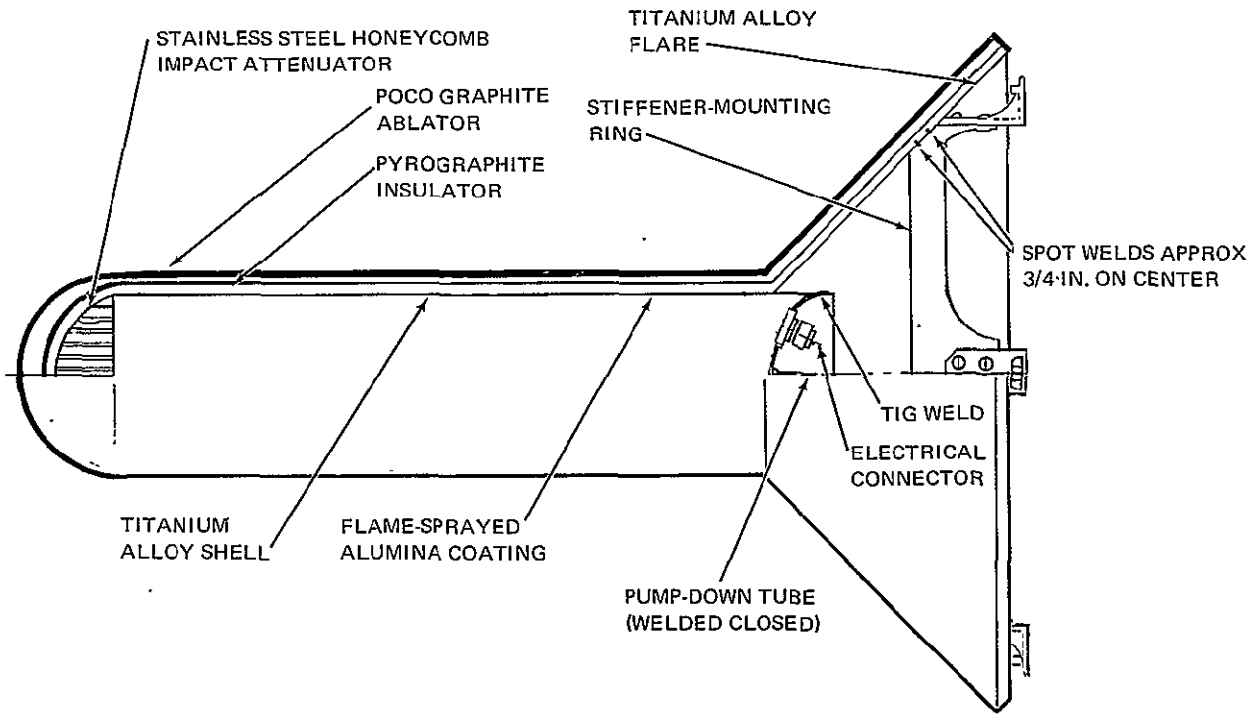

Figure 6-1. Aeroshell Structure

SHAPE SELECTION

Selection of the specific generator aeroshell geometry is governed by four principal objectives.

1. To maximize the flexibility and efficiency of the aeroshell as an operational housing for converter modules.
2. To optimize the ablative, thermal, and impact protection of the radioisotope source material within the scope of present technology.
3. To achieve an integrated generator of high specific power.
4. To minimize volume and (for some missions) cross section.

A passively stable self-orienting reentry structure in the form of a flared cylinder was selected as a representative candidate which is consistent with these goals. The Isomite cells advantageously share a common aeroshell structure, insulator, and ablator. Use of the hemispherical graphite nose allows the brunt of the aeroheating to be absorbed and re-radiated at high temperatures forward of the directly coupled converter radiator area on the sides of the cylinder. Reentry heat input to the converters is relatively low. Use of the flare aft of the cylinder ensures a passive flight orientation control, ballistic coefficient control, and high-drag surface for low aeroheating, stability, and low impact velocity. The self orienting effect aids tracking procedures to permit location of the earth impact point for recovery if desired. Prior knowledge of the orientation at impact allows an impact energy absorbing structure to be designed for minimal weight. Such a structure greatly enhances probabilities of non-rupture of the helium pressure-containing aeroshell, at the first level of containment, and non-rupture of the individual Isomite collector and emitter structure at the second and third level of containment, respectively. At the final level of safety, provided by the fuel form structure, the impact structure minimizes PuO_2 fine powder production and related potential hazards. The flared cylinder configuration is also amenable to detailed aerothermal analysis and is within the scope of present technology.

The flared cylinder is a representative configuration allowing significant flexibility in cell stacking. In the case where the number of cell columns is fixed, the total generator power and reliability can be modified by varying the number of rows without directly perturbing converter performance or operating characteristics. The axial stacking arrangement also reduces the radiation

dose rate in the preferred direction (axial) through self-shielding. The flare structure allows for mounting mechanisms and for reentry tracking/recovery aids if desired. The length/diameter ratio of the aeroshell can be increased with only a small decrease in specific power to provide a low drag, minimum cross-section configuration if these are mission requirements.

Other passive self-orienting configurations such as blunt cones and omnidirectional configurations such as high drag cubes have undergone design and safety study in DWDL IRAD programs. Spherical Isomite modules encased in common insulator and ablator cubic structure have been identified as a promising concept to achieve high specific power. An estimation of generator specific power using omnidirectional aeroshell configurations is presented in the review of advanced technology in Section 10.

AEROSHELL BALLISTIC COEFFICIENT

The aeroshell vehicle is assumed to be constrained by a fixed ballistic coefficient, selected as 30 lb/ft^2 on the basis of impact velocity, weight, and heating requirements. The impact velocity corresponding to this ballistic coefficient is just under 200 fps. Selection of the ballistic coefficient (β) involves an optimization process. An increase in β means a size and weight reduction for the flare, but an increase in ablation, insulation, and impact structure requirements. A typical weight and impact velocity analysis is presented in Appendix E.

The generator design value of β=30 lb/ft^2 is conservative for impact survival. Impact tests of simulated cylindrical Isomite converters (Reference 19) indicate that unprotected devices can survive impact on granite at velocities exceeding 200 fps. In the space mission configuration, converters are protected by the aeroshell and crushup structure which is designed to absorb a major portion of the impact energy. Furthermore, the space between cells within the aeroshell will enable the devices to absorb energy by compacting.

NUCLEAR SAFETY IN LAUNCH-PAD ABORT CONDITIONS

The combination of aeroshell structure and multicell array presents an attractive system for safety in a launch-pad abort environment. Although the aeroshell will absorb impact forces, the primary containment structure is

contributed by the emitter and collector layers. A thin platinum-rhodium layer around the fuel liner prevents high temperature oxidation and is protected against impact by the collector. A platinum alloy layer (of equal thickness) around the aeroshell is more weight efficient, but direct thermal contact with the fuel is lost. A platinum layer on the aeroshell is also more vulnerable to impact penetration. The oxidation barrier is incorporated in the converter with negligible weight penalty, because it can be used as a component of the emitter capsule.

Analysis (Reference 20) shows that typical plutonia fuel containers clad with platinum will survive the currently most-severe chemical propellant fires, provided that good thermal coupling is maintained with the fuel. This is because melting, not oxidation or thermal shock, is the prime concern. Platinum-rhodium alloys have almost negligible corrosion rates in contact with sea water, air, soil, and many other materials. The 18-mil design thickness is conservative for corrosion protection.

REENTRY, IMPACT, AND BURIAL

Design and safety requirements for the generator assumed in this analysis are presented in Table 6-1. Reentry envelope conditions extend to super-orbital reentry. Figure 6-2 shows the effect of these conditions on the type of trajectory attained. For a maximum velocity of 36,300 fps, there are two possible types of trajectories. One is the multi-elliptical orbit reentry with the body grazing the earth's atmosphere until final reentry. The second is a prompt, immediate trajectory. Above 36,300 fps, reentry at shallow angles results in a hyperbolic trajectory with no return while steep angles result in prompt reentry and a narrow corridor exists for multi-orbit reentry.

Selection of the worst-case reentry conditions depends upon the accident analysis of a given mission. For a large class of missions, abort probabilities are highest on ascent to an earth orbit and on boost to a superorbital trajectory. For aborts prior to earth orbit, the only type of trajectory is a prompt one with a maximum velocity of 26,000 fps. For integrated heating and ablation, these abort trajectories are less severe than orbital decay trajectories. Thermal stresses and mechanical erosion are considerations at improbably steep reentry angles. The survivability of graphite heat shields at these extreme conditions, while under study, has not been fully characterized.

For superorbital trajectories, the escape boost normally proceeds with a combined gradual rise in velocity and angle. The region of hyperbolic trajectories provides a potential method of complete emergency disposal. Mission control and backup contingencies can restrict credible combinations of abort reentry velocity and angle to an envelope typified by that assumed for the present generator design as shown in Figure 6-2. In lieu of specific mission constraints, selection of this envelope was necessarily somewhat arbitrary. An advantage of the present generator design is that it is easily scaleable to other envelopes. For other trajectories, added ablator and insulator weight requires drag augmentation by enlargement of the flare to maintain a constant ballistic coefficient. The attendant overall weight penalty, the major perturbation to the system, is then easily determinable.

For the reentry vehicle with a fixed ballistic coefficient, graphite ablator thickness requirements can be calculated from worst-case trajectory heating and pressure transients. Previous studies of graphite-protected radioisotope

Table 6-1
SAFETY CRITERIA AND GUIDELINES

Safety Criterion	Guideline
Fuel release	None under normal or credible accident conditions
Minimum design life	12 yr (10-yr mission)
Intact reentry	Including impact and partial earth burial
Impact at terminal velocity	Intact impact on granite
Partial earth burial maximum temperature	2500°F (1644°K)
Hydrostatic water pressure	Sufficient to limit ocean surface contamination below 10^{-2} MPC
Corrosion life	10 half-lives
Reentry velocity	36, 300 fps (max)
Reentry angles	All prompt reentry trajectories
Launch-pad explosion	10, 000 psi static overpressure 10, 000 ft-lb debris energy
Launch-pad fire	Liquid chemical propellant

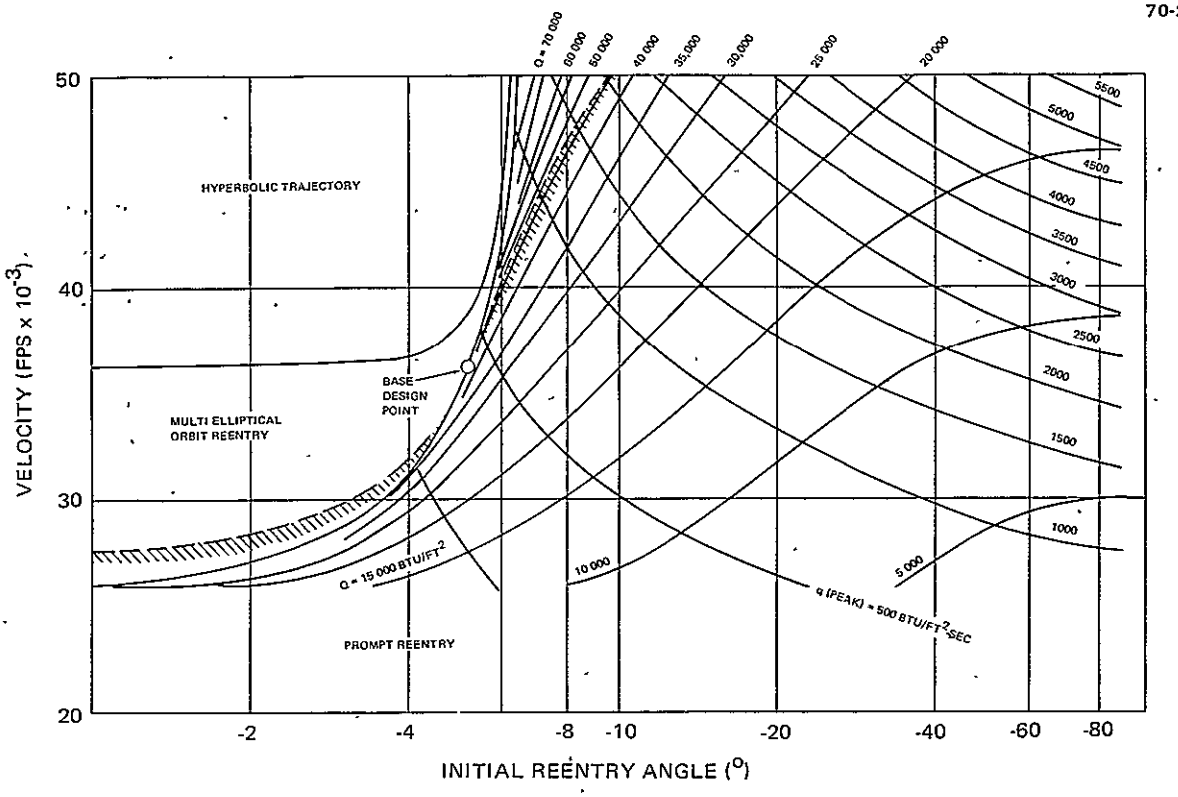

Figure 6-2. Envelope of Design Reentry Conditions (β = 30 lb/ft^2)

heaters (Reference 20) show that, at a given reentry velocity, the worst prompt trajectory for graphite ablation and internal temperatures occurs at the shallowest prompt entry angle. At 36,300 fps, this angle is -5.2° as shown in Figure 6-2 for β = 30 lb/ft^2.

The point V_o = 36,300 fps and γ = -5.2° was used to define the design worst-case trajectory and the corresponding envelope of equivalent or less severe reentry conditions in Figure 6-2. The envelope boundaries are derived considering the effects of integrated heating and peak heating (for which isovalue curves are plotted as a background grid in Figure 6-2) as well as air pressure on maximum ablation and internal temperatures. Trajectory, aeroheating, and thermal analysis of the reference generator design for this worst-case condition are presented in Section 8.

The present design reentry envelope is consistent with current superorbital reentry constraints of active radioisotope heat source programs for both small and large systems. The multi-orbital reentry domain is not included because of

the steep increase in ablator requirements which accompanies a moderately large number of grazing orbits prior to reentry and the expectation that aborts leading to these conditions will have low probability.

The flare aft of the cylinder acts to prevent complete burial of the generator on earth impact in soil. The forward cylinder also presents a moderate impact loading surface. Calculations based on experimentally derived penetration equations such as those used in Reference 21 indicate that the generator will not bury (nose first)beyond about the fifth row of cells in typical soil conditions. For partial burial,surface temperatures are maintained low enough by natural convection to prevent soil, aeroshell,and fuel melting. Surface temperature rise for the low probability case of complete burial in sand or soil is calculated in Appendix E.

The aeroshell structure is not expected to be breached on land impact because of the low impact velocity and crushup material. In the highly unlikely event that converters spill out after impact, no temperature problem exists for individual converter burial, even in low conductivity soil.

THERMAL DESIGN ASSUMPTIONS

Among the various ablator material choices, fine-grain high-density graphite appears best for generator applications within the context of present technology. POCO AXF-5Q and ATJ-S graphites have excellent thermal stress and ablation characteristics and are commercially available. POCO has been extensively tested and characterized under Transit, SNAP-19, and MDAC-W nose cone (RESEP) programs. MDAC-W has found this material to have high survival capability at heating rates considerably above those calculated for the multicell generator at steep entry angles. Physical and thermal property data are presented in Appendix E.

Thickness requirements of the POCO® ablator were derived for the generator configuration in Figure 6-1. Ablator thickness distribution around the generator is based on Newtonian flow theory for hypersonic continuum (laminar) heating.

Insulation requirements depend in large measure on the material type, heat treatment, and density of insulator selected. On the nose section, severe

heating and high temperature thermal impedance requirements dictate selection of an insulator such as heat-treated pyrographite. On the sides, reentry heating is less severe and normal operating temperature considerations are more important. A moderate impedance insulator such as aluminum oxide, reinforced pyrographite, or as-deposited pyrolytic graphite could be used. Potential insulators are compared in Appendix E.

Heat-treated (delaminated) pyrographite is the prime choice for the nose section because of its thermal conductivity advantage and its highly anisotropic characteristic which makes it a good heat conductor circumferentially. Under normal operation, waste heat will flow along the skin to the nose section and, to a lesser degree, to the flare section to increase the effective radiation area. The PG also provides backup ablation protection at moderate air pressures.

For insulation on the cylindrical sides, as-deposited pyrographite is selected. In addition to the natural thermal choking effect of the PG insulator, reentry temperatures are minimized by provision of copper "shoes" brazed to the converters and pressing on the inside of the aeroshell. Provision is made to electrically isolate converters from the shell structure with an alumina layer applied to the aeroshell. The copper provides good heat transfer during normal operation but melts on reentry to reduce thermal contact. Titanium is assumed in this analysis for the aeroshell and flare structural material because of its light weight, moderately high melting point, and good strength. Impact data also exist for titanium structures (Reference 22) which categorizes this material with 4130 steel. A titanium thickness of 0.03 in. is assumed throughout.

CONVERTER ARRAY CONFIGURATION

Converters may be arranged within the cylindrical housing in two possible stacking arrangements. One is mating the flat ends of the cylindrical cells to the inner curved surface of the housing. The second is paraxial stacking with curved surfaces of the converters parallel to the inner curved surface of the housing. It can be shown, for cylindrical converters with L/D near unity, that paraxial stacking is the optimum packing arrangement (minimum wasted space). In this analysis, paraxial stacking is assumed throughout.

For a given total generator power and a given cell size, there are various paraxial stacking arrangements. Figure 6-3 shows the internal cross-sectional area of the housing per cell for a typical converter module and selected radial groups. This curve shows that an arrangement of four or five cells around the circular cross-section of the housing results in optimum stacking. A greater number of cells around the circumference, assuming no internal cells, results in more wasted space. Conversely, a stacking of two or three cells does not result in as dense a packing as four or five cells.

A design weight analysis for spherical and cylindrical shapes (Reference 23) shows that, for a given volume, the optimum length of a cylinder to attain minimum weight occurs when $L_a/D_a = 1$. On the other hand, a preliminary pressure distribution analysis based on Newtonian flow theory, indicates an L_a/D_a close to 2 ensures aerodynamic stability. Therefore, optimum weight will occur for the reentry vehicle when converters are arranged in radial groups of 4 and 5 with enough rows to give an aeroshell L_a/D_a between 1 and 2.

70-2157

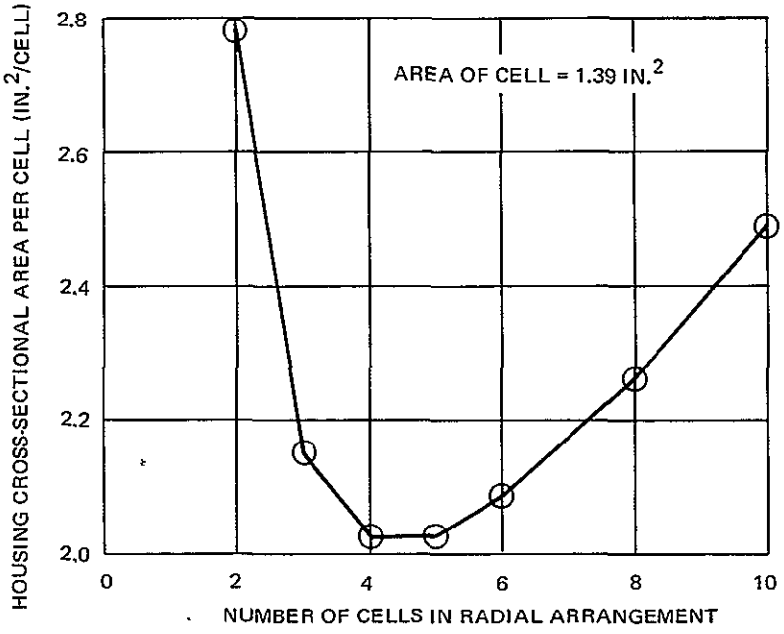

Figure 6-3. Packing Density of Circular Converters in a Cylinder

AEROSHELL DESIGN OPTIMIZATION

To explore the weight parametrics with different cell stacking options. a DWDL computer program was used to calculate the total generator weight including reentry vehicle with a constant ballistic coefficient of 30 lb/ft^2. In this program, individual cell dimensions and power are input and reflect the baseline converter design. For all practical combinations of columns around the aeroshell circumference and up to 200 w_e total power, the program solves the total system weight and resulting normal operating temperature at the graphite surface assuming radiation to space at a constant emissivity of 0.8 (Reference 24). The code starts with three columns and takes a progressive number of rows until 200 w_e is reached. The process is iterated for a greater number of columns. Detail of the iterative weight analysis are contained in Appendix E.

Trajectory and aeroheating are available from previous studies (Reference 20) to estimate ablator thickness. Table 6-2 summarizes the aeroshell component thicknesses assumed for the parametric weight analysis.

Table 6-2

ASSUMED AEROSHELL COMPONENT THICKNESS

Component	Material	Thickness (in.)
Ablator:	POCO AXF-5Q	
Nose region		0.5
Cylinder region		0.15
Flare		0.25
Insulation	Pyrographite	0.1
Aeroshell Structure	Titanium	0.030

Using the computer program, generator design and weight characteristics are determined for four module powers (1, 2.5, 5, and 7 w_e) of the baseline converter design (Table 1-1). These converters are characterized by Ta-O-Cs surfaces with 1-mil spacing, vented cylindrical emitter geometry (L/D = 1), and plutonia SSC fuel. Diameters (including 10 mils for electrical insulation), lengths (with 0.5-in. clearance for helium vent tubes), thermal powers, and converter weights are inputs to the code. All possible combinations of number

of columns (between 3 and 20) and number of rows (between 1 and 20) corresponding to generator powers up to 200 w_e are calculated. Some combinations result in generator L/D ratios less than unity which are considered unacceptable for reentry vehicle design for reasons previously discussed.

Acceptable converter combinations are typically shown for the 5-w_e module size in Table 6-3. Corresponding generator powers, radiation surface temperatures, and specific powers are delineated. Similar matrices were generated for other cell sizes of interest.

The resulting specific powers for the various combinations are plotted against total generator power in Figure 6-4 for all module powers. Solid curves are drawn through the maximum specific power attainable at any given generator power level. Spacing of the data bands illustrates a monotonic increase in specific power with module power, the rate of gain diminishing in the range 5 to 7 w_e power.

This analysis neglects a basic requirement to provide sufficient radiator area and allow radiator temperatures consistent with optimum collector temperatures and a temperature differential across the layered structure of the aeroshell. Temperature and area matching of the aeroshell/converter array assembly is discussed in Section 8.

Component thickness in Table 6-2 are chosen to provide safety margin in the parametric analysis. Definition of a specific generator configuration as described in Section 8 permits refinement of the aeroheating analysis and leads to a more precise assessment of aeroshell weight. A detailed thermal description and weight analysis of the 100-w_e generator is contained in Section 8 and related Appendix F.

Table 6-3

MATRIX OF GENERATOR CHARACTERISTICS FOR ALL ACCEPTABLE COMBINATIONS USING 5 W_e ISOMITE CELLS

NUMBER OF COLUMNS (N)

NUMBER OF ROWS (M)	3	4	5	6	7	8	9	10
					L/D < 1			
2	30 3.82 703							
3	45 3.95 719	60 4.06 749	75 4.12 768	90 4.15 780	105 4.17 788	120 4.18 794		
4	60 4.01 727	80 4.13 759	100 4.19 779	120 4.22 793	140 4.24 802	160 4.25 808	180 4.26 813	200 4.26 816
5	75 4.05 732	100 4.17 765	125 4.23 786	150 4.27 801	175 4.29 811	200 4.30 818		
6	90 4.08 736	120 4.19 769	150 4.26 791	180 4.29 806			MAXIMUM SPECIFIC POWER	
7	105 4.10 739	140 4.21 772	175 4.28 794					
8	120 4.11 741	160 4.23 775	200 4.29 797			GENERATOR POWER > 200 W_e		
9	135 4.12 742	180 4 24 777						
10	150 4.13 743	200 4.25 778						
11	165 4.14 745			LEGEND: FIRST NO. IN BOX = GENERATOR POWER (W_e) SECOND NO. IN BOX = SPECIFIC POWER (W_e/LB) LAST NO. IN BOX = TEMPERATURE (^oK)				
12	180 4.15 745							
13	195 4.15 746							

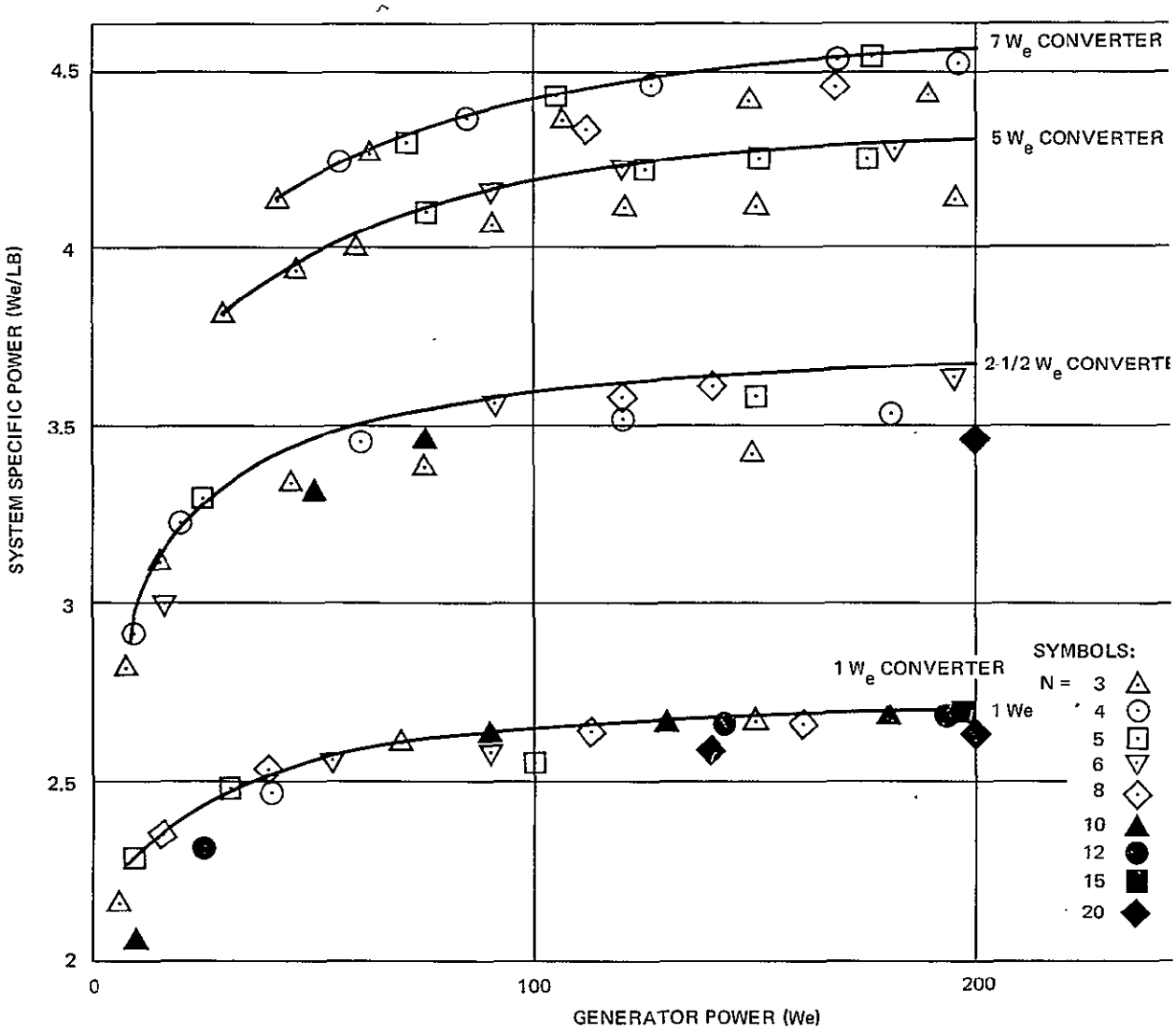

Figure 6-4. Isomite Array and Reentry System Specific Power vs Total Generator Power for Selected Cell Powers

Section 7
PARAMETRIC GENERATOR CHARACTERIZATION

Using the parametric information developed in the preceding sections, generators with nominal output power of 50, 100, and 200 w_e are characterized, reflecting component choices and system requirements which are summarized in Table 7-1. Two additional assumptions are made.

1. All converters except failed modules are designed to operate at peak efficiency and do not drift off-optimum during operation.
2. Converter short-circuit failure propensity is four times the open-circuit failure rate.

RELIABILITY CONSTRAINTS

Figure 5-4 can be used to determine the excess power requirement (redundancy) to achieve the generator reliability goal because the assumed converter reliability of 90% at 10.5 years is approximately equivalent to 95% reliability at 5.5 years. As an example, considering 20 converters (10 rows, 2 columns), Figure 5-4 shows a 98% probability of achieving 66% or more of full array power. For a nominal 100-w_e generator, failure is defined by an output less than 70 w_e at 5.5 years. The design redundancy required at 5.5 years, therefore, is $[(0.7 \times 100)/0.66 = 106]$ w_e with no failures. Redundancy requirements for other arrays are obtained similarly. As stated in Section 5, with converters having higher short-circuit than open-circuit failure propensity, 3-column arrays are inferior to 2-column arrays and hence are not considered in this study.

The design redundancy calculated for a nominal 100 w_e generator is plotted in Figure 7-1 against number of converters (2 x number of rows). Similar curves are obtained for other power levels by ratioing. Figure 7-2 shows the required individual module power vs number of converters, obtained by dividing the redundant array power (Figure 7-1) by the number of converters. The range of module power interest is shown in Figure 7-2 between 1 and 6 w_e. The lower value is shown in Section 4 to be associated with rapidly

Table 7-1

COMPONENT CHOICE AND SYSTEM REQUIREMENTS FOR PARAMETRIC GENERATOR CHARACTERIZATION

Component or Requirement	Description
Fuel Form	PuO_2 :- Solid Solution Cermet, BOL thermal power density 3.2 w_t/cm^3, density 10.5 g/cm^3
Fuel Capsule	Vented cylinder, L/D = 1
Electrode System	Emitter and collector Ta-O-Cs, all surfaces active, 1-mil spacing
Weight of converter structure	2.15 g/cm^2 based on thin shell emitter and collector with total 50 mil thickness
Converter reliability	90% at end of 10 year mission (10.5 years after BOL)
Generator shelf life	0.5 year
Generator reliability	0.98 at BOL + 5.5 years (including shelf life). No single failure catastrophic
Generator failure statement	(1) Power <70% (nominal BOL + 5.5 year) rated power. (2) Voltage <3 v.
Aeroshell geometry	Flared-cylinder.
Ablator choice and thickness	POCO graphite; 0.5 in. on nose; 0.15 in. on cylinder, 0.25 in. on flare.
Insulation choice and thickness	Pyrographite, 0.1 in.
Aeroshell structure	Titanium, 0.030 in. thick.

70-2159

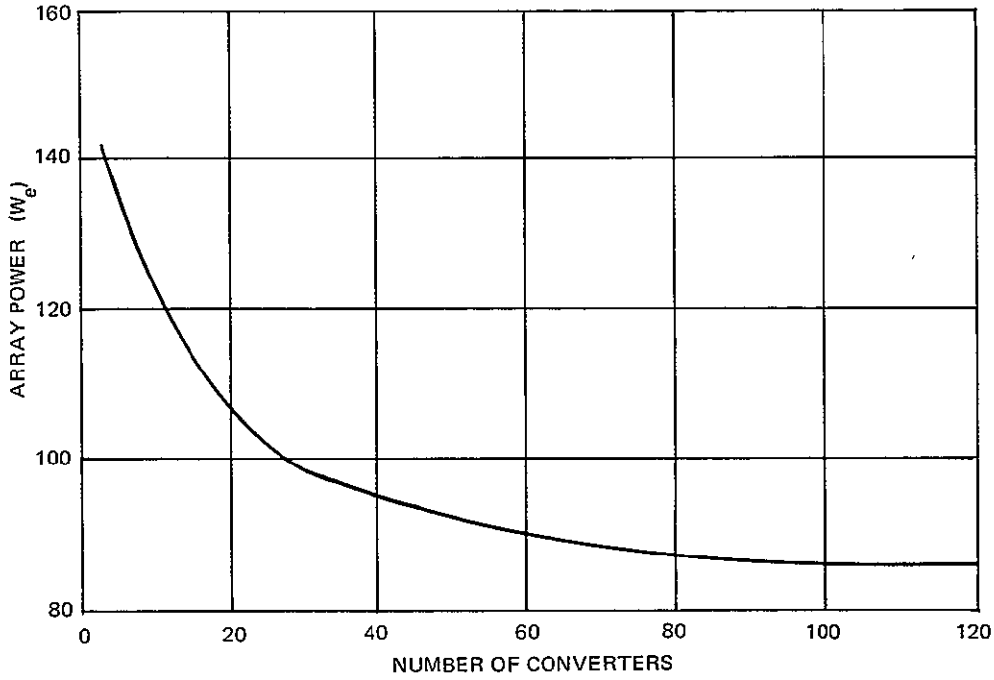

Figure 7-1. Full Array Power vs Number of Converters in 2-Column Array

70-2160

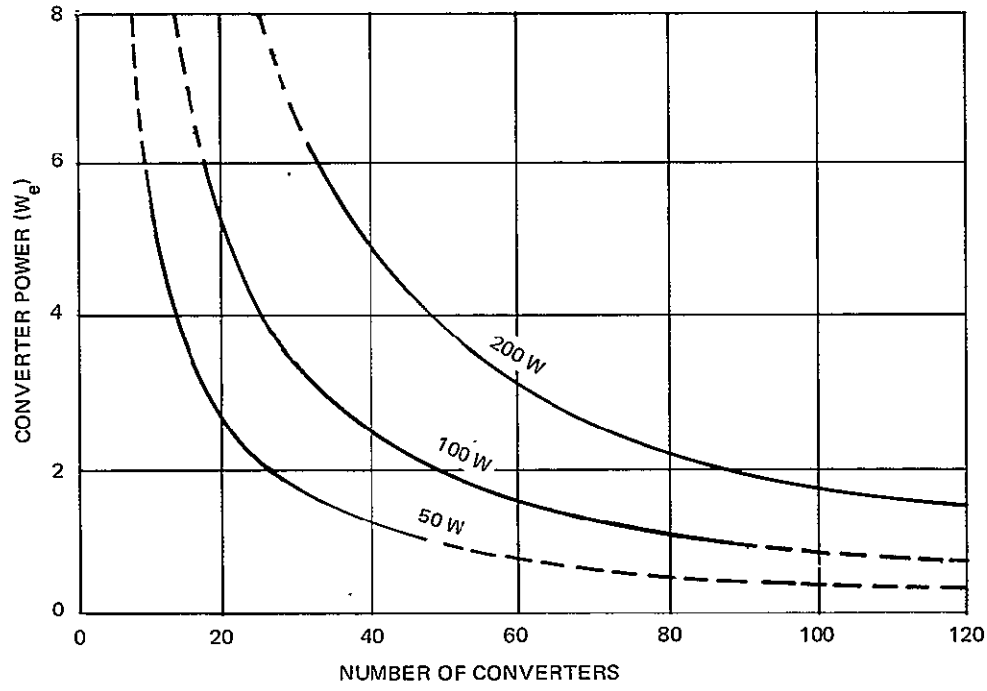

Figure 7-2. Converter Power vs Number of Converters

decreasing efficiency. The upper power value shown in Section 6 is the point at which aeroshell specific power is becoming insensitive to converter module power.

The failure statement for minimum generator voltage (3 v at 5.5 years) is a requirement which places further restriction on the number of design alternates. Figure 7-3 shows the fraction of full-array voltage (derived from reliability information in Figure 5-4) achieved with 98% probability as a function of the number of rows in a 2-column array. Individual converter voltage and efficiency are shown in Figure 7-4 as functions of converter power in the range 1 to 6 w_e using data from Section 2. Figure 7-5 plots the 98% probable generator voltage as a function of number of converters derived from Figures 7-3 and 7-4. The 3-v minimum is satisfied for all options except the nominal 50 w_e generator case with less than 20 converters.

FUEL THERMAL INVENTORY AND WEIGHT

The thermal power required at 5.5 years is calculated by considering the redundant array power and converter efficiency. BOL thermal inventory is larger by a factor of 1.045, representing the 5.5 year decay of the plutonia fuel. The results are plotted in Figures 7-6, 7-7, and 7-8 for nominal 50, 100, and 200 w_e generators, respectively. Each shows a minimum in the BOL thermal source as a result of the interaction between a declining array redundancy requirement and simultaneous decrease in converter efficiency as the number of modules increases.

Parametric generator weights may be derived by interpolation from Figure 6-4 where specific power is shown as a function of generator power with converter power as a parameter. Generator weight is plotted in Figure 7-6, 7-7, and 7-8 for each respective generator power. Generator weight rises with increasing number of converters for all cases.

With the source and weight trends opposed, there is no well-defined optimum design. However, an upper boundary on the number of converters may be placed at the minimum of the heat source curve.

The combined influence of converter characteristics, fuel thermal power density, generator reliability goal and aeroshell stacking established a range of interest for the number of converter modules which permit acceptable

70-2161

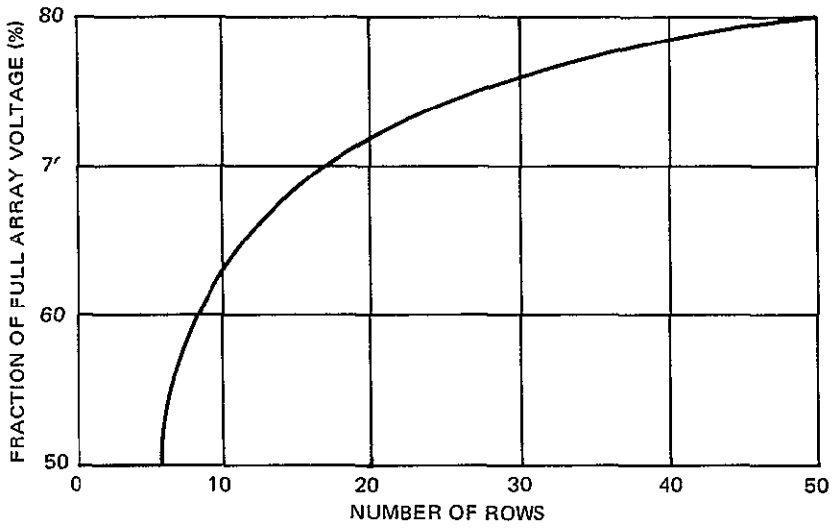

Figure 7-3. Percent of Full Array Voltage Available with 98% Probability

70-2162

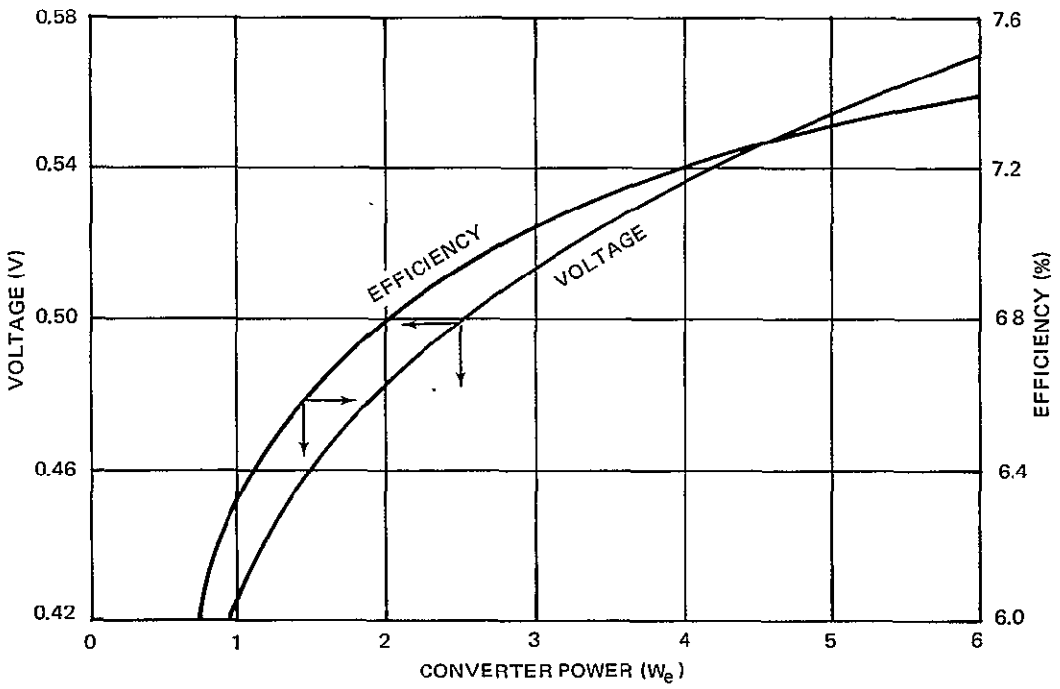

Figure 7-4. Converter Voltage and Efficiency vs Power

70-2163

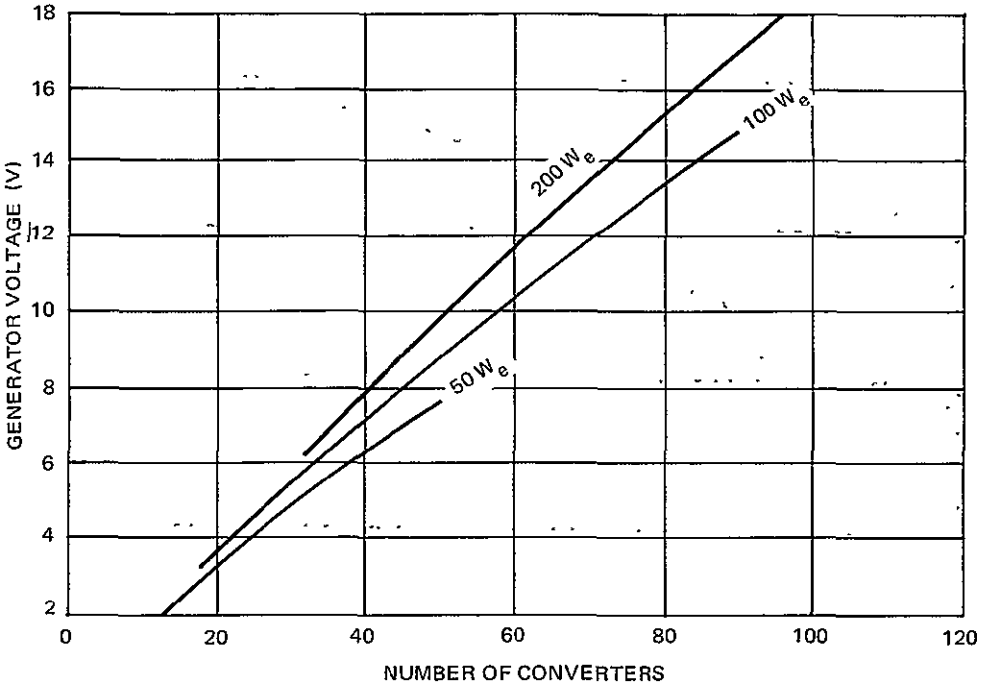

Figure 7-5. 98% Probable Generator Voltage as a Function of Number of Converters in Generator

70-2164

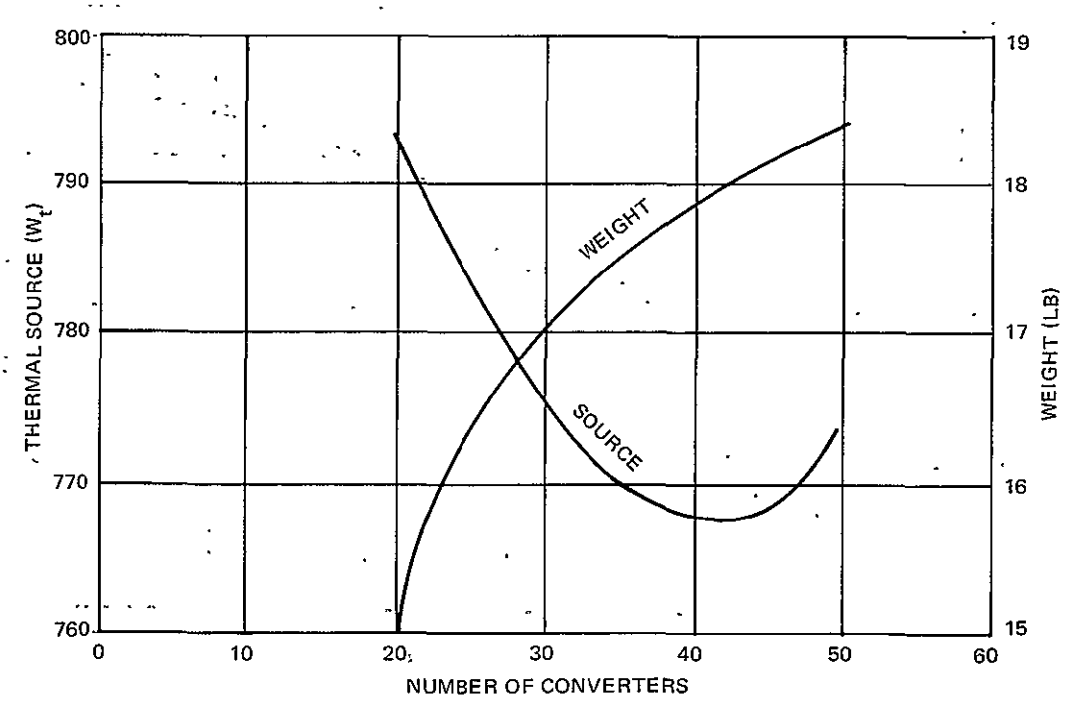

Figure 7-6. Thermal Source and Weight for 50-Watt Generator

70-2165

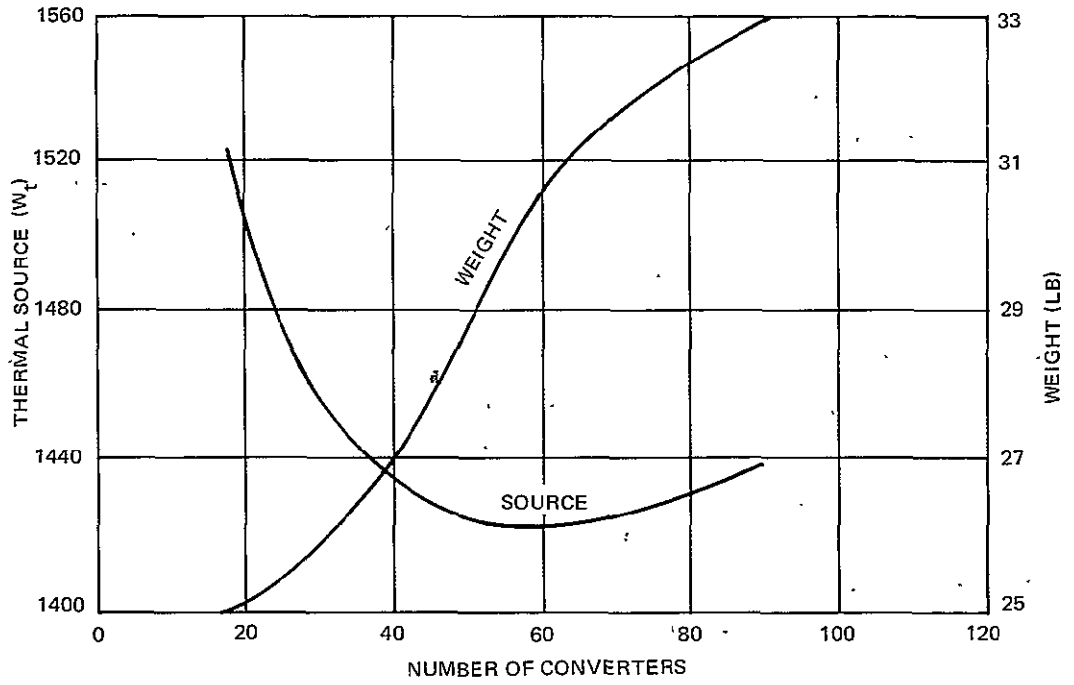

Figure 7-7. Thermal Source and Weight for 100-Watt Generator

70-2166

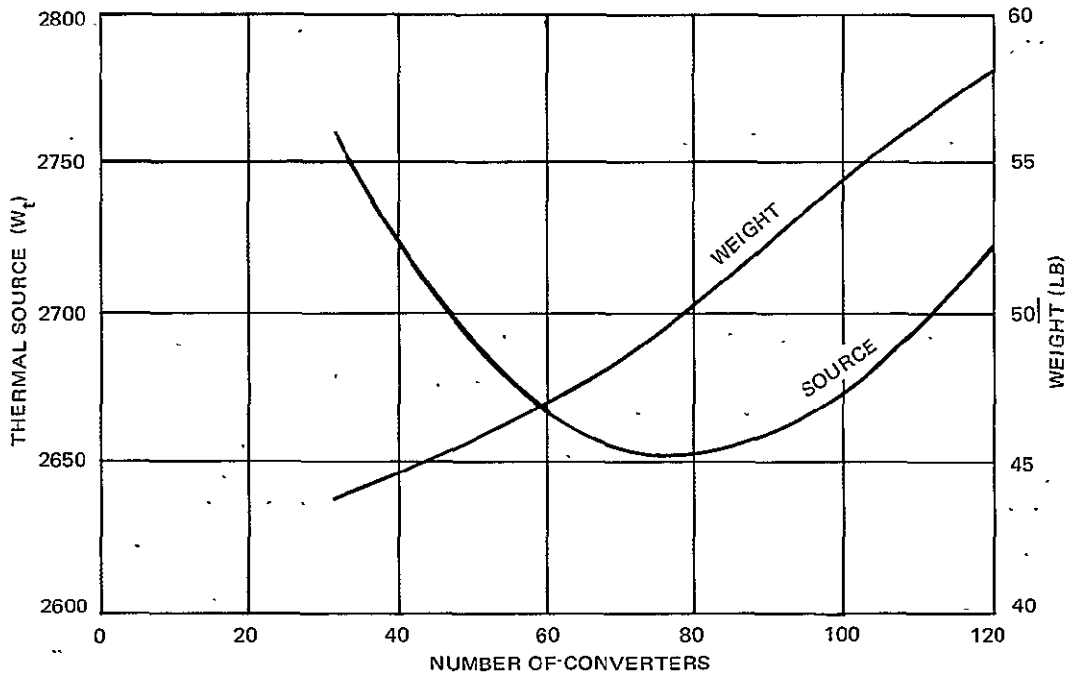

Figure 7-8. Thermal Source and Weight for 200-Watt Generator

generator designs. Table 7-2 summarizes the design range at each generator power level.

Table 7-3 lists pertinent data for several potential designs at each generator power level. An optimum choice cannot be readily made from these options based on parametric data alone. This problem is discussed in Section 8. However, gross characterization in terms of common converter use, efficiency, and specific power can be identified.

Table 7-4 summarizes the range of module power, efficiency, and specific power derived from Table 7-3 for each nominal generator power level.

In general terms, this parametric analysis shows that current technology thermionic multicell space power generators in the 50 to 200 w_e power range theoretically achieves specific power between 2.78 and 4.5 w_e/lb and efficiencies from 6.46% to 7.34% depending on converter size, generator power, and the assumed reliability goal. Minimum voltage requirements at the 50-w_e generator level preclude the use of 3 to 4 w_e modules. Lower module power, proportionately higher redundancy, and a less suitable aeroshell structure result in lower efficiency and specific power for the nominal 50 w_e generator. The nominally 200-w_e generator designs offer little improvement in efficiency and specific power over 100-w_e generator options. A convenient basic generator module size appears, therefore, to lie within this power range. Several design options for 100 and 200 w_e generators use a common module size between 3 and 4 w_e. Thus, a common "building-block" approach to generator design is suggested for the multihundred watt power range.

Table 7-2
MODULE POWER RANGE PROVIDING ACCEPTABLE GENERATOR DESIGN[1]

Generator Power (w_e)	Minimum Number of Modules	Maximum Number[2] of Modules
50	20[3]	40
100	18[4]	60
200	32[4]	80

(1) Two-column array
(2) Established at minimum BOL source power
(3) Minimum voltage constraint
(4) Maximum converter size constraint

Table 7-3

GENERATOR PARAMETER DESIGN SUMMARY

Nominal Generator Power (w_e)	Number of Converters	Array Power (w_e)[1]	Module Power (w_e)	Module Efficiency (%)	Generator Voltage (v)[2]	Thermal Source BOL (w_t)	Generator Weight (lb)
50	20	53.0	2.65	6.98	3.18	793	15.0
	30	49.5	1.65	6.70	4.80	772	17.0
	40	47.5	1.19	6.46	6.36	768	18.0
100	20	106	5.30	7.34	3.53	1508	24.9
	30	99	3.30	7.10	5.34	1456	25.9
	40	95	2.38	6.90	7.14	1438	27.0
	50	92	1.84	6.75	8.84	1424	29.4
	60	90	1.50	6.61	10.49	1422	30.6
200	40	190	4.75	7.29	7.92	2722	44.5
	50	184	3.68	7.16	9.86	2684	45.7
	60	180	3.00	7.04	11.73	2671	47.6
	70	177	2.53	6.94	12.56	2664	48.3
	80	174	2.18	6.85	15.23	2653	50.4

(1) Array power with no failed elements to provide 70% of nominal power with 98% probability after 5.5 years, using elements 90% reliable after 10.5 years.

(2) Generator voltage achieved with 98% probability.

Table 7-4

MODULE POWER, EFFICIENCY, AND SPECIFIC POWER RANGE

Nominal Generator Power (w_e)	Module Power Range (w_e)	Efficiency Range (%)	Specific[1] Power Range (w_e/lb)
50	1.19 - 2.65	6.46 - 6.98	2.78 - 3.34
100	1.50 - 5.30	6.61 - 7.34	3.26 - 4.02
200	2.18 - 4.75	6.85 - 7.29	3.96 - 4.50

(1) Calculated by nominal generator power/generator weight

Section 8

DETAILED GENERATOR DESIGN

The parametric generator design options discussed in Section 7 provide a basis for analysis of optimum generator configurations at each power level. In this section, a detailed design is presented for a 100-w_e generator based on constraints listed in Table 7-1. In addition to the assumptions which govern the parametric study of previous sections, the detailed generator design involves:

1. A detailed reliability analysis
2. Refined aeroheating calculations for ablator and insulator sizing.
3. A tradeoff between aeroshell structure weight, converter weight, and efficiency penalties to achieve adequate radiator area.
4. Consideration of system integration component configuration and weight.

RELIABILITY ANALYSIS

From previous parametric designs, the range of interest for the number of converters in the nominal 100 w_e is between 18 and 60. In this range, generator weight increases monotonically with the number of converters (Figure 7-7). Because a near-minimum weight generator is desirable, the detailed investigated is further restricted to between 20 and 32 converters. The design is based on 90% converter reliability at 10.5 years (10 year mission plus 0.5 years shelf life) which implies a converter mean life of 99.7 years. With this mean life, the calculated reliability for an individual converter at 5.5 years becomes 94.63%. The previous assumptions of a 2-column series/parallel connected array and a short-circuit/open-circuit failure ratio of 4:1 are retained.

Probabilistic output calculations are summarized in Table 8-1 for electrical arrays of 2-columns and 10 to 16 rows (20 to 32 converters) using a converter reliability of 94.63%. The tabulated results represent a 6000-case analysis by the Monte Carlo code described in Section 5. Table 8-1 shows the

Table 8-1

SUMMARY OF ARRAY RELIABILITY CALCULATIONS

Probable Power (%)	Reliability at 5.5 years (Number of Converters)						
	20	22	24	26	28	30	32
75	91.4	90.3	91.3	95.0	93.7	93.9	94.9
74	91.4	90.3	9.13	95.0	93.7	93.9	94.9
73	92.5	93.0	96.3	95.1	94.7	95.8	97.2
72	92.5	93.0	96.3	95.1	94.7	95.8	97.2
71	92.5	93.0	96.4	95.8	96.4	97.7	97.2
70	94.4	97.2	96.4	95.8	96.4	97.8	97.6
69	94.4	97.2	96.9	97.3	98.2	97.8	97.6
68	94.4	97.2	96.9	97.3	98.3	98.2	98.8
67	97.9	97.2	96.9	97.3	98.3	98.2	98.8
66	97.9	97.7	97.8	98.7	98.6	98.9	99.2
65	97.9	97.7	97.8	98.7	98.6	98.9	99.2
64	97.9	97.7	97.8	98.7	98.6	98.9	99.2
63	98.2	98.4	98.9	99.0	99.2	99.3	99.2
62	98.2	98.4	98.9	99.0	99.2	99.3	99.2
61	98.2	98.4	99.1	99.4	99.4	99.4	99.6

probability of achieving any percentage of full array power for each number of converters.

At the 98% probability level, (shown by boxed numbers in Table 8-1) the percentage of full array power which can be achieved is shown in Figure 8-1. The erratic appearance of the results is almost completely attributable to the discrete nature of the failures; for example, in the 2 x 10 array there is no combination of failures which will lead to 66%, 65%, or 64% of full array power.

Statistical fluctuations can be almost completely eliminated as a cause. The 6000 histories were accumulated in two runs, one of 2000 and one of 4000 cases. The differences between the results for each set are not sufficient to change the 98% probable power fraction.

Using the results shown in Figure 8-1, the required full array power and derived converter power at 5.5 years are plotted in Figure 8-2 as functions of number of converters.

70-2167

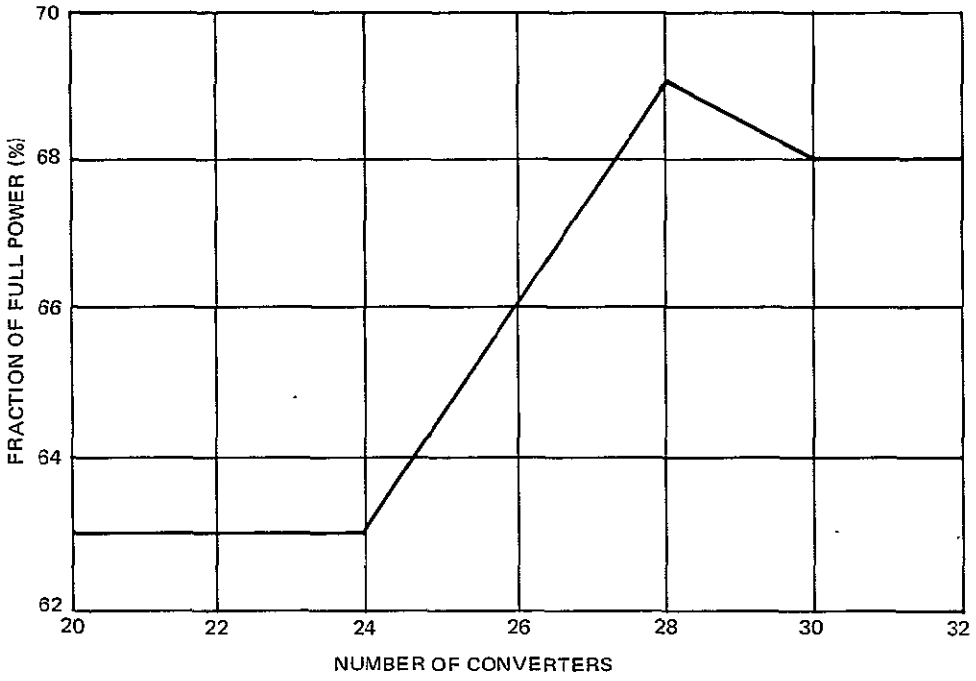

Figure 8-1. Fraction of Full Power Available with 98% Probability vs Number of Converters

70-2168

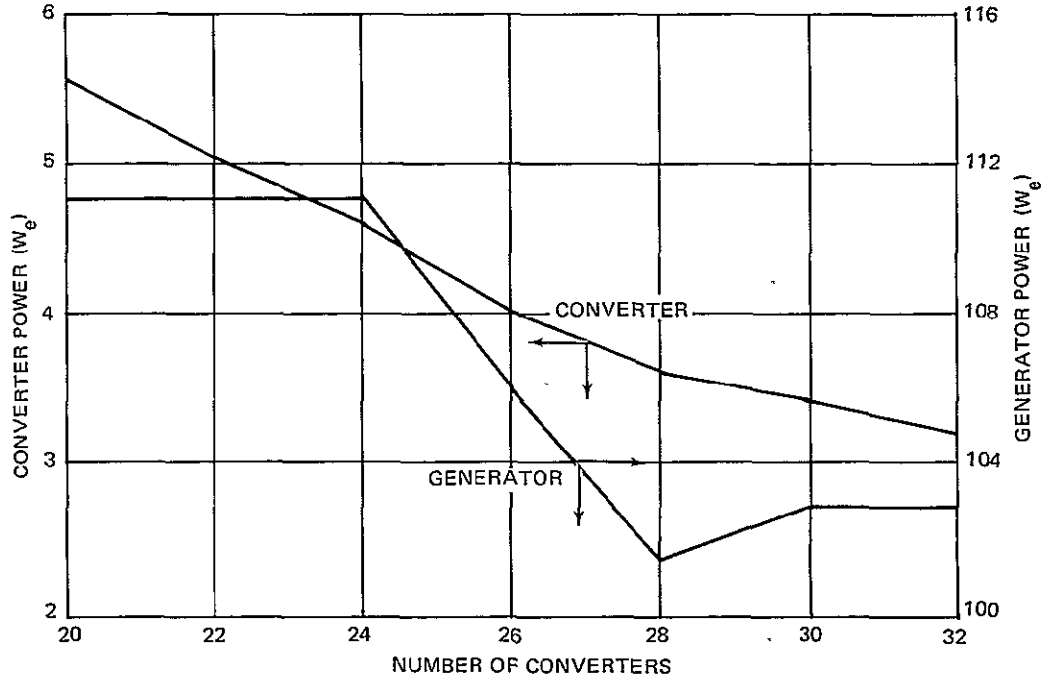

Figure 8-2. Generator and Converter Power for Various Numbers of Converters

REFINED AEROTHERMAL ANALYSIS

An aerothermal analysis was performed for a flared cylinder with a ballistic coefficient of 30 lb/ft^2 to derive required graphite ablator and insulation thicknesses and normal operating and worst-case reentry temperature. An oblate rotating earth atmosphere model for a free-moving point mass was used to simulate reentry trajectory characteristics. A computer program was used to solve the equations of motion and compute the aerodynamic heat rate, stagnation point air pressure, and enthalpy. Results for a worst-case trajectory (entry velocity = 36, 300 fps, entry angle at 400, 000 ft = -5.2°) are plotted against time in Figure 8-3. The heating rate is the actual (radius corrected) cold-wall heat rate to the center of the hemispherical nose (stagnation point).

These parameter transients were input to a graphite ablation code which solves for the time behavior of the oxidation and sublimation rates. The total ablation rate at the stagnation point is shown in Figure 8-4 together with the oxidation rate. Areas under these curves are total amounts of ablation (per unit surface area). Dividing by the graphite density yields the total depth of graphite ablated.

These results indicate that 0.24 in. are removed from the front face for the assumed worst-case trajectory. Evaluation of current-technology analytical methods and confidence levels (Reference 25) indicates that a safety factor on the order of 1.5 is well advised to absolutely ensure a conservative design. Consequently, a design thickness of 0.35 in. at the nose point was selected.

Ablation distributions around the generator are dependent on the pressure and aeroheating distributions. Modified Newtonian theory can be used for locations on the nose within about 60 degrees of the stagnation point. Calculated graphite ablation distributions are summarized in Table 8-2 and discussed further in Appendix F.

70-2169

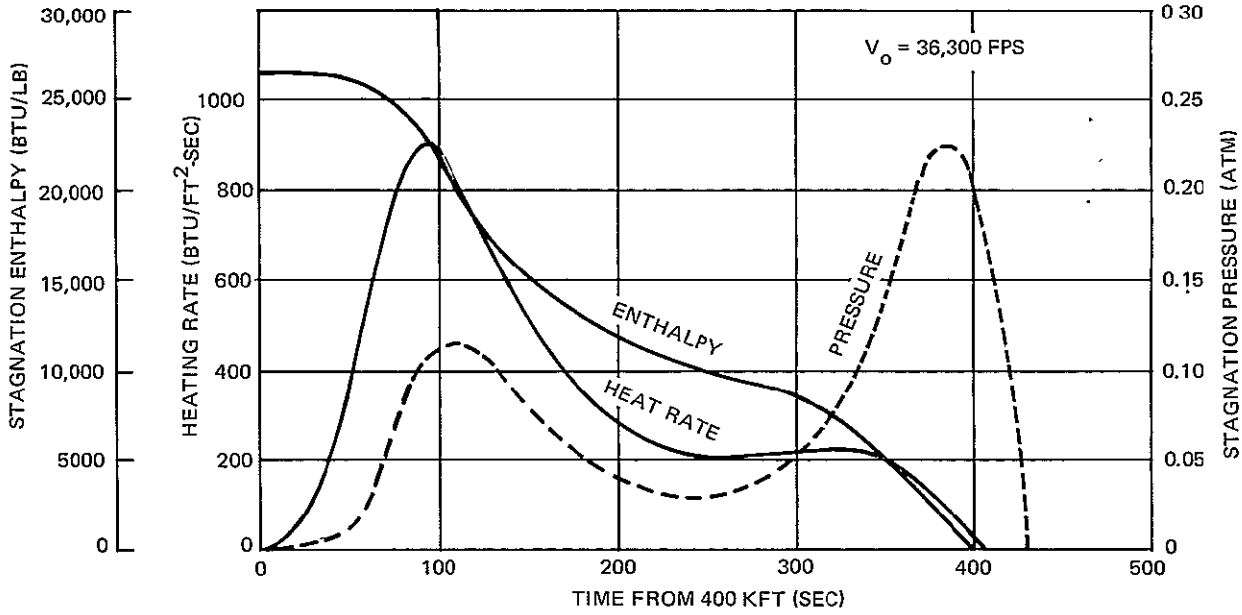

Figure 8-3. Stagnation Point Reentry Parameters for -5.2° Superorbital Return

70-2170

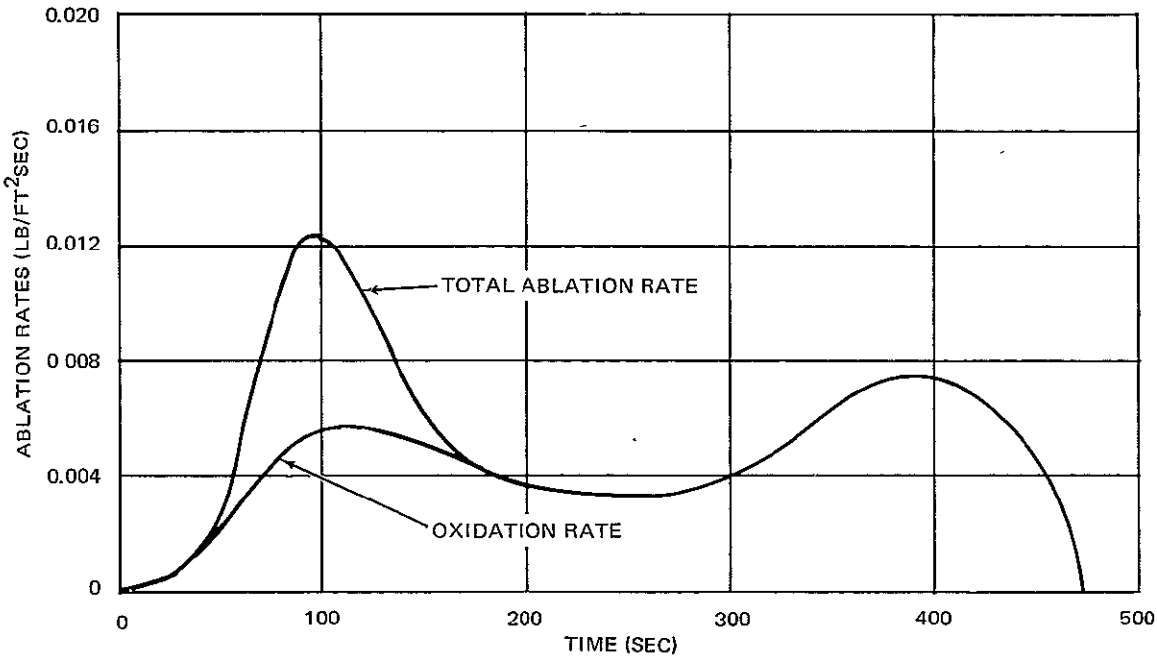

Figure 8-4. Total Ablation Rate at Stagnation Point

Table 8-2

POCO GRAPHITE ABLATION RESULTS

Ray Angle (°)	Depth Sublimated (in.)	Depth Oxidized (in.)	Total (in.)	Safety Factor	Design Thickness (in.)
0	0.04	0.20	0.24	1.45	0.35
30	0.03	0.17	0.20	1.45	0.29
45	0.01	0.14	0.15	1.45	0.22
60	0	0.10	0.10	1.5	0.15
90	0	0.04	0.04	2.25	0.10
sides	0	0.04	0.04	2.25	0.10
flare	0	0.10	0.10	1.5	0.15

For ray angles approaching $\pi/2$ and on the cylindrical region, analytical methods are not as well established. As a result, a larger safety factor is introduced.

Aeroheating at locations away from the stagnation point for a hemispherical-ended cylinder may be determined from literature sources for hemispheres and end-on cylinders (Reference 26). Figure 8-5 shows the heating distribution, normalized to the stagnation point, around the nose and along the axial length of the sides (Reference 26). Oxidation and sublimation depth estimates are based on this aeroheating distribution.

REENTRY TEMPERATURES

To determine generator temperatures during a worst-case reentry trajectory, the thermal model depicted in Figure 8-6 was used. This is a one-dimensional radial-heat-transfer model with uniform surface heating, heat conduction through the heat shield and aeroshell layers, and radiation across the gap to the fuel capsule. Four nodes represent the fuel capsule (including emitter) and one node represents the lumped capacitance of collector, copper shoes, alumina electrical insulation, and aeroshell (on a per-module basis). Two nodes each are used for the insulator and ablator, where the outermost node is a zero capacitance node which receives aeroheating, radiates to space, and conducts inward. The insulator thickness shown in Figure 8-6 is 0.15 in., determined on the basis of these heat transfer calculations and represents an increase over that assumed for the parametric

70-2171

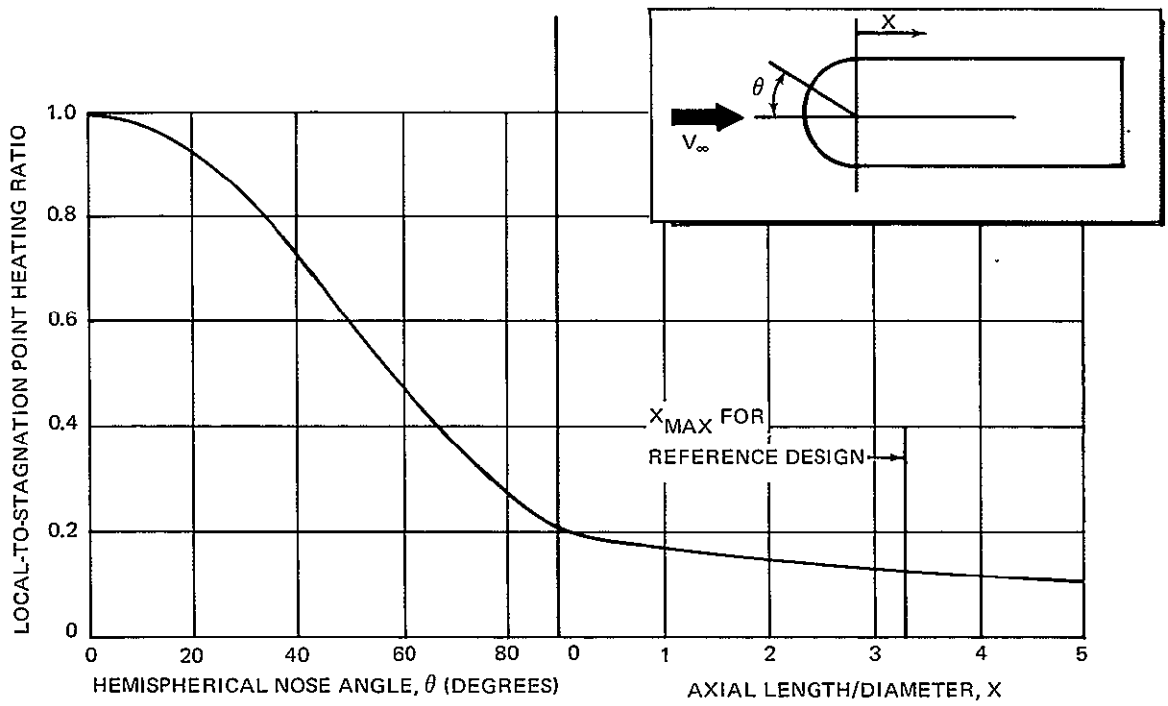

Figure 8-5. Heating Ratios Around Hemispherical-Ended Cylinders at Zero Angle of Attack

70-2172

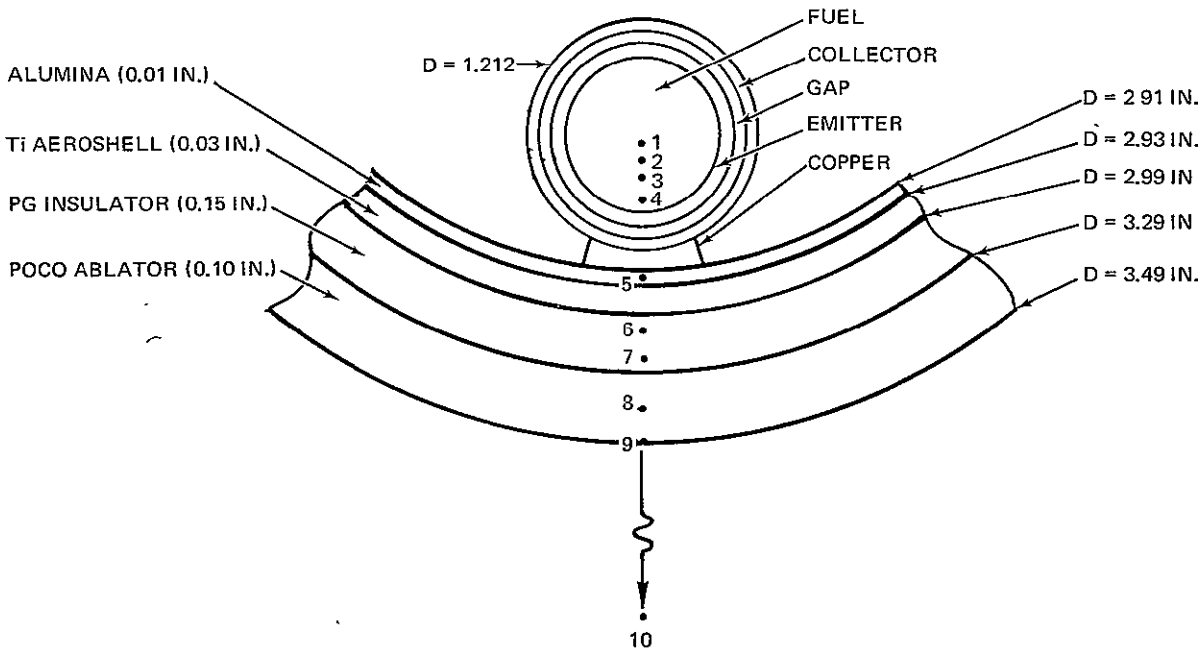

Figure 8-6. Heat Transfer Node Model for Single Converter

analysis in Section 6. A heat transfer computer program is utilized to solve the finite difference equations at discrete time steps.

The surface heating is taken to be 16% of the stagnation point heat rate. This is the approximate average heat rate on the cylindrical sides according to Figure 8-3. Second-order heating corrections such as the hot-wall correction factor, oxidation heating, and transpiration cooling of the carbon monoxide are not included.

Most material properties were held constant in the analysis. An exception is the thermal conductivity of the pyrographite insulation which decreases rapidly with temperature (a tabular interpolation routine was used). An average effective emissivity of 0.08 for the emitter gap was assumed based on known heat transfer characteristics of the emitter/collector surfaces.

Results for a -5.2° trajectory at 36,300 fps entry velocity (design condition) are shown in Figure 8-7. Ablator surface, collector, and emitter temperatures are shown as a function of time to impact. These results are very conservative because the benefit of melting the copper shoes is not considered. Copper will melt at about 1350°K (after 110 seconds) reducing the heat transfer from the aeroshell to the collector. Thus, after about 110 seconds, the collector temperature will separate from the aeroshell temperature and level off at about 1370°K. The emitter temperature will increase at a slower rate than shown and will probably remain below 1400°K. Fuel temperatures will follow the emitter temperature.

A principal result of the refined aerothermal analysis is the reduction of ablator thickness over the whole aeroshell structure compared with thicknesses assumed previously in the parametric study. This gain is partially compensated by the increased insulator thickness required. However, a net reduction in aeroshell structure weight is indicated by the detailed aerothermal calculations.

Maximum helium pressures released from the fuel can be estimated from reentry temperature history (Appendix F). Considering the ultimate stress limits of leading high temperature titanium alloys, it is evident that the aeroshell must be vented for operation at 1370°K under reentry heating conditions. Therefore, the reference design is provided with a rupture diaphragm (built into the aeroshell pump downtube) designed to release helium at pressures below those which impair aeroshell integrity.

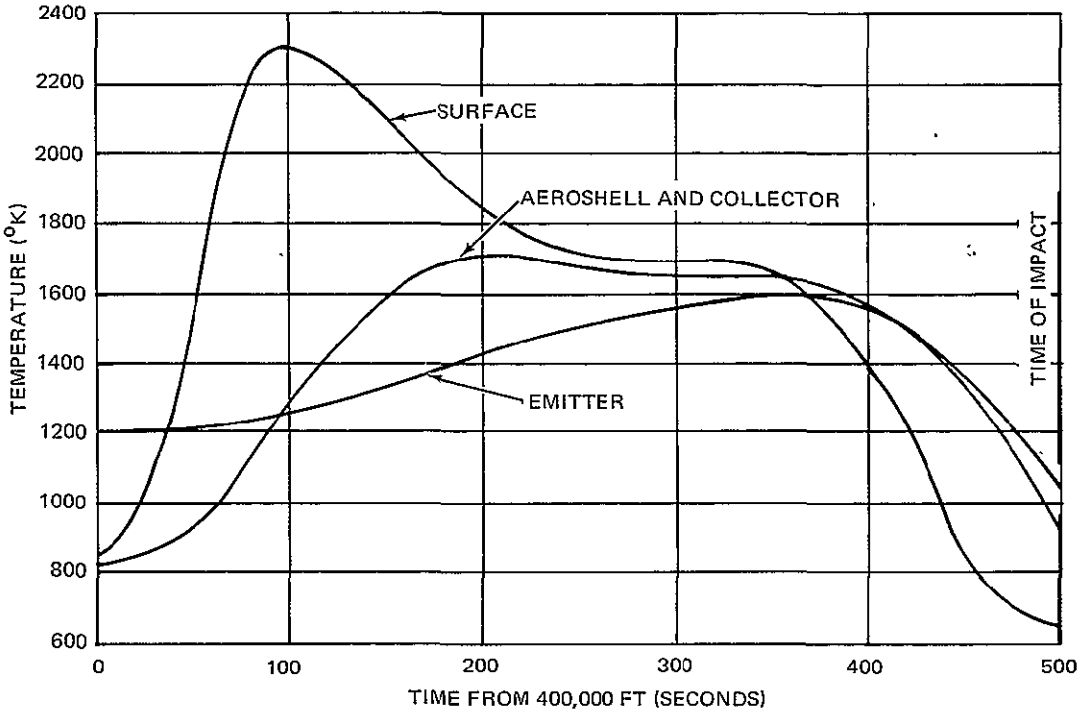

Figure 8-7. Worst-Case Reentry Temperatures (Perfect Aeroshell/Collector Contact)

This provision is considered, however, as an emergency contingency necessitated by the present accuracy of current techniques for predicting the amount of helium release from the fuel. Best available analysis to date (Reference 20) indicates that, at most, 5 percent of the helium will be released at 1370°K in 300 seconds, the approximate time span at temperature. On this basis, the helium pressure will be only 5% of that considered, and no venting should occur.

COLLECTOR TEMPERATURE INFLUENCE

The 5-parameter code described in Section 2 was used to determine sub-optimum converter designs as a function of collector temperature. These calculations provide converter efficiency, diameter, weight, and voltage as a function of temperature for each module power level. A typical set of results, for the 20-converter configuration, is shown in Figure 8-8. The irregularities visible at 780°K are attributable to incomplete convergence of the optimization technique and have essentially no effect on the generator optimization. Sub-optimum converter characteristics for several array options reflecting the influence of T_c, are used to establish an optimum generator configuration.

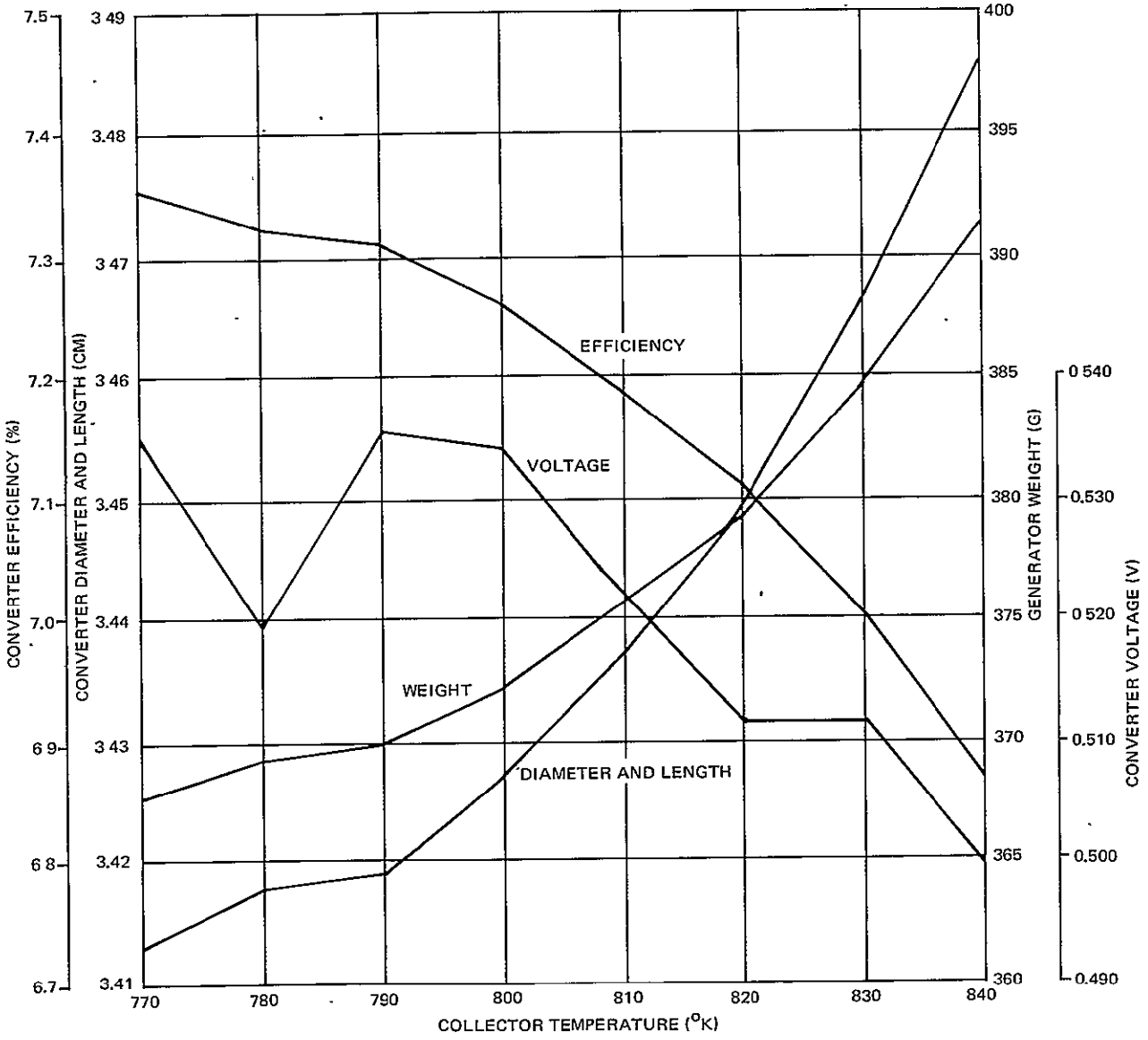

Figure 8-8. Converter Parameters as a Function of Collector Temperature for the 20-Module Generator

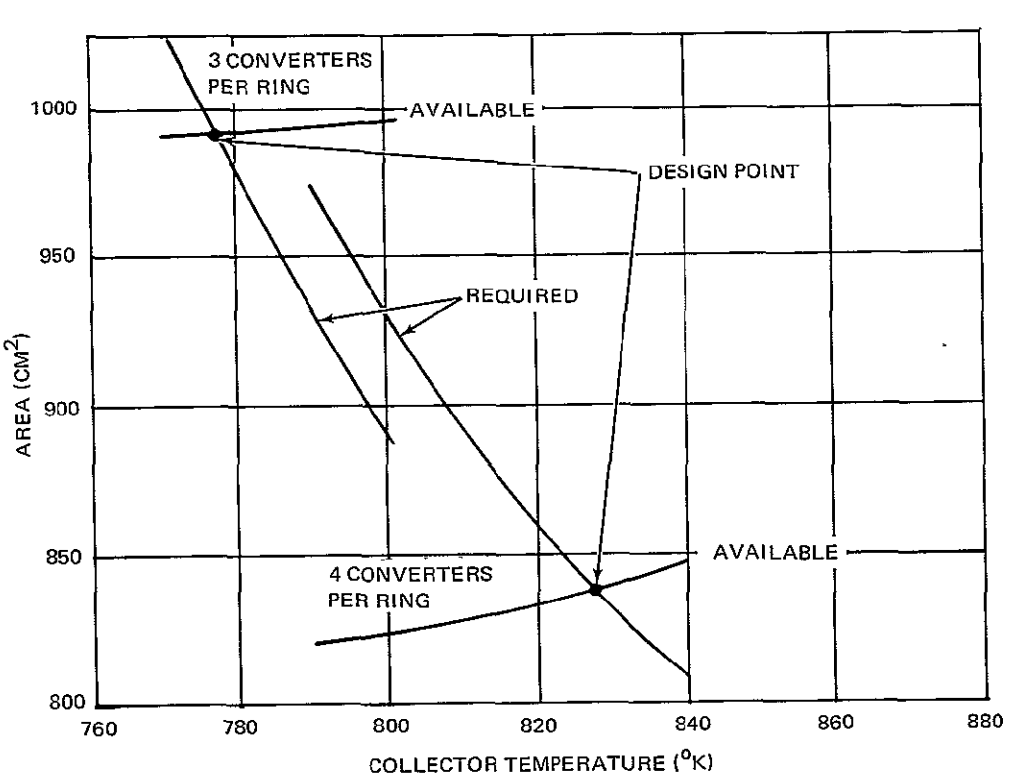

Figure 8-9. Required and Available Radiator Areas for 20-Converter Generators

GENERATOR CONFIGURATION

For each number of converters there are at least two, and usually more, ways in which the cells may be stacked in the flared-cylinder aeroshell while meeting the requirement that the shell aspect ratio be greater than unity. For each stacking arrangement and each collector temperature, aeroshell dimensions and weight are obtained using the detailed aerothermal analysis with specific allowance for changing converter size. The amount of heat to be radiated to space is obtained from converter power and efficiency.

The temperature drop through the aeroshell insulator can be calculated from the conductivity and area of the pyrographite layer. For these calculations, temperature-independent conductivity of 0.83 Btu/hr-ft-F was assumed for the pyrographite (0.15-in. thick) and 35.2 Btu/hr-ft-F for the 0.10-in. thick POCO graphite ablator. With the radiator temperature established, the area required to radiate the waste heat to space is calculated assuming an emissivity of 0.8 and compared with the actual radiator area. For purposes of this study, the effective radiator area is assumed to include the nose hemisphere but not the flare. A radiation

sink temperature of zero is used; the error is less than 0.1% for actual sink temperatures less than about 330°K. Typical results are shown in Figure 8-9 for a 20-converter array with both 3 and 4 converters per ring. In this case, the collector temperature must be greater than about 827°K for the 4 x 5 stacking and about 777°K for the 3 x 7 layout. For each one, the minimum allowable temperature is greater than the temperature for peak efficiency, so the minimum allowable temperature is chosen as the tentative design point. Converter parameters at this temperature were obtained from linear interpolation.

This method was incorporated in a simple computer code. For any number of converters the code starts with a 3-converter row configuration and, for each collector temperature, calculates the required and available radiator areas. The minimum acceptable temperature is chosen as the design point unless it is lower than the optimum collector temperature, in which case, the latter is used. Generator weight is then calculated including an appropriate flare. The code iteratively examines configurations with more converters per row until a configuration which has a cylindrical aspect ratio of less than 1.25 results, at which point the code terminates.

A summary of the results for the 100-W_e generator using this code is included in Table 8-3. The generator weight and thermal source required are plotted against the number of converters in Figures 8-10 and 8-11. The smooth curves shown in parametric designs (Section 7) have been replaced by quite irregular plots. The irregularities have two sources.

1. The required generator power does not change smoothly because of the discreteness of failures.
2. The specific power changes depending on whether a particular stacking arrangement has many open spaces (with 4 converters per ring, 7 rings are needed for either 26 or 28 converters, adversely affecting the generator weight with 26 converters).

Figures 8-10 and 8-11 show that a minimum occurs in both weight and thermal source with 28 converters. For larger numbers of converters, the thermal source requirement drops to still lower values, but the weight increases rapidly. The minimum source is achieved with a stacking arrangement of 3 cells per row, but this arrangement is only marginally better than 4 modules per row which is significantly lighter. Using 4 cells per row

Table 8-3

WEIGHT AND THERMAL SOURCE CALCULATIONS (100-W_e GENERATOR)

No. of Diodes	Generator Power (w_e)	Cell Power (w_e)	No. per Row	No. of Rows	Generator Weight (lb)	Source at BOL (w_t)
20	111.111	5.5556	3	7	23.39	1579
			4	5	23.51	1633
			5	4	24.33	1709
22	111.111	5.0505	3	8	23.98	1587
			4	6	23.70	1600
			5	5	23.85	1615
24	111.111	4.6296	3	8	24.16	1596
			4	6	24.12	1628
			5	5	24.35	1650
26	106.061	4.0293	3	9	23.90	1536
			4	7	23.60	1541
			5	6	23.65	1544
28	101.449	3.6248	3(1)	10	23.69	1483
			4(2)	7(2)	23.05(2)	1490(2)
			5	6	23.14	1497
30	102.941	3.4314	3(1)	10	24.09	1510
			4	8	23.80	1510
			5	6	23.74	1538
			6	5	23.92	1557
32	102.941	3.2169	3(1)	11	24.65	1520
			4(1)	8	24.00	1520
			5	7	24.06	1521
			6	6	24.12	1526

(1) Converters operate at optimum collector temperature.

(2) Optimum design option for minimum generator weight and near-minimum BOL thermal inventory.

70-2176

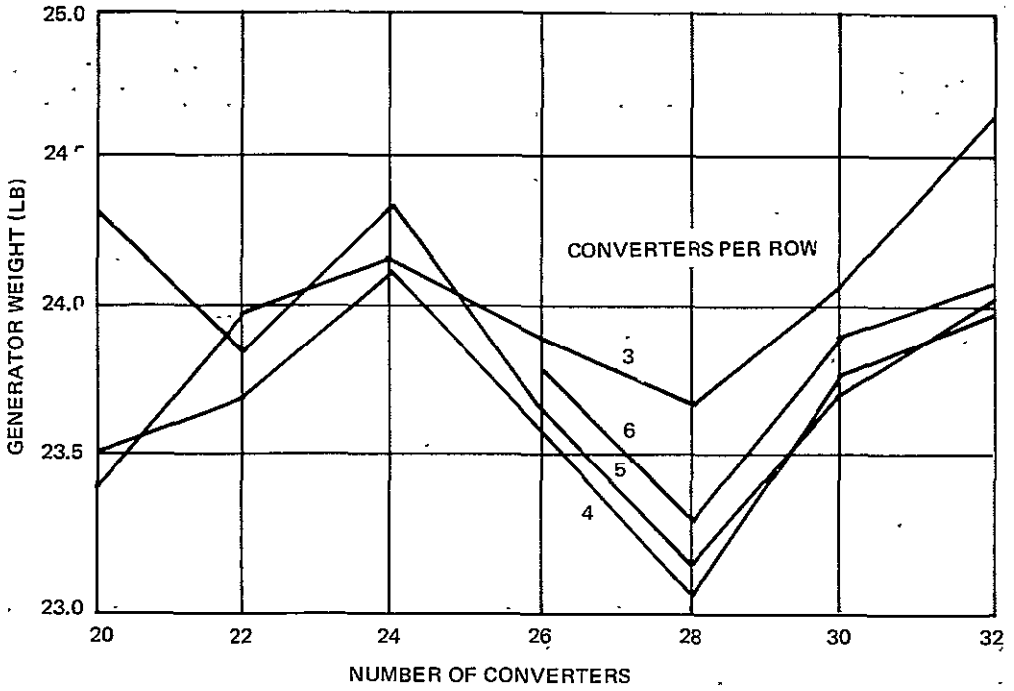

Figure 8-10. Generator Weight vs Number of Converters for 100-W_e Generators

70-2177

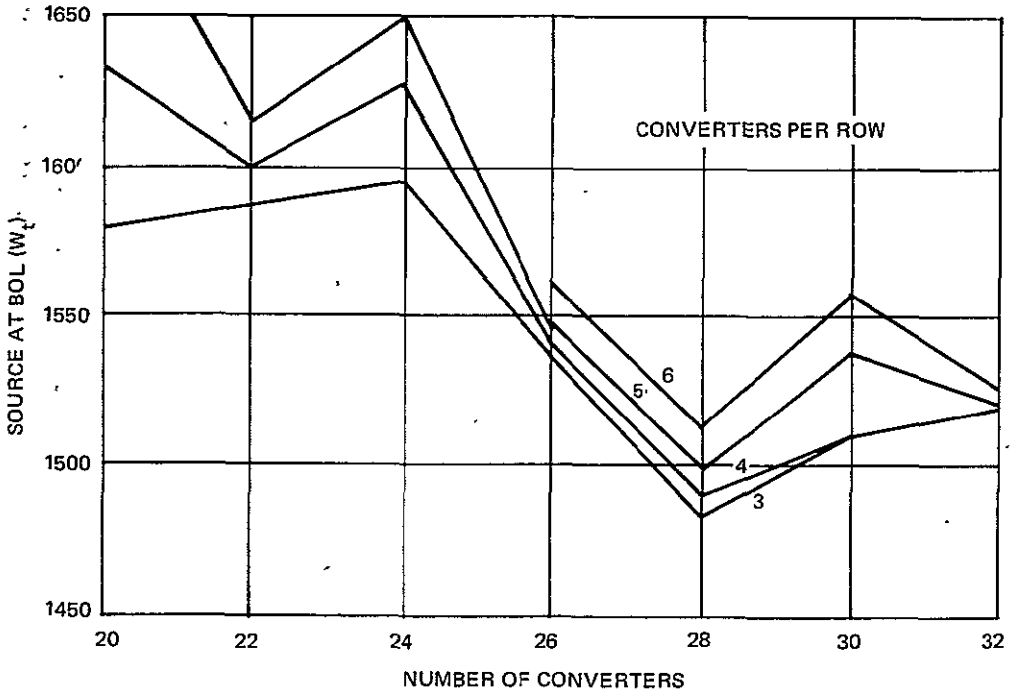

Figure 8-11. Thermal Source at BOL vs Number of Converters for 100-W_e Generator

has two additional advantages: it permits a very simple and light electrical interconnection layout within the generator, and, by having the current flow in both directions, allows for a minimal external magnetic field.

SYSTEM INTEGRATION OF AEROSHELL ASSEMBLY

Mechanical and electrical integration components are required to attach the aeroshell assembly to the space vehicle, provide reentry separation, and bring the electrical output to convenient terminals. Figure 8-12 shows a typical method for mounting the generator on the vehicle structure. Table 8-4 summarizes the mounting component weights required, for example, to isolate a 50-lb aeroshell structure from vehicle-imposed shock and vibration conditions of 100 g for 0.5 ms and 20 g from 0 to 2000 Hz, respectively.

Electrical connection losses decrease with increasing generator voltage. Figures 8-13 and 8-14 show parametric characteristics of the electrical leads, assuming OFHC (oxygen-free high-conductivity) copper for the lead material. OFHC copper is chosen for its high efficiency, low vapor pressure, and high ductility. High ductility minimizes interconverter mechanical load transmission resulting from thermal expansion and launch loading effects. Lead optimization may be expressed in terms of overall generator specific power and voltage. Details of the analytical method are discussed in Appendix F.

Figure 8-13 shows minimum weight connector sizing data for a nominal generator specific power of 4 w_e/lb. Except for the parallel interconnects (Figure D-1), the cross-sectional area of all electrical connectors is established by current flow, independent of connector length.

Figure 8-14 shows connector power loss and weight characteristics as a function of generator output voltage, per foot of effective connector length. The effective connector length may be determined approximately by summing

1. Main bus lengths
2. One-half of collector bus lengths
3. Total length of series interconnects in one column

The collector bus carries, on the average, one-half the generator current. Because current divides proportionally among the columns in the generator, series interconnector weight is proportional to generator power output and

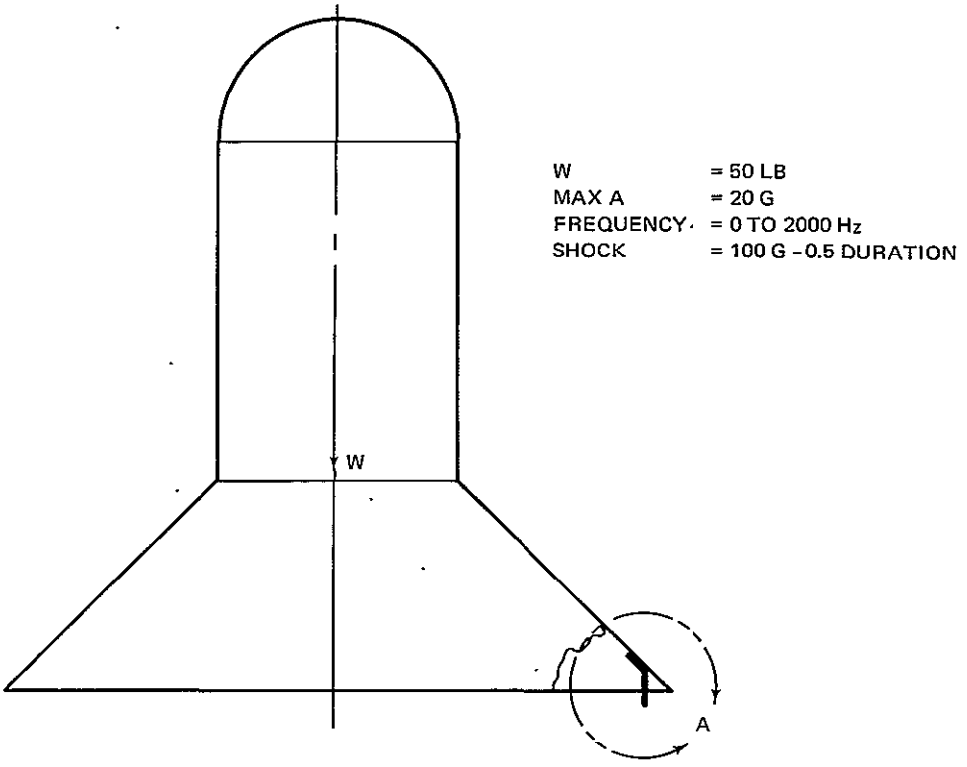

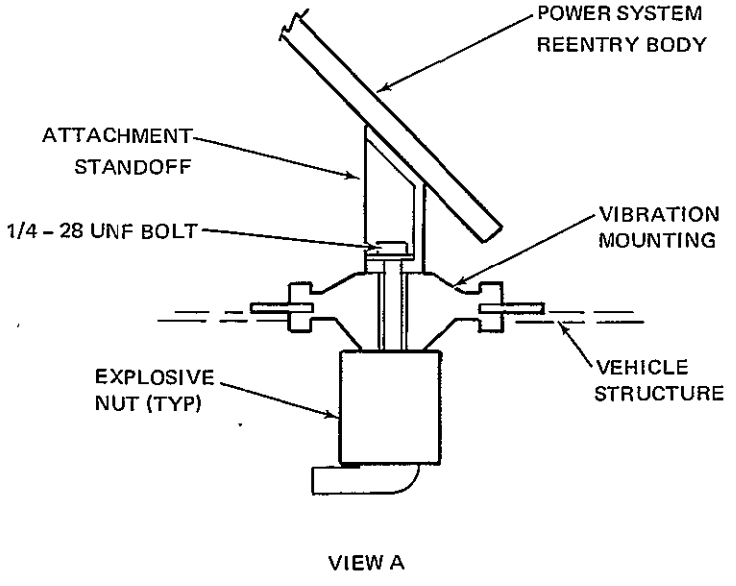

Figure 8-12. Vibration Mount for Multicell Generator

Table 8-4

MOUNTING AND SEPARATION SYSTEM WEIGHTS

Component	Source	Quantity	Unit Weight (lb)	Total Weight (lb)
Attachment Standoff	(1)	4	0.15	0.60
Vibration Mounting	(2)	4	0.31	1.24
Explosive Nut	(3)	4	0.30	1.20
Mounting Bolts	(4)	4	0.04	0.16
Total Weight				3.20

(1) Standard forged aluminum fitting
(2) Standard HT series mounting, Lord Mfg. Co.
(3) Space Ordnance Systems
(4) Standard 12-pt high strength 1/4-28 UNF bolt

70-1144

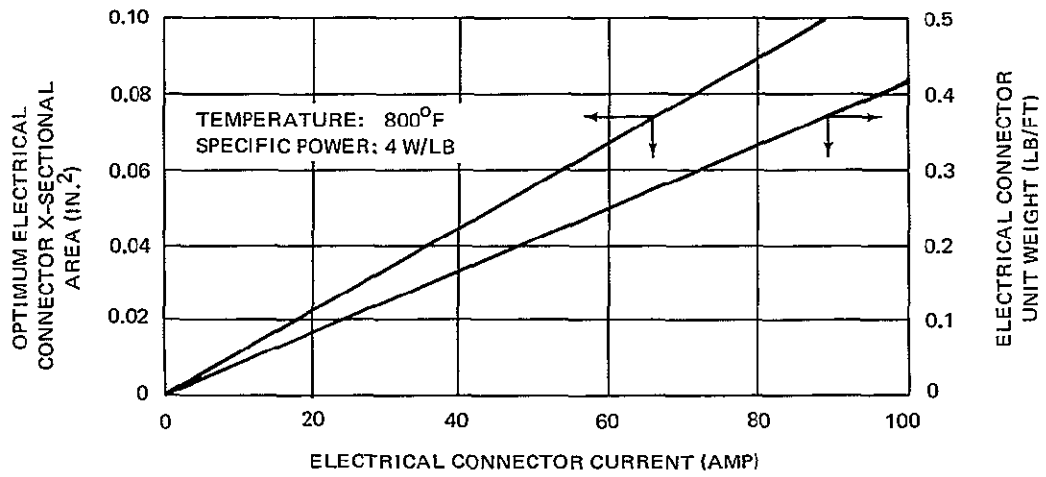

Figure 8-13. Connector Sizing

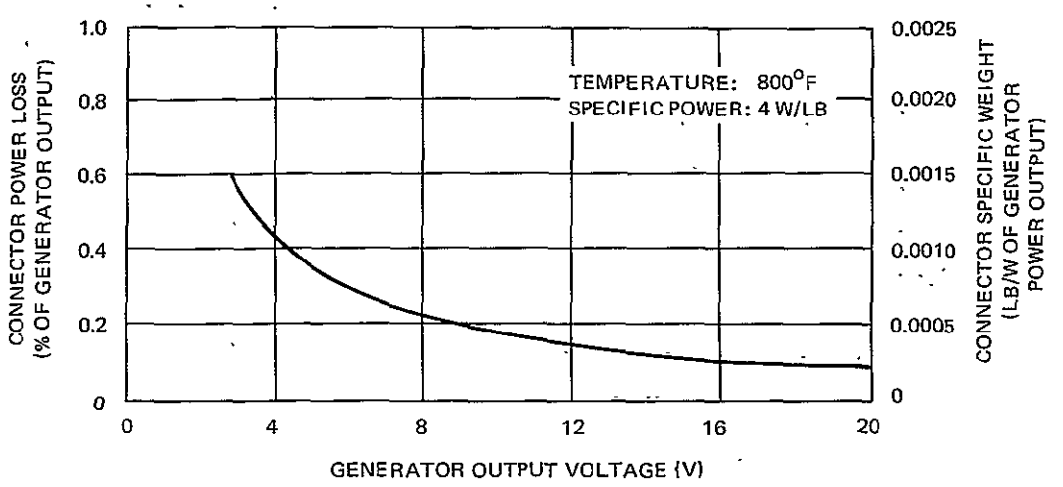

Figure 8-14. Connector Characteristics Per Foot of Effective Length

current but is essentially independent of the number of columns in the generator. The multicell generator configuration is compact, and therefore, the main bus connecting the generator to the power converter can be expected to contribute the predominant weight and power losses which are, in any case, small and typically less than 1% of generator weight and power output, respectively.

DETAILED 100 w_e GENERATOR DESIGN

The optimum design of a 100 w_e multicell generator, reflecting all constraints described previously, is shown in Figure 8-15 and incorporates 28 converters arranged in the reentry vehicle as a 4-column, 7-row array. Electrically, the converters are connected as a 2-column, 14-row array to meet reliability criteria. Figure 8-15 shows major dimensions and component descriptions of converters, aeroshell, and system integration structure.

The basic structure of the aeroshell is a pressure vessel made of titanium alloy. Thermal insulation is provided by a layer of pyrographite 0.150 in thick on the cylinder, 0.100 in. thick on the flare cone, and a maximum of

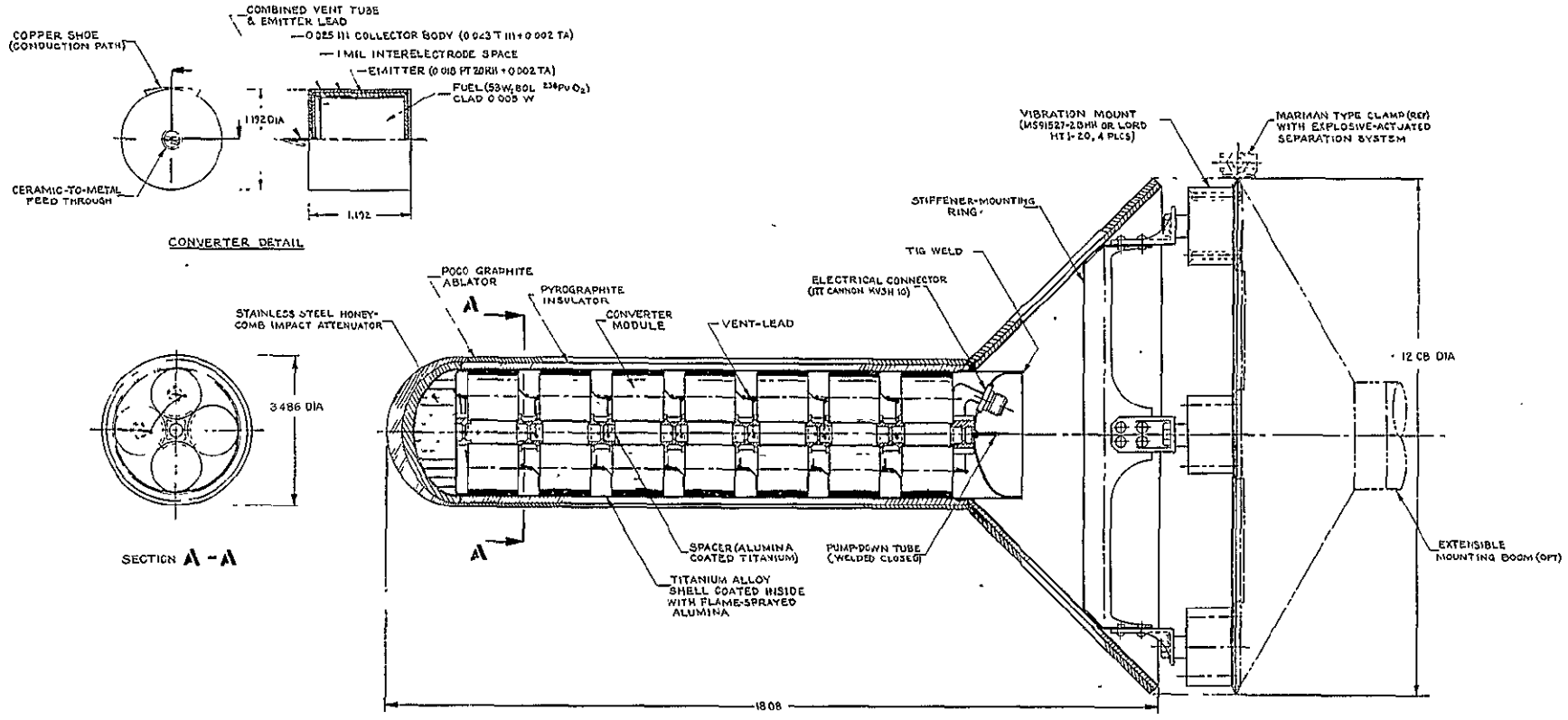

Figure 8-15. 100-Watt Multicell Generator

0. 250 in. thick on the nose of the vehicle. A POCO graphite ablator is applied to the outer surface of the pyrographite to a thickness of 0. 100 in. on the cylinder, 0. 150 in. on the flare and up to 0. 35 in. thick on the nose (Table 8-2 summarizes radial ablator thickness on nose). Stainless-steel honeycomb is incorporated in the nose of the vehicle to provide impact attenuation. The flare cone is welded to the cylinder aft of the last converter row to provide an unimpaired thermal radiation surface. All parts of the cylinder, nose, aft shell, and flare are 0. 030 in. thick titanium alloy.

A ring 0. 030 in. thick is welded to the inside of the flare cone to provide stiffness to the flare and for attachment of the mounting fittings. Standard vibration mounts are, in turn, attached to a base plate whose edges are formed to match a modified Marman clamp. This mates with the spacecraft support structure. An explosively actuated release device is attached to the clamp to ensure that the reentry vehicle can separate from the spacecraft and orient itself as it enters the atmosphere.

The shock mounts specified for the configuration shown in Figure 8-15 are Lord Mfg. Co. HT1-20, or equal. This type of mount utilizes an elastomeric material as the damping medium in which internal friction provides a nonlinear spring rate. Snubbing characteristics of this material increase at an exponential rate and permit gentle bottoming under heavy shock forces. Transmissibility at resonant frequency varies slightly with temperature between -220° and +420°K. At the higher temperature, maximum transmissibility may reach a factor of 3. At the lower temperature, the factor is less than 2. 25. Both maximums occur in a frequency range of 18 to 22 Hz. Above 100 Hz, the transmissibility factor drops to less than 5% throughout the full temperature range.

Other features of the chosen mount include a fail-safe design in which the inner member has a flange larger in diameter than the opening in the outer housing. The maximum axial deflection of each HT1-20 is 0. 25 in under a load of 440 lb. In the radial direction the mount deflects about 0. 20 in under a load of 200 lb.

Details of the reference design include:

1. Flame sprayed alumina on the inside of the pressure vessel prevents electrical shorting of the converters.
2. Titanium alloy spacers coated with alumina maintain the position of the converters and isolate them electrically.
3. Minimum electrical lead runs save connector weight.
4. A hermetically sealed electrical connector is welded into the aft shell.
5. Flare stiffener ring cut out and smoothly tapered provides a strong attachment point for the vibration mounts. (Attaching these mounts directly to the thin shell of the flare would cause acute stress discontinuity and impair the reliability of the flare.)
6. Each converter is supplied with a copper shoe brazed to the outer surface of the collector body. This shoe provides efficient heat conduction to the graphite surface. Melting of the shoe upon reentry acts as a thermal switch.
7. The cylindrical body shell is fitted with a pump-down tube through which the completed assembly is evacuated and the tube welded shut in the final process. This provides a large void volume into which helium generated by decay of the plutonium fuel is vented. This feature minimizes the structural weight of the converter and maximizes the reliability and long-term safety of the generator. The pumpdown tube contains a frangible section to relieve excessive helium pressure stress in the aeroshell.
8. The reference mounting system using an extensible boom ensures removal of the generator to a safe distance to void interference with experiments by nuclear radiation.

Table 8-5 gives a detailed breakdown of design characteristics.

The detailed 100-w_e generator design generally substantiates the performance trends identified in the parametric study, indicating an overall nominal specific power of 4 w_e/lb and 7% conversion efficiency. Generator design is significantly influenced by assumed system constraints.

A change in reliability requirements or a mission constraint involving operation in, for example, a gravity field will favor other design options. Missions which require low drag and/or small cross section could be accommodated with different converter array and aeroshell configurations. Appropriate design choices could provide the multicell generator with up to an order of magnitude smaller cross section than that of the flared cylinder treated in

Table 8-5

100 W_e-GENERATOR DESIGN SUMMARY

Generator nominal design power (w_e)	100
Generator mission life (years)	10
Generator shelf life (year)	0.5
Generator reliability goal	1) 0.98 at BOL + 5.5 years 2) No single converter failure catastrophic
Generator failure statement	1) Power <70 w_e 2) Voltage < 3 v
Converter emitter	Ta-O-Cs
Converter collector	Ta-O-Cs
Converter electrode gap (mil)	1
Converter geometry	Cylinder, all surfaces active
Helium management	Vented
Converter reliability	90% at 10.5 years
Converter failure mode	Short circuit:open circuit = 4:1
Aeroshell geometry	Flared cylinder
Aeroshell inner diameter (in.)	2.9
Aeroshell outer diameter (in.)	3.5
Aeroshell cylindrical length (in.)	11.5
Aeroshell overall length (in.)	18.1
Flare diameter (in.)	12.1
Ballistic coefficient (lb/ft^2)	30
Radiator temperature (°K)	801
Temperature difference across insulation (°K)	27
Aeroshell weight summary (lb)	
Graphite on nose	0.55
Graphite on sides	2.20
Copper shoes and alumina	0.59
Impact plate and crushup	0.23
Titanium aeroshell	0.63
Graphite on flare	2.74
Flare structure	0.74
Total aeroshell weight (lb)	7.68
Number of converters	28
Converter stacking arrangement	
Array columns	4
Array rows	7
Converter electrical connection	
Columns	2
Rows	14
Converter diameter and length (in.)	1.19
EOL converter power (w_e)	3.63
EOL converter efficiency (%)	7.1
BOL thermal power per converter (w_t)	53.2
Converter weight (lb)	0.57
Converter array weight (lb)	15.96
Total aeroshell and converter array weight (lb)	23.64

Table 8-5

100 W_e-GENERATOR DESIGN SUMMARY (Continued)

Fuel centerline temperature (°K)	1235
Emitter temperature (°K)	1205
Collector temperature (°K)	828
Emitter Q/A (w_t/cm^2)	1.35
Generator nominal specific power (w_e/lb)	4.23
Generator voltage (v)	6.92
Generator current (A)	14.45
Electrical connector weight (lb)	0.10
Flare stiffener and titanium spacer weight (lb)	0.13
Aeroshell mount weight[1] (lb)	0.68
Connector power loss (w_e)	0.25
EOL overall efficiency[2] (%)	7.08
Overall generator weight (lb)	24.55
Overall nominal generator specific power (w_e/lb)	4.07
Dose rate at 20-ft from flare along major axis[3][4]	
Neutron current (N/cm^2 sec)	3.4
γ dose rate (mrad/hr)	0.03

(1) Shock mounts only charged to generator. Mounting weight is influenced by generator weight. (Example is included in Table 8-4 for 50-lb generator).
(2) Allowing for additional connector loss.
(3) Calculated at 5 years into mission for current grade PuO_2 (1.2 ppm Pu-236 and 10^4 neutrons/sec-g Pu-238)
(4) Shielding calculations were based on Arnold's Handbook (Reference 27). Arnold's data were corrected with a self shielding factor to account for generator L/D ratio and materials in the source region.

this report or of an RTG of equivalent power. The gross performance level of this concept has, however, been established with a high degree of confidence for the stated assumptions of current and/or near-term technology. This performance level, which is attractive and competitive with the next generation of RTGs, in combination with long-term growth potential discussed briefly in the next section, provides strong motivation for development of the multicell thermionic conversion system.

Section 9

SUPPORTING EXPERIMENTAL EVIDENCE OF QUASI-VACUUM MODE CONVERTER PERFORMANCE

Effort in a DWDL Independent Research and Development (IRAD) program has been undertaken to provide a limited check on the validity of the calculational methods used in this study. A simulated converter (Figures 9-1 and 9-2) incorporating Ta-O-Cs electrodes with an electrical heater for the thermal source was instrumented to yield data on the emitter thermal balance.

Emitter and collector temperatures were measured using thermocouples. The effective emissivity was obtained from the cooling curve by subtracting a first-power temperature dependent component from the heat loss and fitting the remainder to a $\Delta(T^4)$ relationship. Correction was made for the heat losses

70-1591-A

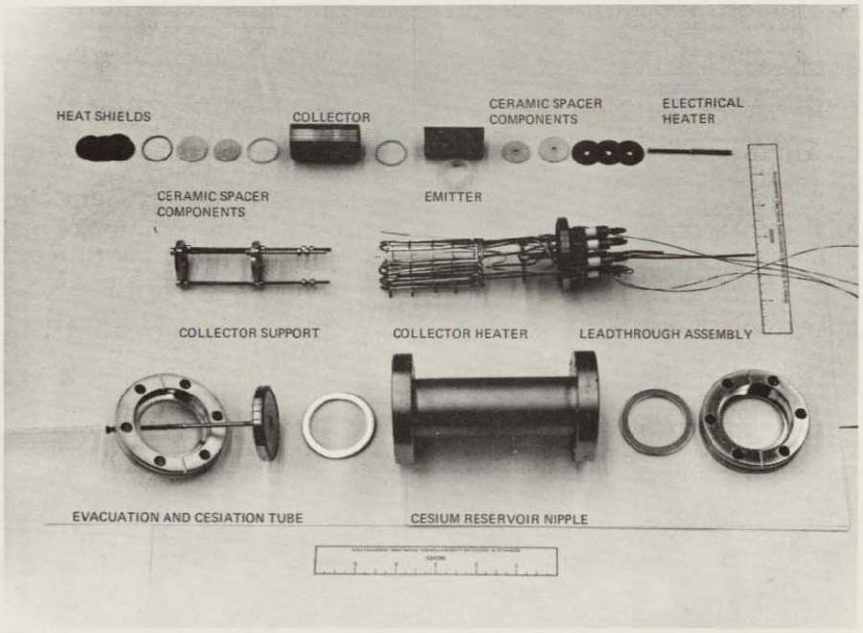

Figure 9-1. Components of Converter Simulation Experiment

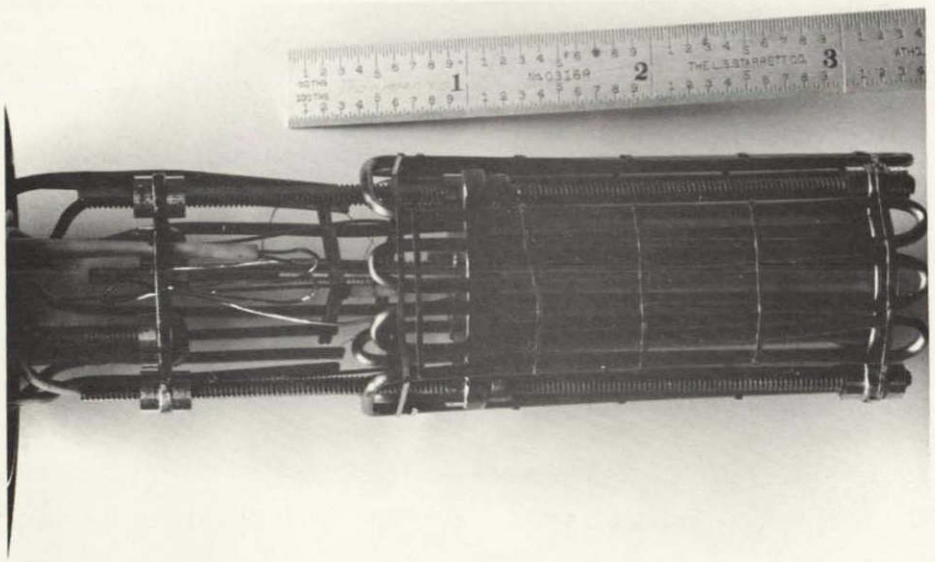

Figure 9-2. Emitter and Collector Assembly

through the ends of the experimental apparatus. To calculate electron cooling, the emitter and collector work functions were estimated from the saturation currents and measured electrode temperatures.

A set of results is compared in Table 9-1 with a calculation using the same materials, electrode spacing, collector temperature, and approximate gross power output. General agreement between theory and experiment are observed. The largest disagreement in the thermal balance is the gas conduction, which can be attributed to a difference in the cesium accommodation coefficient used in the calculation; the computer calculation used 0.6, while 1.0 was used in the calculation for the experimental device.

In Figure 9-3, the error bar indicates the operational region of the device on the efficiency vs Q/A plane. Output in excess of 600 mw_e was achieved at approximately 0.7 w_t/cm^2. Indicated conversion efficiency ranged from 3.8% (Table 9-1) to 5.2% depending on the degree of conservatism exercised in the estimation of end loss. The mean indicated efficiency agrees closely with

the theoretical value shown by the 600 mw_e isopower line, which includes the effect of gravity on the conduction loss. The theoretical isopower curve was derived from the same parameters and materials properties used for generator performance calculations in this study. The close agreement of a practical demonstration with a relatively unrefined experiment provides strong support for the feasibility of the quasi-vacuum mode thermionic concept.

Table 9-1

COMPARISON OF EXPERIMENTAL AND CALCULATED RESULTS

Emitter Thermal Balance		
	Experimental	Calculated
Thermal Input (w_t)	16.7	15.5
Radiation (w_t)	7.5	7.18
Electron Cooling (w_t)	5.4	5.92
Gas Conduction (w_t)	3.3	1.66
Support Conduction (w_t)	0.6	0.61
Lead Conduction (w_t)		0.14

Converter Parameters		
	Experimental	Calculated
Thermal Input (w_t)	16.7	16.5
Power Generated (w_e)	0.63	0.64
Efficiency (%)	3.8	4.1
Emitter Temperature (°K)	1073	1030
Emitter Work Function (ev)	1.82	1.55
Collector Temperature (°K)	828	828
Collector Work Function (ev)	1.54	1.48
Emission Barrier (ev)	1.94	1.84
Spacing (mil)	1	1
Cesium Reservoir Temperature (°K)	490	490

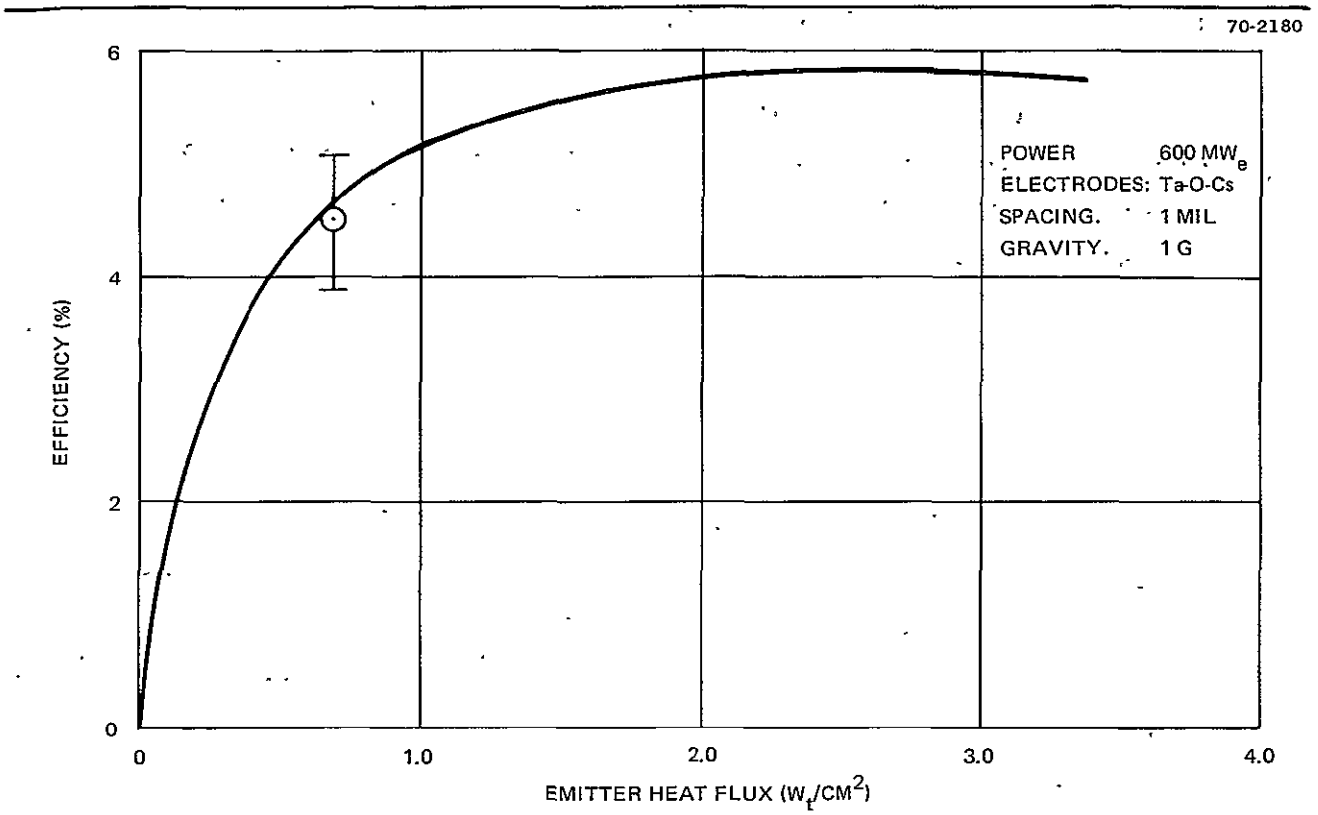

Figure 9-3. Comparison of Theoretical and Experimental Efficiency for 600 mw_e Converter

Section 10
ADVANCED TECHNOLOGY REVIEW

Growth potential of the Isomite multicell generator concept may be expected to involve high thermal power density radionuclide fuel development and evolution in converter and aeroshell design. Significant improvement in conversion efficiency, specific power, and cost result from anticipation of a suitable curia fuel form. A comparison of future Pu-238 and Cm-244 fuel forms projects curium cost as one-fifth that of plutonium per thermal watt (Reference 28). For comparison with the plutonia-based system discussed previously, curia cermet properties discussed in Section 4 are assumed in the following analysis.

CUBIC OMNIDIRECTIONAL VEHICLE FOR CURIUM-FUELED CONVERTERS

Integration of a reentry protection system with advanced technology, spherical, curium-fueled converters has been analytically scanned using techniques described previously for several potential reentry configurations (flared cylinder, blunt cone, and cube). Arrangement of the spherical cells within a common cubic heat shield is found to be promising for high specific power with safety advantages in several areas.

For a simple lattice structure of hard spheres, a face-centered cubic (cubic close-packed) arrangement minimizes interstitial volume (Reference 29) and is therefore an optimum packing arrangement. As shown in Figure 10-1, 14 spheres are placed in a cubic lattice, eight spheres in corners and six in the faces. The interstitial volume fraction is 0.26 and the sphere volume fraction is 0.74. The spheres can be placed to vent at the cube center with a curia vapor absorbant material in the interstitial volume. This assures that traces of radioactive material would not vent along with the helium. The inactive helium would be vented through the cubic graphite heat shield.

The cubic heat shield geometry advantageously reduces reentry aeroheating, ablation depth, and the impact velocity to a minimum (Reference 30). The cube is omnidirectional and has an advantage in increased reliability as a reentry

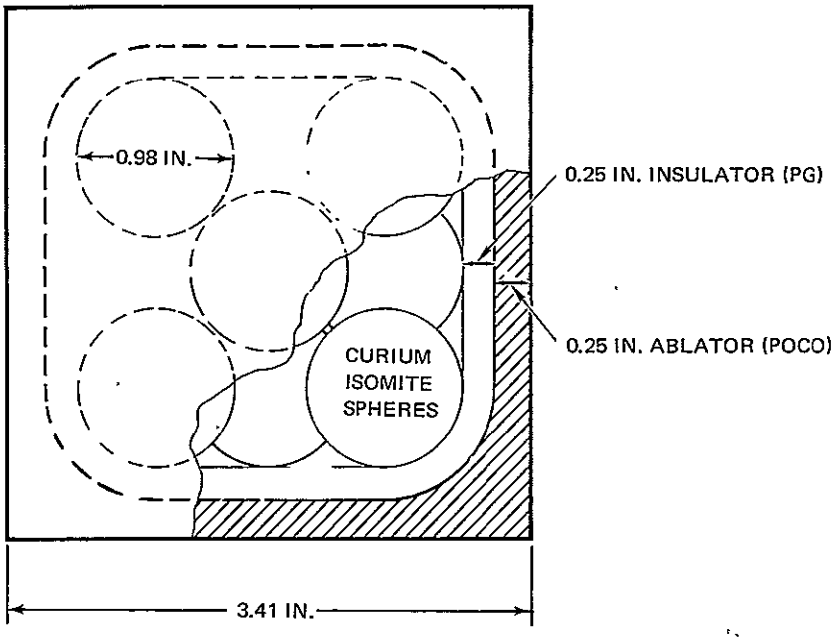

Figure 10-1. Cubic Omnidirectional Reentry Vehicle Concept with Spherical Curium Isomite Converters ($\sim$100 w_e)

protection vehicle. Use of spherical modules coupled with the low impact velocity of a cubic aeroshell eliminates the need of an impact-attentuation structure. The cubic aeroshell provides a high-area radiation surface for maximum flexibility in accommodating converter operating temperatures and, for some missions, low orbital drag and radar cross sections.

Further analysis and experimental testing is needed to verify the potential of this concept. Major problem areas requiring investigation are:

1. Launch pad abort fire and debris safety
2. Mechanical and thermal shock integrity
3. Design of non-detrimental electrical leads through the heat shield
4. Achievement of adequate flexibility in generator design
4. Safety verification of selective venting helium management

For the purposes of an advanced technology review, however, this representative configuration provides significant growth potential for the multicell generator concept.

ADVANCED TECHNOLOGY MULTICELL GENERATOR

Figure 10-1 shows a schematic section of a spherical converter/cubic aeroshell assembly. Advanced technology converter design is characterized by spherical vented emitter capsules in place of cylindrical capsules, curia fuel in place of plutonia SSC, and W-O-Cs electrode surfaces in place of Ta-based surface systems. Future generator design would incorporate any of these advanced individually or in other combinations, but analysis of each of these is not within the scope of this study.

Typical characteristics of curium-fueled system with the sphere/cube configuration are presented in Table 10-1 and Figure 10-2, and reflect the generator design approach and insight gained from the parametric study portion of this report.

The optimized spherical modules (considered at integer power levels from 1 to 7 w_e) are encased with a cubic pyrographite insulator and POCO ablator each of 0.25 in. thickness (the insulator has rounded corners). An electrical insulation standoff distance of 0.02 in. between modules is assumed. The interstitial volume is assumed to be occupied by a hypothetical impact/heat sink/Cm_2O_3 vapor absorber material of density 0.2 lb/in.^{3}.

Table 10-1

CHARACTERISTICS OF 14 SPHERICAL CURIUM-FUELED CONVERTERS IN CUBIC REENTRY VEHICLE

Cell Power (w_e)	Cell Diameter (in.)	Cube Length (in.)	Surface Area (in.^{2})	Generator Weight (lb)	Generator Power (w_e)	Specific Power (w/lb)	Surface Temp (°K)	Emitter Temp (°K)
1	0.591	2.48	36.8	1.47	14	9.50	619	1480
2	0.694	2.72	44.5	2.12	28	13.21	695	1570
3	0.776	2.92	51.2	2.68	42	15.65	731	1600
4	0.840	3.08	56.8	3.20	56	17.50	763	1635
5	0.888	3.19	61.1	3.71	70	18.86	786	1680
6	0.933	3.30	65.4	4.21	84	19.96	813	1700
7	0.978	3.41	69.7	4.72	98	20.78	832	1720

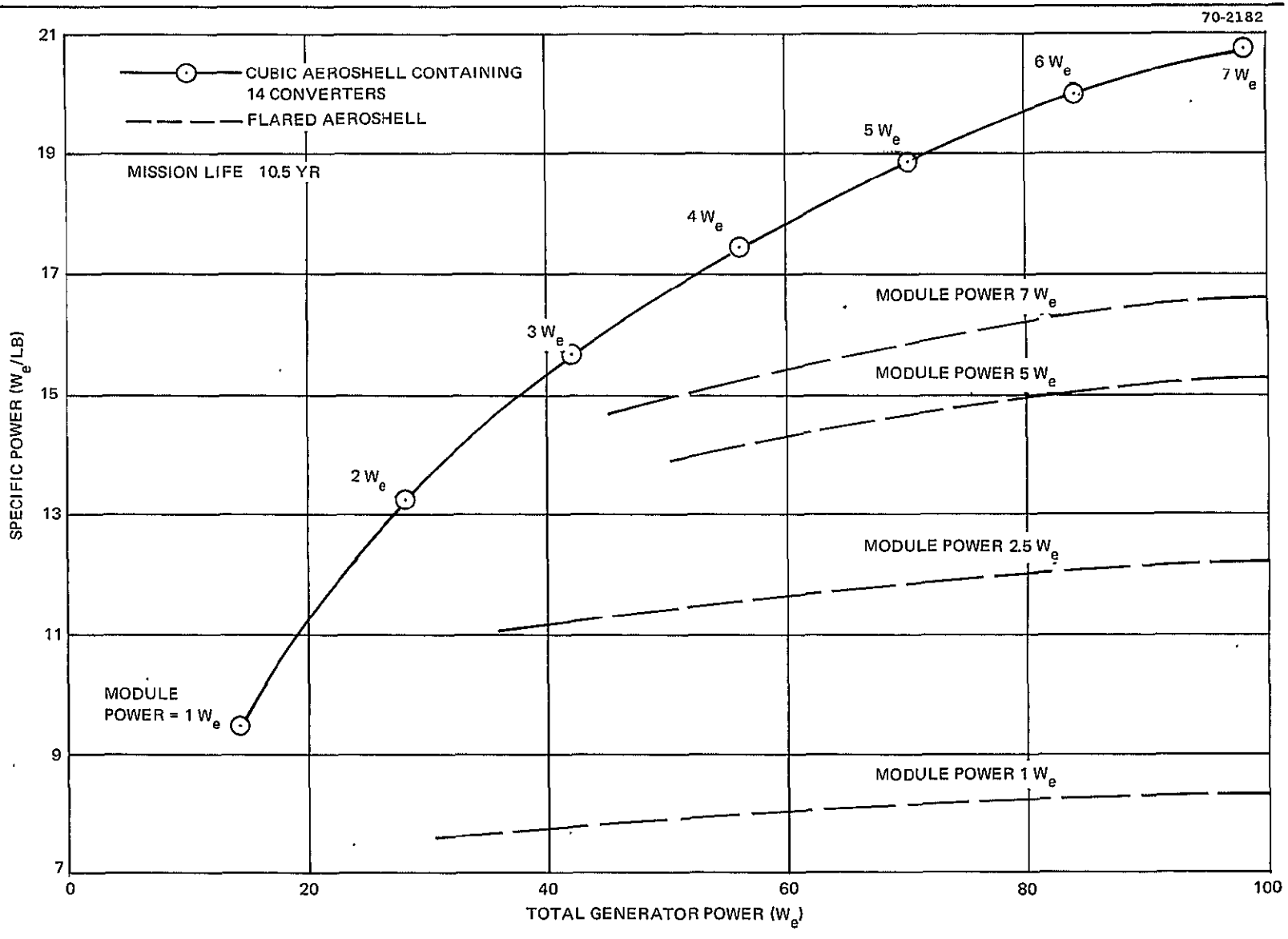

Figure 10-2. EOL Specific Power of Advanced Technology Spherical Curium-Fueled Generators

The results describe converter performance at the end of a 10.5-year mission and corresponding decay in full power density. For 7-w_e converter arrays, a specific power of over 20 w_e/lb is obtained. Generator weights do not include electrical leads, mounting structure weights, or structural changes required to assure that optimum collector temperatures can be obtained in all cases. In Table 10-1 emitter temperatures of the larger power modules exceed 1600°K. As a result, these converters may have more favorable performance by operating in the conventional thermionic arc discharge mode. This possibility is worthy of further study.

A similar analysis was performed for spherical curia-fueled converters arranged in the more conservative flared-cylinder aeroshell discussed in this report. Results are included in Figure 10-2 for comparison with the cubic structure. The flared-cylinder aeroshell places an arbitrary constraint on potential specific power of the concept. The specific power of the curia-fueled flared-cylinder configuration is, however, approximately a factor of 3 to 4 times that of the flared-cylinder plutonia-fueled generator and thus indicates a substantial performance gain within an aeroshell technology spectrum of relatively higher credibility than is currently associated with the omnidirectional cube.

For missions requiring low radiation levels, additional shielding is required for the curia-fueled generator to approach the neutron and gamma levels associated with plutonia-fueled systems. DWDL calculations show that the weight of the additional shield added to the curia generator provides a system still with twice the specific power of the equivalent plutonia-fueled device.

Section 11
CONCLUSIONS AND RECOMMENDATIONS

All objectives of the Phase I and Phase II design study have been satisfied. The plutonia-fueled quasi-vacuum mode thermionic multicell space power generator is shown to provide a highly flexible and redundant modular power supply satisfying space power requirements in the 50 to 200 w_e range with total accommodation of system requirements. A basic "building block" module power in the range 3 to 4 w_e is identified for generators with nominal power between 100 and 200 w_e. The feasibility of a wide range of generator power and configuration options using a single basic module has tremendous economic benefit, both in the development and qualification program stages. Special mission requirements, such as low orbital drag, small radar cross section, and radiation resistance can be incorporated in the generator design by relative simple configurational changes in the aeroshell without modification to the converter modules.

The flared-cylinder is representative of an aeroshell configuration which provides, in conjunction with the modular Isomite array concept, four levels of fuel containment. The modularity of the array divides the total fuel inventor into approximately 50 w_t units operating with center line temperatures no more than 30°K above emitter temperature. At emitter flux densities characteristic of the plutonia-fuel generator, Ta-O-Cs emitter temperatures optimize between 1150° and 1250°K. Quasi-vacuum mode thermionic conversion is, therefore, compatible with the current and developing plutonia fuel technology required fo planned RTG and Brayton aerospace systems.

This concept using current and/or near-term technology provides a space power source for multihundred-watt requirements with practically constant specific power of 4 w_e/lb and 7% overall conversion efficiency allowing for both redundancy to meet reliability goals and system integration losses. High confidence is placed on the performance predictions identified in this study becaus technology assumptions and basic design features are generally conservative.

The current and/or near-term technology generator appears to be competitive with the next generation of RTGs. Potential performance growth offered by high thermal power density fuel and credible converter development exceeds most long-term projections for thermoelectric devices. Advanced technology multicell generators theoretically can achieve specific power in excess of 20 w_e/lb and 10% conversion efficiency, considered at the end of a 10-year mission. This performance growth offers a potentially significant contribution of improved capability and flexibility in space missions scheduled for the late 1970s and early 1980s.

A curia fuel form and advanced electrode surfaces would permit operation at emitter flux densities between 2 and 4 w_t/cm^2. The corresponding emitter temperatures range from 1480° to 1720°K which is significantly lower than temperatures (1600° to 2000°K) required in conventional thermionic converters. By analogy with uranium-based reactor fuel development, curia fuel could be expected to function and be compatible with converter structural materials in the temperature regime of the advanced generator.

Several aspects of this generator study are worthy of additional consideration. Further weight and design refinement will result from study of the following areas:

1. The optimization of emitter thermal flux concentration (achieved by shielding the emitter into thermionically active and inactive areas).
2. Generator design in response to ranges of reliability goals and other specific mission constraints.
3. Investigation of optimum array connection considering other matrix arrangements, optimization of parallel connector impedence, and three-dimensional networks.
4. Consideration of system performance with other fuels, electrode surfaces, and aeroshell configurations.
5. Design effort to accommodate fuel swelling and the influence of long term operation on materials stability.
6. Optimization of structure (for example emitter and collector capsule thickness) to enhance generator nuclear safety and survival of accident conditions.
7. Consideration of curium-fueled converter operation in the arc mode regime.

An inherent advantage of the multicell concept is that many alternate design options (including growth) are readily available once single cell technology is

established. An important related advantage is that this design flexibility permits exceptionally early utilization of advanced technology developments after they are demonstrated in single cells.

MULTICELL GENERATOR DEVELOPMENT PROGRAM

A program to develop multiwatt power modules and related integration technology of the multicell generator concept would consist of the following tasks:

1. Construct proof-of-principal devices.
2. Construct electrically heated demonstration devices.
3. Construct fueled demonstration device.
4. Show helium vent feasibility.
5. Test demonstration devices in simulated system conditions.
6. Construct and test fueled and vented device.
7. Develop component technology.
8. Develop theoretical generator model.

These tasks define milestone achievements each of which is a relatively small extrapolation of the previous task. Concept feasibility would thus be demonstrated by a sucession of incremental steps and at a very low cost. Any fundamental weakness in the concept (although none is anticipated) would be identified early in the program before major development effort is expended. Redirection of generator development goals would be readily and inexpensively introduced as a result of the relatively low unit power and fuel inventory of the basic converter module.

The novelty and promise of the multicell generator warrant support and interest in an early hardware demonstration program to substantiate the conclusions of this study regarding performance at the current technology level.

Section 12
NEW TECHNOLOGY

Pursuant to the new technology provisions of the contract, no reportable items of new technology have been identified.

PRECEDING PAGE BLANK NOT FILMED

Section 13

REFERENCES

1. E. W. Williams and R. C. Howard. Development of a 100-W_e Isotope Thermionic Electrical Power Module. Proc. 2nd International Conference on Thermionic Electrical Power Generation, Stresa, Italy, May 1968.

2. Radio Corporation of America. Final Technical Report--The Development of Thermionic Isotope Space Power Technology (Volume 1, 2, and Appendix II - Classified Confidential, Appendix I - Unclassied. Contract NASw-1254, 1967.

3. J. G. DeSteese and J. S. Holmgren. A Radiantly Heated Radioisotope-Powered Thermionic Generator. Proc. Thermionic Conversion Specialist Conference, Palo Alto, California, October 1967.

4. R. L. Ryan and J. W. Graham. Isotope Reentry Vehicle Design Study. Preliminary Design Phase II - Final Report. NASA-CR-72555, August 1969.

5. AiResearch Manufacturing Div. Study of Radioisotope Fueled Brayton Cycle Electric Power System for MORL. M-1800 August 29, 1964 - Classified Confidential.

6. Donald W. Douglas Laboratories. Preliminary Design Study of a 250 W_e Promethium-147 Radioisotope Space Power System. DAC-59999, September 1967.

7. I. Langmuir. The Effect of Space Charge and Initial Velocities on the Potential Distribution and Thermionic Current Between Parallel Plane Electrodes. Physical Review, Vol. XXI, No. 4, 419, April 1923.

8. P. A. Lindsay and F. W. Parker. Potential Distribution Between Two Emitting Electrodes II. Thermionic Engines. J. Electronics and Control, Vol. 9, No. 2, 81, August 1960.

9. N. S. Rasor and C. Warner. Correlation of Emission Processes for Adsorbed Alkali Films on Metal Surfaces. J. Appl. Phys. Vol. 35, No. 9, 2589, September 1964.

10. B. A. Khrustalev and A. M. Rakov. Radiative Properties of Tantalum, Niobium, Graphite and Niobium Carbide at High Temperatures. Heat Transfer-Soviet Research. Vol. 1, No. 4, July 1969.

11. Y. S. Touloukian. Thermophysical Properties of High Temperature Solid Materials. Vol. 1 Elements, MacMillan 1967.

12. J. M. Houston and H. F. Webster. Advances in Electronics and Electron Physics. 17, 147, 1962.

13. C. G. Suits. The Collected Works of Irving Langmuir. Vol. 3, pages 285, 311, and 321, Macmillan 1961.

14. J. Leary. Passout for Isotope Fuels and Materials Committee Meeting, Oak Ridge National Laboratory, February 25-26, 1970.

15. W. M. Pardue, et al. Final Report for the Program to Develop Composite Fuel Forms of $Pu^{238}O_2$. BMI-1869, September 1969.

16. J. D. Watrous. DWDL Private Communication.

17. J. R. Long. Output Power Characteristics of Thermionic Converter Arrays Under Partial Failure Conditions. Advances in Energy Conversion Engineering, 1967 Intersociety Energy Conversion Engineering Conference, August 13-17, 1967, Miami Beach, Florida, pp. 163-170.

18. K. Shimada and F. de Winter. Optimization of Thermionic Generator Systems of High Reliability. Fifth Space Congress, Cocoa Beach, Florida, March 1968.

19. A. W. Barsell. Safety Analysis Report for a 4-Watt ^{147}Pm Isomite Miniature Radioisotope Thermionic Converter. MDAC Report DAC-60771 (October 1968).

20. M. W. Hulin. Radioisotope Heater Development Program. MDAC Report DAC-63364 or NASA-CR-101840, June 1969.

21. Hittman Associates, Inc. Spherical Capsule Technology Program. Heat Source Technical Report. HIT-370, January 1969.

22. D. F. Haskell. Impact Failure Criterion for Cylindrical and Spherical Shells. The Shock and Vibration Bulletin 39, Part 5 (December 1968).

23. A. W. Barsell and T. H. Smith. Optimum Configurations for Reentry Safety of 5 to 50 Wth Radioisotope Heaters. MDAC Paper WD 1343, presented at 16th Annual ANS Meeting, June 28 - July 2, 1970, Los Angeles, California.

24. D. W. Larson. Ablation and Thermal Analysis of the Apollo Lunar Radioisotope Heater. SC-RR-69-303, July 1969.

25. R. A. Rindal. An Evaluation of Design Analysis Techniques for High Performance Ballistic Vehicle Graphite Nose Tips, Appendix D (Thermochemical and Thermomechanical Ablation). AFML-TR-69-73, Volume IV, January 1970.

26. R. D. Klett. Drag Coefficients and Heating Ratios for Right Circular Cylinders. SC-RR-64-2141, December 1964.

27. E. D. Arnold. Handbook of Shielding Requirements and Radiation Characteristics of Isotopic Power Sources for Terrestrial, Marine, and Space Applications. ORNL-3576.

28. J. D. LaFleur, Jr. Nuclear Power Systems for Spacecraft. IEEE Transactions on Aerospace and Electronic Systems, Vol AES-6, No. 2, March 1970.

29. C. Kittel. Introduction to Solid State Physics. John Wiley and Sons, Inc., New York (1953).

30. A. W. Barsell and T. H. Smith. Optimum Configurations for Reentry Safety of 5 to 50 W_t Radioisotope Heaters. Presented to 16th Annual Meeting, ANS, Los Angeles, Calif., June 28-July 2, 1970.

Appendix A

QUASI-VACUUM-MODE THERMIONIC CONVERTER CALCULATION AND OPTIMIZATION CODES

Thermionic converter calculations and optimization are carried out on the IBM-1130 computer using calculational methods developed under associated IRAD programs. Two computer codes are available for optimization: one called MM10 has up to five free parameters and uses a so-called "direct-search" technique; the other MSM5, has 3 free parameters and cycles through two more using a stepping search. Both codes use the same subroutines for the converter calculations.

THEORY

Typical potential distributions to be found in a quasi-vacuum-mode diode are shown in Figure A-1, the points in the I-V coordinates being shown in the lower half of the figure. Terms are defined in the symbol table. Near the peak power point, about 0.3 volt, and at lower voltages, the net random electron current across the gap is determined to a large extent by the electron cloud in the interelectrode space, and the diode is in the so-called space-charge mode. Somewhat past 0.3 volt in Figure A-1, the diode operates in the non-space charge mode, implying that the density of electrons in the interelectrode space is so low that volume effects are essentially absent, i.e., no potential barrier is formed in the interelectrode space. If the approximation is made that the electron gas in the emitter has an essentially Maxwellian distribution of electron velocities, the net current density for a given barrier height ψ and emitter temperature T_e will be, from Richardson's equation:

$$J_n = J^+ - J^- = A_R \left(T_e^2 e^{-\psi/kT_e} - T_c^2 e^{-\phi_c'/kT_c} \right) \qquad \text{(A-1)}$$

If space charge effects are absent, $\phi_c' = \phi_c$, the collector work function (right-hand curve). The output power to a load is

$$P = AJ_nV = AJ_n \left(\psi - \phi_c' \right) \qquad \text{(A-2)}$$

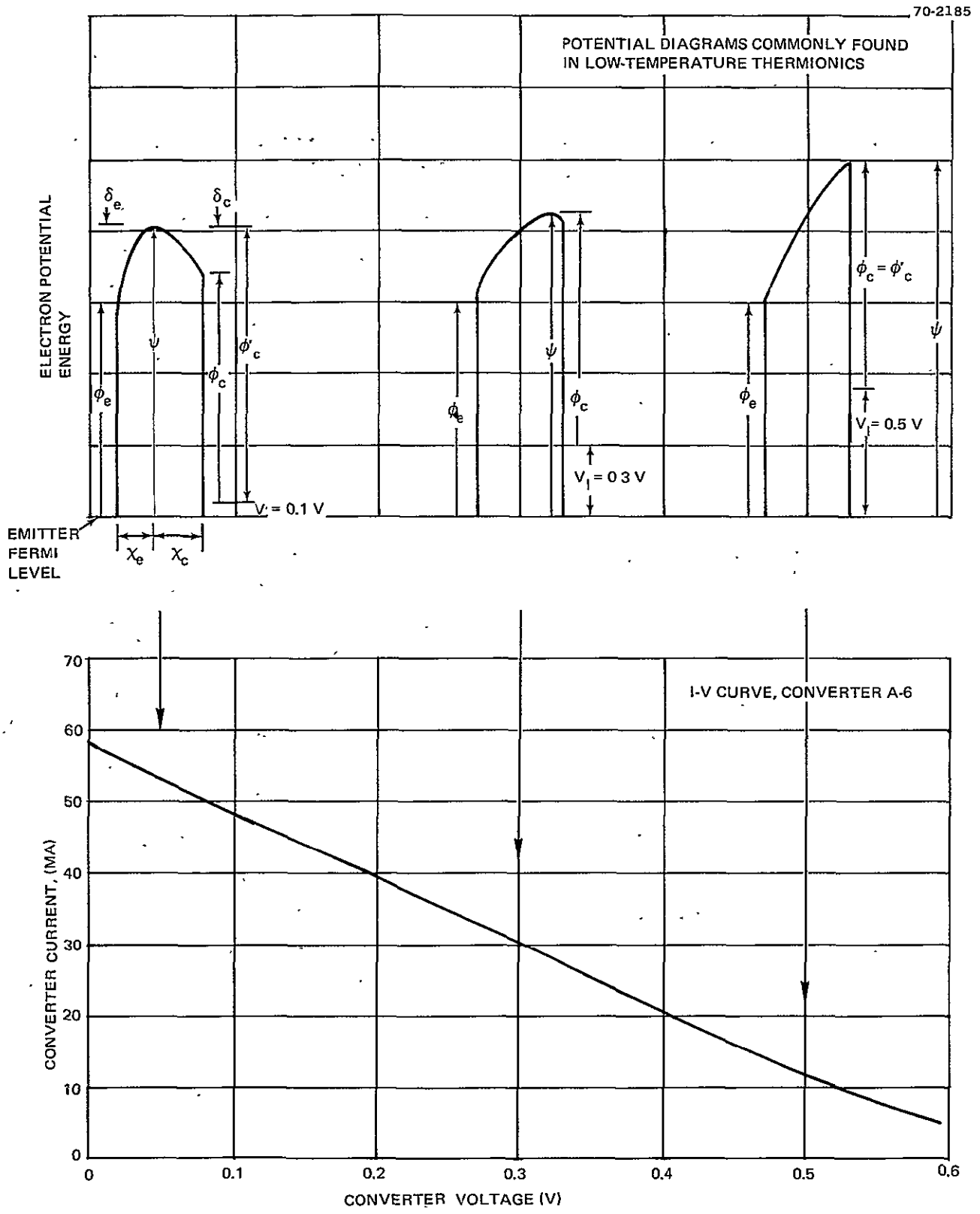

Figure A-1. Potential Diagrams and I-V Plot for Typical Quasi-Vacuum-Mode Thermionic Converter

The present interpretation of thermionic emission with a space-charge barrier has remained essentially unchanged since the first part of the century, when pioneering theoretical and experimental work was done by Epstein, Fry, Gans, and Langmuir (References A-1 through A-4, respectively). Little change in the theory has been forthcoming primarily because of the success of their treatments in describing thermionic emission.

In what might be called classical vacuum mode theory, the following assumptions are made:

1. No interelectrode collisions
2. No ionization effects
3. No back emission
4. Maxwellian distribution of electron velocities

The steps for solving the plane-parallel problem are as follows:

Step 1. Solve the collisionless Boltzmann diffusion equation for the electron distribution function in the interelectrode spacing.

Step 2. Integrate in velocity space to determine the electron density as a function of distance (usually from the potential minimum).

Step 3. Substitute the density function $\eta(x)$ into Poisson's equation to determine the potential distribution u(x):

$$\frac{\partial^2 u}{\partial x^2} = \frac{\eta(x)}{4\pi\varepsilon_o} \qquad \text{(A-3)}$$

From tabulated or graphical presentations of u(x), the potential characteristics associated with a specific emission current can then be calculated, with a number of these solutions then forming a complete I-V curve.

In analysis of the low temperature Isomite battery, points 1, 2, and 4 are either assumed or deviations from them neglected. Of these three assumptions, number 1 may in certain circumstances be incorrect. The electron and Cs atom have a considerable probability of collision. The number of collisions per centimeter is

$q_c = N_v A_c$

N_v = atoms/volume

A_c = atom-electron collision cross-section per atom

In terms of pressure and temperature, the atom density N_A is

$$N_A = 9.656\,(10^{18})\frac{p}{T} \qquad (cm^{-3} - torr - °K) \tag{A-4}$$

The collision cross-section for cesium is about 3 (10^{-14}) cm^2, which gives the collision rate as

$$q_c = 0.74\,\frac{p_r}{(T_r\,T_g)^{1/2}} \qquad (collisions/mil) \tag{A-5}$$

The temperatures T_r and T_g are in thousands of degrees Kelvin. For a gas pressure of 0.1 torr and a temperature of 750 °K, the collisions per mil of interelectrode spacing are on the order of

$$q_c = 0.12 \text{ collisions/mil} \tag{A-6}$$

At spacings on the order of 1 mil the effect of collisions will be negligible.

However, effects of back emission on the electrode potential distribution can not in general be neglected in a device where the emitter-collector difference is on the order of a few hundred degrees Kelvin. The effect of back emission is to inject a high concentration of collector electrons into the collector region, and increase considerably the collector space charge barrier height ϕ_c'. The effect of these electrons is considerable less close to the emitter, which is already immersed in a dense cloud of emitter electrons.

Lindsay and Parker have treated the problem analytically (Reference A-5 and A-6). The steps involved in obtaining the solution for non-negligible back emission are essentially the same as those previously outlined as Steps 1, 2, and 3, with addition to the density function $\eta(x)$, of a density component caused by back emission. Inclusion of back emission is not a difficult analytic step, but poses considerable difficulty from a computational point of view. Description of the emission characteristics with back emission is patterned on the Langmuir formalism, with inclusion of a new parameter, $\bar{a}$. The potential distribution is treated otherwise identically, with dimensionless emitter and collector potentials and distances describing the interrelationships of current, potential, and distance in the interelectrode space. The dimensionless distances X_e and X_c are given as

$$\chi_e = 9.186 \times 10^5 \frac{\sqrt{J^+}}{T_e^{3/4}} X_e \tag{A-7}$$

$$\chi_c = 9.186 \times 10^5 \frac{\sqrt{J^+}}{T_e^{3/4}} X_c \tag{A-8}$$

with the further equations

$$X_e = \int_0^{\eta_e} \frac{dy}{\left[h^-(y) + \bar{a} h^+ \left(\frac{y}{\theta}\right)\right]^{1/2}} \tag{A-9}$$

$$X_c = \int_0^{\eta_e} \frac{dy}{\left[h^+(y) + \bar{a} h^- \left(\frac{y}{\theta}\right)\right]^{1/2}} \tag{A-10}$$

$$h^+(y) = (e^y - 1) - 2\sqrt{\frac{y}{\pi}} - e^y \operatorname{erf}(\sqrt{y}) \tag{A-11}$$

$$h^-(y) = 2(e^y - 1) - h^+(y) \tag{A-12}$$

$$\theta = T_c / T_e \tag{A-13}$$

$$\bar{a} = \sqrt{\theta}\, \frac{J^-}{J^+} \tag{A-14}$$

$$\eta_e = \frac{\delta_e}{kT_e}, \quad \eta_c = \frac{\delta_c}{kT_c} \tag{A-15}$$

where δ_e and δ_c are defined by Figure A-1.

Lindsay and Parker provide tabulated values of η_e and η_c as functions of χ_e, χ_c, and $\bar{a}$, and for $\theta = 1.0$, 0.8, 0.5, and 0.2. Figure A-2 is a plot of η_e and η_c vs χ_e and χ_c for $\theta = 0.8$, where the parameter ν is related to $\bar{a}$ by

$$\nu = \bar{a}/\sqrt{\theta} = J^-/J^+ \tag{A-16}$$

It is clear that back emission has a significant effect on the collector barrier but a minimal effect on the emitter.

70-2186

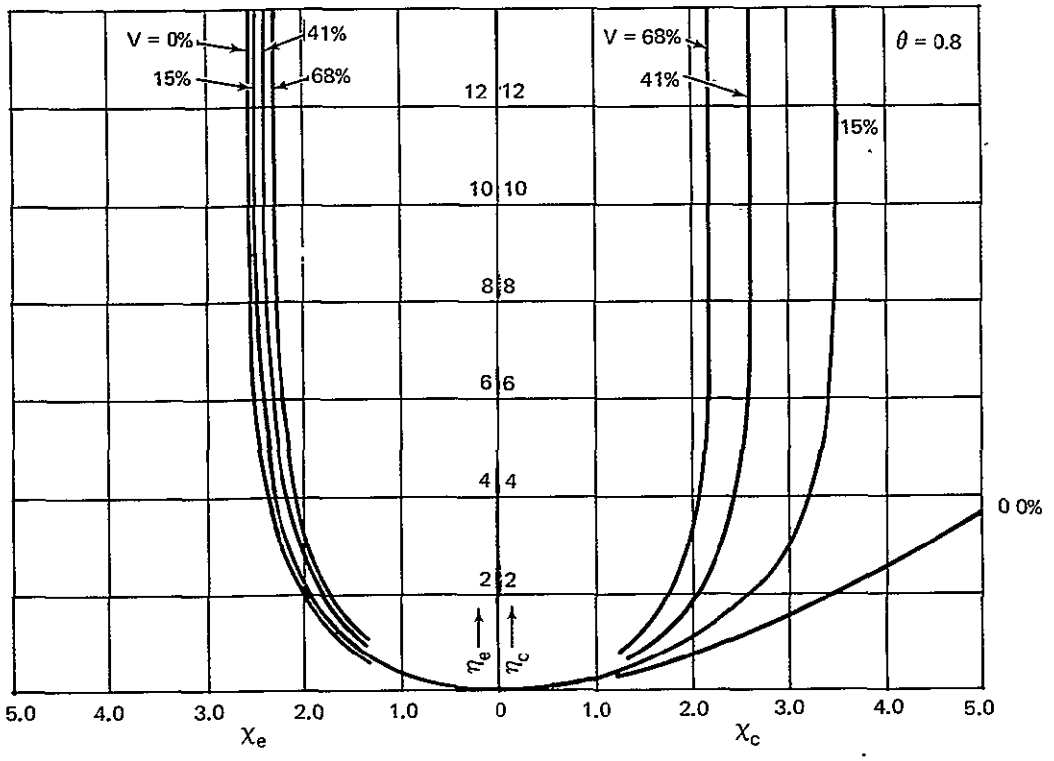

Figure A-2. Dimensionless Emitter and Collector Space Charge Potential vs Dimensionless Distances in Converter

To make the results produced by Lindsay and Parker usable for digital computer calculations, empirical equations were produced by plotting and fitting curves to the results. Although there is no reason to expect the rather complex integral solutions to the potential to be expressible in reasonably simple form, it was decided to attempt to fit the tables with expressions involving θ and $\bar{a}$. In this modeling, it was assumed that the effect of collector back emission was negligible on the emitter potential distribution because of attenuation of collector electrons by the back emission barrier height, and the high density of emitter electrons already in the emitter space. As mentioned before, this behavior is shown qualitatively in Figure A-2, where the value of $\bar{a}$ (which is proportional to back emission) has little effect on the emitter potential until $\bar{a}$ becomes on the order of 0.5. This being the case, the η_e vs X_e relationship was assumed given with adequate accuracy by classical vacuum-mode theory, and expressions given by Rittner (Reference A-7) are used to calculate X_e for a given η_e.

In the collector space, it was found that description of η_c vs χ_c was much simpler than expected. For constant θ, Figures A-3, A-4, and A-5 show that over a considerable range of η_c, there is a very close power-law dependence of η_c on χ_c:

$$\eta_c = \beta(\theta, \bar{a})\, \chi_c^{m} \tag{A-17}$$

where m is a sluggish function of $\theta, \bar{a}$

To maintain some degree of physical reality in the parameterization, the back emission ratio v replaced $\bar{a}$ as the variable other than θ describing the relationship of η_c and χ_c;

$$\eta_c = \beta(\theta, v)\, \chi_c^{m(\theta, v)} \tag{A-18}$$

In this log-log region, it is found that to a good approximation, the dimensionless collector space charge barrier is linearly dependent on v for constant θ and χ_c.

70-2187

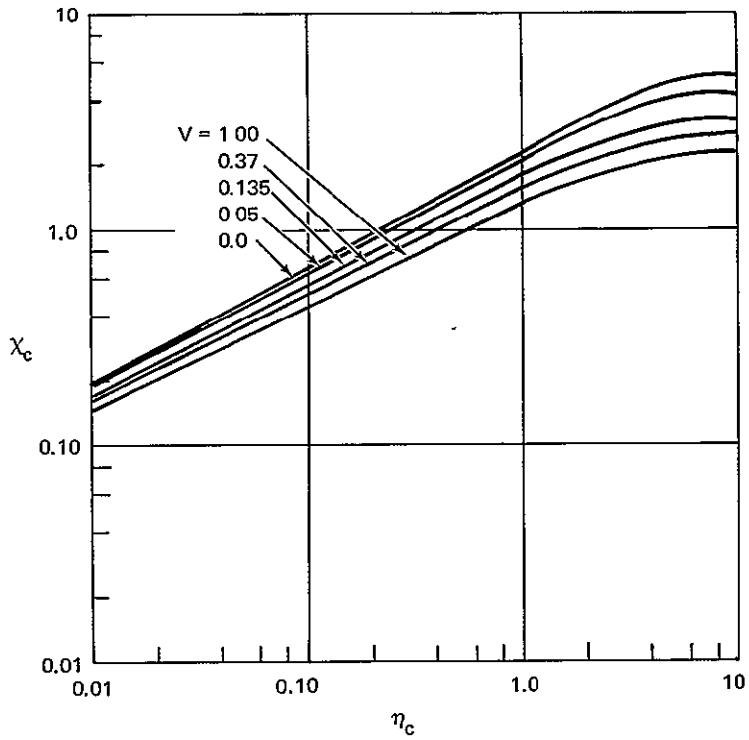

Figure A-3. Log-Log Plot of χ_c vs η_c for θ = 1.0

70-2188

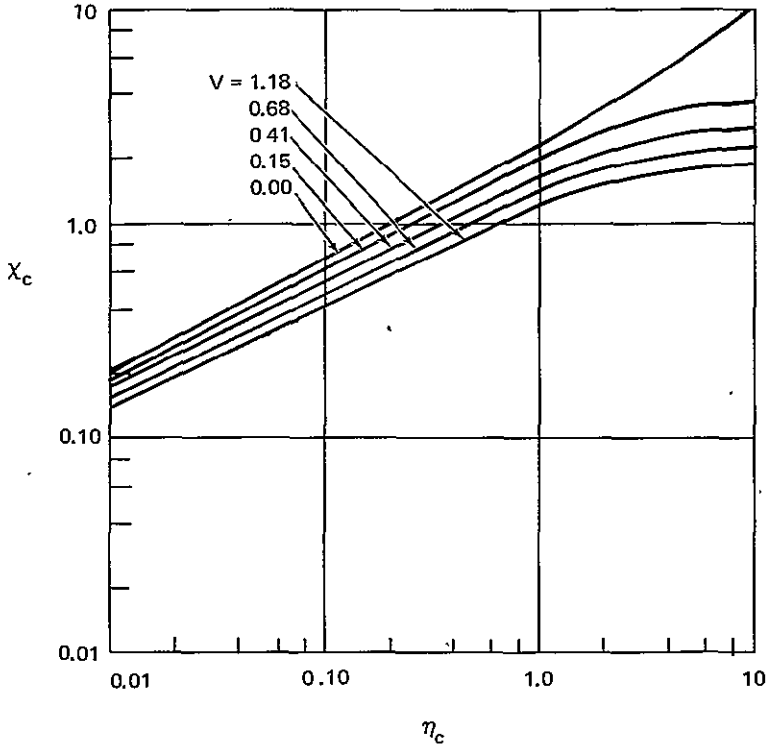

Figure A-4. Log-Log Plot of χ_c vs η_c for $\theta = 0.8$

70-2189

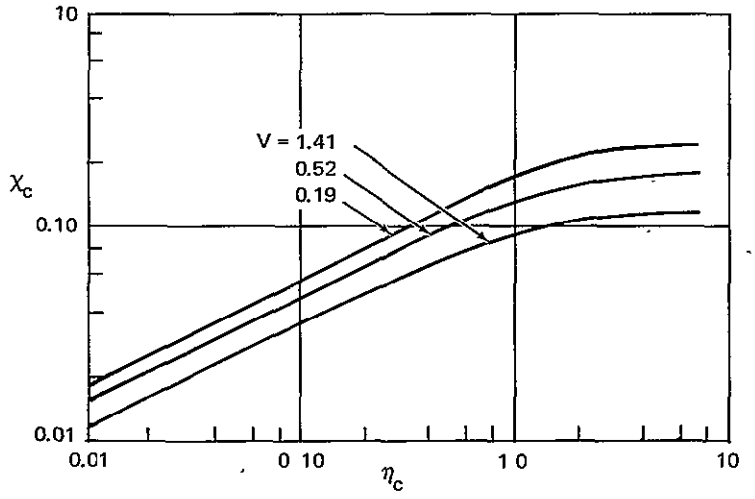

Figure A-5. Log-Log Plot of χ_c vs η_c for $\theta = 0.5$

$$\eta_c = (K + \alpha(\theta) \cdot \nu)\, \chi_c^{m} \tag{A-19}$$

Cross-plotting yields $\alpha(\theta) = 0.30\, \nu/\theta^{0.92}$ (A-20)

The constant, K, is the dimensionless collector space charge barrier with zero back emission. This value is about 0.21 at $\chi_c = 1.0$.

The power 'm' in the fitting equation is determined by plotting the slope of log η_c versus log χ_c for the θ range, and parameterizing in back emission. The equation

$$m = 1.85 + \left(\frac{\nu}{12.5}\right)^{0.521} \tag{A-21}$$

fits the power dependence satisfactorily. The total fitting equation is then

$$\eta_c = (0.21 + 0.30\, \nu/\theta^{0.92})\, \chi_c^{(1.85 + (\nu/12.5)^{0.521}} \tag{A-22}$$

Table A-1 compares calculated values using the above fitting equation and tabulated values of Lindsay and Parker.

In all cases considered, the error in collector barrier height is less than 10% relative or $0.01 kT_e$ absolute. For higher values of χ_c, η_c rises very rapidly until it reaches infinite proportions (for all practical purposes) at a critical value of χ_c. It was necessary to separate the η_c, χ_c space into two sections because of this behavior. In the first section, the log-log equations describe the behavior adequately, while in the second asymptotic region, it was necessary to form a more complex solution which will describe the behavior and match the log-log expression at the boundary.

The derivation of this fitting equation was somewhat tedious. The equation is

$$\eta_c = \frac{\beta\, \theta^{1.09}}{\nu^{0.128}} \left[x \ln\left(\frac{1}{1-x}\right)\right]^{0.97\nu^{0.09}} \tag{A-23}$$

$$x = \chi_c / \chi_o \qquad 0.45 \leq x \leq 1 \tag{A-24}$$

$$\chi_o = -0.42 + (0.312 + 0.657\,\theta)\ \ln(16/\nu) \qquad \text{(A-25)}$$

The coefficient β is determined from the requirement that at $x = 0.45$, the log-log expression (Equation A-22) and Equation A-23 give the same value of η_c. When the parameter $x \cong 0.45$ the two expressions are closest to yielding the same value of η_c, and the same rate-of-change of η_c with respect to χ_c. This ensures that lines of constant back emission are duplicated as closely as possible.

Table A-1

CALCULATED VALUE COMPARISON

θ	χ_c	ν	η_c (Exact)	η_c (Approx)	Relative Error	Absolute Error
1.0	0.25	0.00	0.0157	0.016	2%	0.003 kT_e
		0.135	0.0170	0.0169	<1%	0.0001
	1.00	0.00	0.21	0.21	0%	0.0
		0.135	0.253	0.25	1%	0.003
		0.370	0.323	0.321	<1%	0.002
	2.00	0.135	0.950	0.964	2%	0.016
	3.00	0.0	1.53	1.60	<5%	0.07
	3.00	0.05	1.80	1.827	2%	0.027
0.80	0.266	0.0	0.017	0.018	7%	0.01 kT_e
		0.151	0.020	0.020	0%	0.0
	0.261	0.678	0.030	0.0285	5%	0.0015
	1.0	0.0	0.21	0.21	0%	0.0
	1.067	0.151	0.30	0.301	<1%	
	1.050	0.452	0.40	0.416	4%	0.016
	2.356	0.151	1.50	1.41	6%	0.09
0.50	0.25	0.0	0.0157	0.016	2%	0.0003 kT_e
	1.0	0.0	0.21	0.21	0%	0.0
	3.0	0.0	1.53	0.60	<5%	0.07
	1.067	0.191	0.35	0.362	3%	0.012
	1.0405	0.52	0.55	0.548	<1%	0.12
	1.5209	0.191	0.75	0.673	10%	0.077

CALCULATIONAL METHOD

In mechanizing the vacuum-mode thermionic converter calculations, several choices existed. The method adopted uses the following sequence:

1. Choose T_c and ψ
2. From the emitter heat balance, obtain T_e
3. Calculate δ_e and δ_c
4. Calculate voltage, current, and power out of the converter.
5. Correct for electrical losses in the emitter lead.

Each of these steps is described in more detail below.

1. Choose T_c and ψ. The method of choosing and varying T_c and ψ is different in the two codes and depends on the purpose of the analysis.

2. Obtain T_e. For a diode with specified dimensions and heat source the heat balance is written as

$$\text{Source} = (\text{Radiation}) + (\text{gas conduction}) + (\text{support conduction}) + (\text{Emitter lead conduction}) + (\text{Electron cooling}) \quad \text{(A-26}$$

$$Q = \sigma \varepsilon A (T_e^4 - T_c^4) + G_g A (T_e - T_c) + G_s (T_e - T_c) \quad \text{(A-27}$$

$$+ k_L (T_e - T_c)/(\ell/a) + A_R A T_e^2 (\psi + 2kT_e) e^{-\psi/kT_e}$$

T_e is obtained by successive estimations. The first estimate is the converged value from the last calculation, the second estimate is 25°K larger or smaller depending on the sign of the difference between Q and the right-hand side of the equation and successive estimates are based on interpolation to bring the difference to zero. Successive guesses on T_e less than 0.1 °K apart bring the iteration to a close.

3. Calculate δ_e and δ_c. With ψ known, δ_e is given by

$$\delta_e = \psi - \phi_e \quad \text{(A-28}$$

χ_e and χ_c are then calculated using equations developed by Rittner (Reference A-7). Letting $u = \delta_e/kT_e$, (A-29

$$\chi_e = -2\sqrt{u} + 0.376126u + 0.0251956u^{3/2} + 6.9163 \times 10^{-4} u^2 \qquad \text{(A-30)}$$
$$-9.9409 \times 10^{-4} u^{5/2} \qquad u \leq 0.2$$

$$= -\frac{6.156143u + 65.69123u^2 + 59.48926u^3 - 4.103353u^4}{0.2629089 + 14.62018u + 49.59515u^2 + 16.06387u^3 - u^4}$$

$$0.2 < u < 3.0$$

$$= -2.55389 + \sqrt{2e^{-u}} - 0.0123e^{-u} + (1 + \sqrt{u/\pi})\sqrt{e^{-3u/18}}$$

$$u \geq 3.0$$

$$\chi_c = 9.186 \times 10^5 \left[A_R T_e^2 e^{-(x + \phi_e/kT_e)}\right]^{1/2} \frac{d}{T_e^{3/4}} + \chi_e \qquad \text{(A-31)}$$

If χ_c is non-positive, δ_c is set to 0.0; otherwise δ_c is calculated iteratively using the expressions developed earlier which take back emission into account. The first step is to determine which set of expressions to use. The ratio of χ_c to χ_o (χ_o is the asymptotic dimensionless collector distance; i.e., the distance at which the back emission barrier height approaches infinity) is symbolized by x, and is initially set to 0.5; ν, the back-emission ratio, is then obtained by rearranging the expression for χ_o:

$$\nu = 16 \exp\left\{(-\chi_c/x - 0.42) / (0.312 + 0.657\theta)\right\} \qquad \text{(A-32)}$$

Using this value of ν, δ_c is calculated by two different expressions:

$$\delta_c(1) = (0.21 + 0.3\nu\theta^{-0.92})\chi_o^{1.85} + (0.8\nu)^{0.521} \qquad \text{(A-33)}$$

$$\delta_c(2) = -\theta \ln \frac{e^{\phi_c/kT_c - \Psi/kT_e}}{\theta^2} \qquad \text{(A-34)}$$

For $\delta_c(2)$ greater than $\delta_c(1)$, the non-linear equations are used; otherwise, the linear set is appropriate.

If the $\chi_c - \eta_c$ equations are in the linear region, ν is used as the independent variable in the two equations for δ_c and adjusted until the two yield the same result for δ_c. If the non-linear set is appropriate, iteration proceeds on x:

for each value of x, a value of ν is calculated using the above equation. Normalizing then is performed so that the two sets of equations will agree, and δ_c is calculated two ways and compared.

4. Calculate voltage, current, and power. Once δ_c has been calculated, the gross voltage output is calculated from

$$V = (\phi_e + \delta_e) - (\phi_c + \delta_c) \tag{A-35}$$

The current is next calculated, using

$$I = A_R A \left[T_e^2 e^{-\psi/kT_e} - T_c^2 e^{-(\phi_c + \delta_c)/kT_c} \right] \tag{A-36}$$

Finally, the power is

$$P = I V \tag{A-37}$$

5. Electrical losses in emitter lead. Electrically, the emitter lead is part of the load seen by the converter. Net voltage and power are calculated as

$$V_{net} = V - IR_{Lead} = V - I\rho(\ell/a) \tag{A-38}$$

$$P_{net} = P - I^2 R_{Lead} \tag{A-39}$$

$$R_L = (V/I) - R_{Lead} \tag{A-40}$$

THREE-PARAMETER OPTIMIZER CODE (MSM5)

This computer code optimizes a converter with respect to collector temperature T_C, emission barrier height ψ, and emitter lead length-to-area ratio W. The coding is set up to step through a series of values of source strength Q and emitter area A; for each combination of Q and A an optimum configuration with respect to T_C, ψ, and W is computed.

The code is made up of a main program and 8 subroutines. The main program directs the logic and performs the optimization along with some calculations; the converter thermionic analysis is performed in two subroutines. A logic flow diagram for the main program is shown in Figure

A-6; each of the major program blocks is discussed in more detail in succeeding sections of this appendix.

Clear Storage. On the first entry only, all data storage locations are cleared. This is necessary, as the system monitor does not perform this function.

Read Input. Data input is handled by subroutine INPUT. Either a card reader or the console keyboard, or both, may be used as the source of input.

List Input. All input data is listed on the printer, properly identified. An essentially complete record is thus available.

Select Emitter Area, Perform Geometric Calculations. The lower and upper bounds for a dimension variable are input, along with the number of values to be used. The actual value of this variable (DE) is determined by DO-loop incrementing. Subroutine MSM5B calculates emitter area (GAREA), device length and diameter, weight excluding fuel, and any other required geometric data. Several different versions of subroutine MSM5B have been written.

Select Isotope Source Strength. In a similar fashion to DE, the isotope thermal source QX (at beginning-of-life) is also incremented under DO-loop control. The end-of-life source is calculated at this time, as is the void-to-fuel ratio, source weight, and total system weight.

Select Emitter Lead. The length-to-area ratio (W) of the emitter lead is an important optimizing parameter: too large a value will result in increased electrical power loss while too small a value degrades the thermal economy of the emitter. A stepping search is used to find the optimum value; the logic is given in detail in the appendix section titled "Logic Block A."

Select Collector Temperature. For any value of W, there is an optimum collector temperature. Logic Block B uses a stepping search, described in more detail later, to identify this value.

Select Thermionic Barrier Height. For any value of W and T_c there is an optimum value of load resistance R_L, corresponding to a barrier potential ψ. The effect is to trace a portion of the I-V curve to locate the peak power.

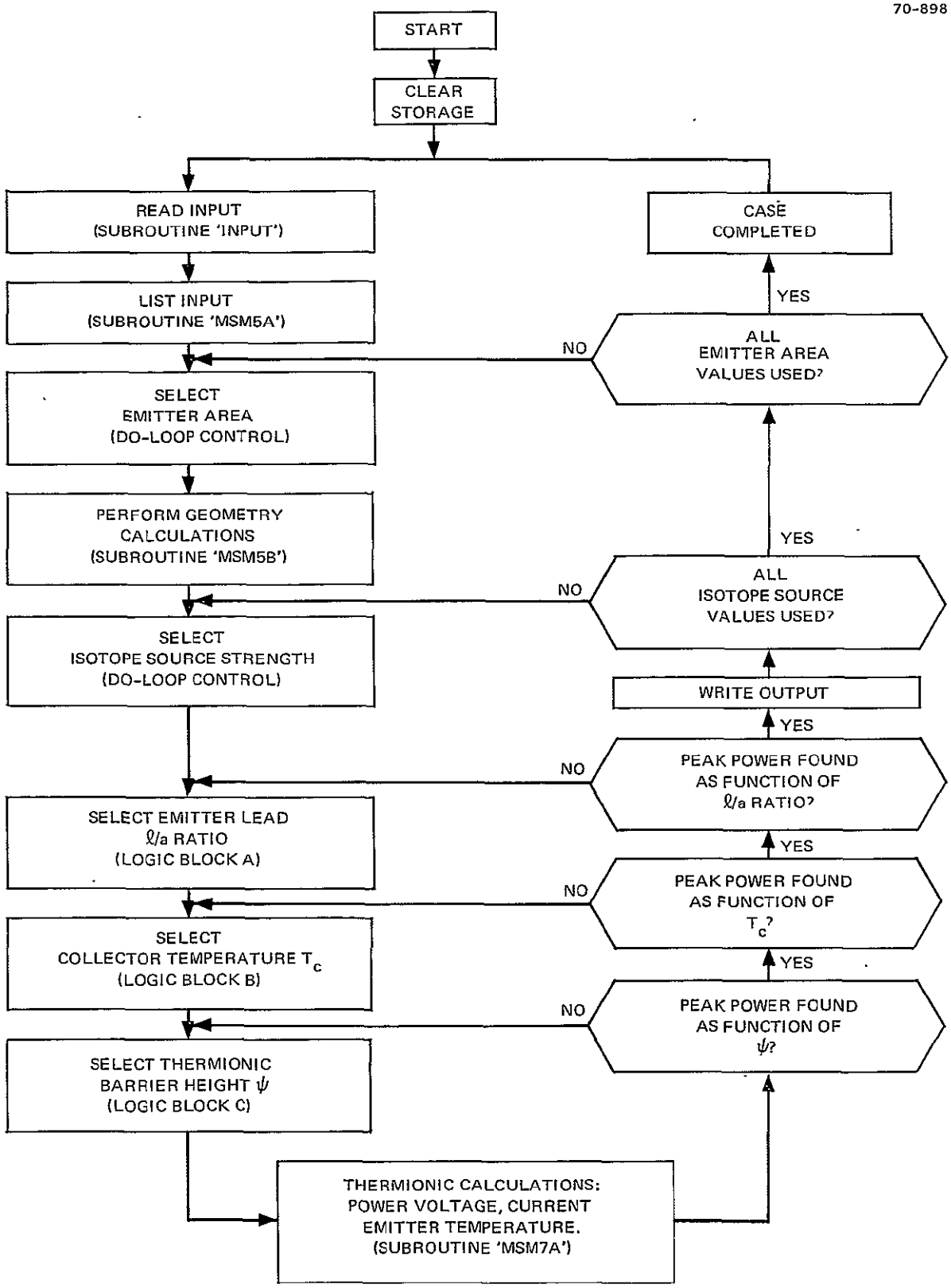

Figure A-6. Logic Flow Diagram of DWDL Vacuum-Mode Converter Computer Code

Machine implementation is simpler with ψ treated as the variable rather than R_L or output voltage.

Thermionic Calculations. Subroutines MSM7A and MMA1 perform the actual converter calculations. A converter can be characterized by Q, Q/A, W, T_c, and ψ; the resulting output is single-valued. Data furnished by the routine to the main program includes electrical power, voltage, current, and emitter temperature, as well as other parameters.

Control Logic. The remainder of the logic determines where to return control. The control statements are actually included in the logic blocks, but the straight-line diagram used here is designed to make the flow more apparent. Values of ψ are selected by Block C, until the value is found which produces the maximum net power for a particular combination of Q, GAREA, W, and T_c. This is the peak power as a function of ψ. A new value of T_c is selected, and iteration is performed on ψ with this latest T_c. Eventually a maximum net power is found for a particular combination of Q, GAREA, and W. Although designated as the peak power as a function of T_c, it is really the peak as a function of both T_c and ψ. Similarly, each value of W requires outer iterations on T_c and inner iterations on ψ, until eventually the maximum power is obtained for a particular Q and GAREA.

Optimization with respect to Q and GAREA is not performed. These parameters are stepped through; each pair has a particular optimum W, T_c, and ψ combination. Once this optimum is found, two lines of output are produced on the printer, with all data identified. After all requested pairs of Q and GAREA have been run, the case is complete. Control then passes to the input routine and the next case is started.

Subroutine INPUT. The input routine, used in many programs at DWDL, was written to minimize the number of cards required in programs where cases are stacked, and also to provide flexibility of input. Each input datum has an associated location number (LOC) on the input cards; the datum is preceded by the appropriate LOC. Since each datum is identified, they may be entered in any sequence, and any number of times (in which case the last-entered value is used). Furthermore, data not entered remains unchanged from the previous case, or zero if no value has been entered. As a result,

only that data which changes from one case to the next need be entered. Provision has been made by using console data switches for entering data from the console keyboard following, or instead of, the card reader. This feature permits the programmer to use results from one case in setting up succeeding cases, without having to reload the program each time.

Subroutine MSM5A. This short subroutine lists and identifies the input data including that which is unchanged from the previous case. A case title precedes the data listing, which includes the LOC of the data. A complete record of data used in the calculations is, therefore, available at later times.

Subroutine MSM5B. Geometric calculations are performed in this routine, which also lists input data peculiar to the particular subroutine version in use. A frequently-used version uses the emitter area as the geometric variable DE; the subroutine will perform the necessary calculations for a sphere and for cylinders with any length to diameter ratio and any combination of active and inactive surfaces. From the emitter area, shape, and (for cylinders) number of active surfaces and aspect ratio, the routine calculates the emitter outside diameter. Once this is found the length, collector diameter and length, material volumes and weights, and volume available to the fuel are found. Control then returns to the main program.

Logic Block A. This block performs two functions shown separately on the logic flow chart. It selects the value of W to be used for the next series of iterations and it includes the decision point, "peak power found vs function of ℓ/a ratio?" On the first entry to the block for a given Q and GAREA, an initial guess is made for the lead ℓ/a ratio, WIRE. Control then leaves Block A. On the second entry the first-guess results are stored and a second value of WIRE is provided using another empirical expression. On the third entry the results of the first two trials are compared; the value of WIRE leading to the higher net power is retained as a base, and a step size DWIRE = 0.1 x WIRE is calculated. If the second guess is used as a base the results are stored.

The third value of the parameter is at WIRE-DWIRE. A check is then made to ensure that stepping is proceeding in the correct direction, if not, DWIRE is changed in sign and the next step is at WIRE + DWIRE. Thereafter, WIRE is decremented by DWIRE at each step until the net power is lower than

on the previous step. DWIRE is then reduced by a factor of 10 and the sequence repeats once more. When the net power again diminishes from one step to the next the peak power is assumed found.

On the second stepping sequence, a check is made on the rate at which the net power is changing; two consecutive steps in which $\Delta P/P$ is less than 0.01% terminates the logic.

Logic Block B. Two functions are performed by this block: selection of collector temperature, and determination that the optimum TC has been found for a given WIRE. The decision point titled, "Peak Power Found as Function of TC?" is thus, in reality, included in the logic block.

On the initial entry to this block, an initial guess for TC of the converged value from the previous interation +25°K is selected. The step size is chosen as 25°K. The next entry uses TC + DTC; a check is made, as in block A, that stepping is proceeding in the correct direction. When the power peak has been passed, DTC is reduced by a factor of 10, the process repeats, and the next value of TC leading to a peak power is taken as the optimum. As with the iteration on WIRE, a change in power, on successive steps of TC, of less than 0.01% also serves to terminate the logic.

Logic Block C. As with blocks A and B, the choice of ψ and the determination of optimum are combined. On the first entry for a Q, GAREA pair an initial guess at ψ is made by calculating the open-circuit ψ. To do this, a heat balance on the emitter is solved, neglecting electron cooling, by iterating on TE. The open-circuit value for ψ is then obtained from

$$\psi = \phi_c T_e / T_c + 2 kT_e \ell n (T_e / T_c) \qquad (A-41)$$

For all other first entries, ψ is set at the last converged value plus 0.005 ev. When the open-circuit ψ is used, the step size is $0.25 kT_e$; otherwise it is $0.0025 kT_e$.

After an initial ψ is chosen, the same stepping sequence as with WIRE and TC is used, except that direction checking is unnecessary; the code steps until the net power decreases, then decreases step size by a factor of 10 and repeats. If ψ open-circuit is used, two decreases in step size are used, until DPSI = $0.0025 kT_e$; the smallest step used is $0.0025 kT_e$.

Thermionic Calculations. The computer coding follows the calculational method described in an earlier section. Subroutine MSM7A performs the heat balance and calculates δ_e, χ_e, and χ_c. Control passes to subroutine MMA1 for the determination of δ_c. MSM7A then completes the calculation of gross voltage, current and power.

When ψ is decreased to below the optimum value it will usually occur that ϕ_e will be calculated to be greater than ψ. In this case the power is set to -100.0 and the routine terminates. This arbitrary negative power is recognized by the stepping logic as indicating that the optimum ψ has been passed.

Output. After the thermionic calculations are completed the net voltage and power are calculated. These, along with the values of the parameters, converter weight, and a selected number of other variables of interest are printed out when the stepping logic has determined that the optimum combination for a given Q and GAREA has been found.

Additional Points. To minimize the number of iterations, each time a change in parameter results in an increase in power all the values to be output are stored. As a result, it is unnecessary to repeat the calculations for an optimum or intermediate optimum.

Provision is made in the code to hold WIRE or TC constant, rather than stepping them. An initial value is entered; this value will be maintained, and the associated logic block is bypassed.

FIVE-PARAMETER OPTIMIZER CODE (MM10)

The parameters available for optimization by this code are Q, TC, WIRE, ψ, and T_c/T_R (TRAT). The program will search for the maximum-efficiency configuration leading to a specified power (POBJ), or simply for the maximum-efficiency configuration. Any or all of the parameters may be held constant, and in the case of the search with no POBJ the source Q should be held constant.

The program consists of a main program and 10 subroutines, several of which are the same as MSM5. The main program contains little more than initialization logic and output logic; selection of parameter choices is performed in subroutine MM10C. The input, geometry, and thermionic calculation

routines are identical with those in MSM5, and have the same names; INPUT, MSM5B, MSM7A, and MMA1. Subroutine MM10A lists the input, including the case title; output of results is performed by subroutine MM10B.

Optimization Logic. The optimization logic is contained in subroutine MM10C, for which a flow chart is included as Figure A-7. The approach is known as "direct search" in addition to other names. Initial guesses and upper and lower limits are furnished for each variable. The set of initial values is termed a "base point". The routine proceeds by changing the value of one variable at a time in steps around the base point. When a set of steps has been found which produces an improvement in the objective function, steps of accelerating size are taken in that direction in n-space, where n is the number of parameters.

When further steps in the chosen direction produce worsening results, a new base point is established, and the process continues. If neither x + dx nor x - dx produces an improvement, dx is multiplied by 0.1 and the process repeats. When all steps are down to a specified fraction of the initial step size, and no improvement direction can be found, the logic terminates.

The choice of objective function depends on the type of search being performed. If there is no object power, the objective function is simply reciprocal efficiency, since the routine minimizes the function. Where there is a specified power, the function becomes

$$f = \frac{1}{\eta} + \left|\frac{\text{POWER} - \text{POBJ}}{\text{POBJ}}\right| \times \text{PENP} \qquad \text{(A-42)}$$

where PENP is an input number; 100.0 has produced good results. It should be noted that a tolerance on the result is specified; if the relative improvement in objective function for some step is less than the tolerance, it is treated as no improvement.

An input variable is set up to determine the output logic. Depending on its value two lines of output are produced on every step, on every new base point, and for the initial and final steps only. On the final step a considerable amount of additional information is produced, including a heat balance on the emitter.

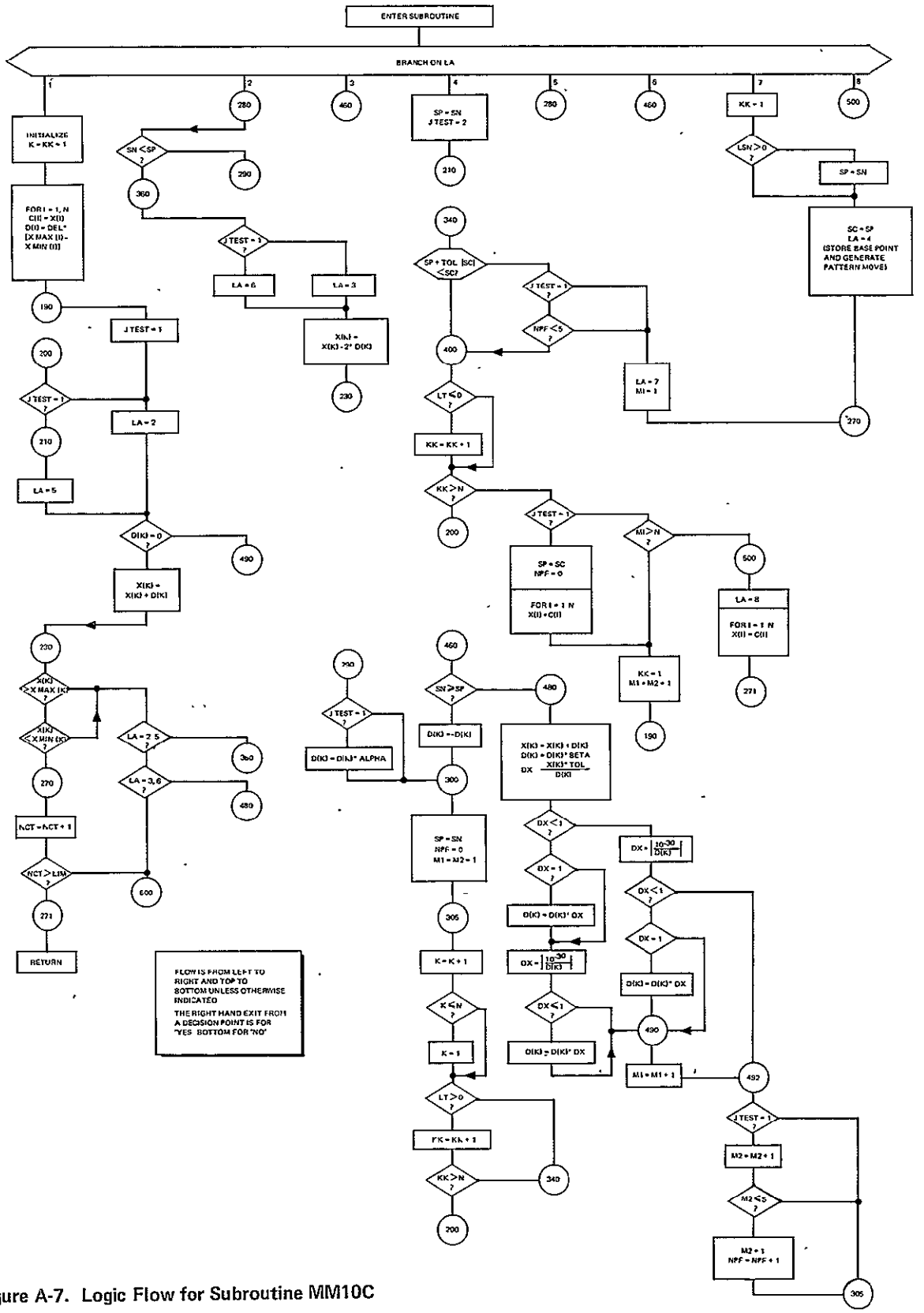

Figure A-7. Logic Flow for Subroutine MM10C

During the detailed design analysis a large number of calculations is performed with TC constant but the other four parameters free. Typically, a 4-parameter search required about 250 steps with a tolerance of 1×10^{-6} and used about 4 minutes.

DATA SUBROUTINES

Subroutines are used to calculate work function, emissivity, and emitter lead electric and thermal conductivity as functions of temperature and other parameters. Use of subroutines permits changes to be made with little difficulty. The following section presents the analytical form of the data as used in the work reported here.

Work Functions (MMA2). Emitter and collector may be different materials; two flags indicate the surface and the material.

Tantalum-Oxygen-Cesium:

$$\phi_o = 1.9641 - 2.08 \times 10^{-3}\, T_c + 1.74 \times 10^{-6}\, T_c^{\,2} \qquad \text{(A-43)}$$

$$\phi_c = \phi_o - 0.353 \times (T_c / T_R - 1.825), \quad \frac{T_c}{T_R} < 1.825 \qquad \text{(A-44)}$$

$$\phi_c = \max \begin{Bmatrix} \phi_o + 0.76 \times (T_c / T_R - 1.825) \\ 1.60\ T_c / T_R - 2.44 \end{Bmatrix}, \quad \frac{T_c}{T_R} > 1.825 \qquad \text{(A-45)}$$

$$\phi_e = 3.07419 - 1.77396\, T_e / T_R + 0.49977\, (T_e / T_R)^2, \quad \frac{T_e}{T_R} < 2.775 \qquad \text{(A-46)}$$

$$\phi_e = 1.60 \frac{T_e}{T_R} - 2.44, \quad \frac{T_e}{T_R} > 2.775 \qquad \text{(A-47)}$$

Tungsten:

$$\phi_c = 1.60 + 0.9807 \left(\frac{T_c}{T_R} - 1.9 \right)^2, \quad \frac{T_c}{T_R} < 2.64 \qquad \text{(A-48)}$$

$$\phi_c = 1.336 \frac{T_C}{T_R} - 1.39 \quad , \quad \frac{T_C}{T_R} > 2.64 \tag{A-49}$$

Same equations for ϕ_e, with T_e replacing T_c throughout.

Tungsten-Oxygen-Cesium:

$$\phi_o = 2.0034 - 2.08 \times 10^{-3} \; T_c + 1.74 \times 10^{-6} \; T_c^{\,2} \tag{A-50}$$

$$\phi_c = \phi_o - 0.289 \left(\frac{T_c}{T_R} - 2.65 \right) \quad , \quad \frac{T_c}{T_R} < 2.65 \tag{A-51}$$

$$\phi_c = \max \left\{ \begin{matrix} \phi_o \\ 1.42 \; \dfrac{T_c}{T_R} - 2.74 \end{matrix} \right. \quad , \quad \frac{T_c}{T_R} > 2.65 \tag{A-52}$$

Same equations for emitter except $\phi_o = 1.663$ for all T_e.

Emissivity (MMA3).

Tantalum:

$$\varepsilon = 0.060 + 0.000095T \tag{A-53}$$

Tungsten:

$$\varepsilon = +0.014 + 0.000110 \; T \quad , \; T < 1000 \tag{A-54}$$

$$\varepsilon = -0.059 + 0.000155 \; T \quad , \; T > 1000 \tag{A-55}$$

Effective Emissivity:

$$\varepsilon = \left[\frac{1}{\varepsilon_e} + \frac{1}{\varepsilon_c} - 1 \right]^{-1} \tag{A-56}$$

This assumes a view factor of unity.

Conductivities (MMA5). Data is for Niobium

Thermal Conductivity:

$$\kappa = 0.40365 - 0.0001495 \left(\frac{T_e + T_c}{2}\right) \tag{A-57}$$

Electrical Resistivity:

$$\rho = 0.112 \times 10^{-6} \left(\frac{T_e + T_c}{2}\right)^{0.865} \tag{A-58}$$

Cesium Vapor Conduction. Equation derived for low pressures. This equation is not in a subroutine but is included here for convenience in keeping all data in one location.

$$G_g = \frac{1.31 \times 10^7 \; e^{-8910/T_R}}{T_R} \tag{A-59}$$

DEFINITION OF SYMBOLS

Symbol	Definition
$\bar{a}$	$\sqrt{\theta}\,\frac{J^-}{J^+}$
A	Emitter area
A_c	Atom-electron collision cross-section
A_R	Richardson's constant
d	Electrode spacing
G_g	Gas conduction
G_s	Support conductance
h^+, h^-	Functions used in definition of X_e, X_c
I	Current
J^+, J^-	Emitter, collector current density
J_n	Net current density
K	Dimensionless collector space charge barrier with zero back emission
k	Boltzmann's constant
k_L	Emitter lead thermal conductivity
ℓ/a	Emitter lead length-to-area ratio
m	Exponent in equation for η_c
N_A	Atom density
N_V	Atoms per unit volume
P	Power
p	pressure
P_R	Reservoir pressure
Q	Heat source
q_c	Collision density
R_L	Load resistance
T_c, T_e	Collector, emitter temperatures

Symbol	Definition
T_g, T_R	Gas, reservoir temperatures
u	Dimensionless emitter potential
V	Voltage
W	Emitter lead length to area ratio
x	χ_c / χ_o
X_c, X_e	Functions used to derive χ_c, χ_e
y	Dummy variable
α, β	Parameters in expression for η_c
δ_c, δ_e	Collector, emitter potentials
ε	Emissivity
η_c, η_e	Collector, emitter electron density
θ	Ratio of emitter to collector temperature
ν	Back emission ratio
ρ	Emitter lead wire resistivity
κ	Emitter lead wire thermal conductivity
σ	Stefan-Boltzmann constant
ϕ_c, ϕ_e	Collector, emitter work functions
ϕ_c'	Collector emission barrier height
ϕ_o	Function used in calculation of work functions
χ_c, χ_e	Collector, emitter dimensionless distance to potential minimum
χ_o	Asymptotic dimensionless collector distance
ψ	Total emission barrier height
GAREA	Emitter area

Symbol	Definition
PENP	Input penalty multiplier
POBJ	Object power in MM10
PSI	Total emission power height
TC, TE	Collector, emitter temperature
TRAT	T_c/T_R
TR	Reservoir temperature
WIRE	Emitter lead length-to-area ratio

REFERENCES

A-1. P. S. Epstein. Verh. dtsch. Phys. Ges., 21, 85, 1919.

A-2. T. C. Fry. Phys. Rev., 17, 441, 1921; Ibid., 22, 445, 1923.

A-3. R. Gans. Ann. Phys. 69, 385, 1920; Ibid., 70, 625, 1923.

A-4. I. Langmuir. Phys. Rev., 21, 419, 1923.

A-5. P. A. Lindsay, and F. Parker. J. Electron, Contr., 7, 289, 1959.

A-6. P. A. Lindsay, and F. Parker. J. Electron, Contr., 1960.

A-7. E. S. Rittner. J. App. Phys., 31, No. 6,

Appendix B

PLUTONIA FUEL FORM

Aerospace applications of radioisotope heat sources require a high level of fuel integrity for maximum safety under both normal operating and accident conditions. Operating requirements typically demand maximum power density. The two requirements are mutually exclusive. Maximum power density is attained using metallic plutonia which is very hazardous; maximum safety appears to be obtained by having plutonium dioxide contained in multiple metal layers which substantially reduce power density. Because safety is foremost, plutonia fuels technology is based on use of plutonia-metal combinations (cermets) in various forms.

PLUTONIA SOLID SOLUTION CERMET

Between midyear 1969 and August 1970, the only plutonia radioisotope fuel form being developed by the AEC was the solid solution cermet (SSC). The SSC was selected by the AEC in the summer of 1969 as the fuel form for future aerospace applications. Development activities on the plutonia-molybdenum cermet and microsphere fuel forms were suspended. The solid solution cermet is best described as particles of a solid solution of plutonia and 10 mole-percent thoria coated with a layer of approximately 15 volume-percent molybdenum which is hot pressed to 95% of theoretical density; this shape is then over-coated with 4 volume-percent of molybdenum. The fuel composition is approximately

96 v/o {95 v/o [85 v/o (90 m/o PuO_2-10 m/o ThO_2)-15 v/o Mo]

-5 v/o void} -4 v/o Mo

The SSC is only about 70% PuO_2 by volume and has a power density less than half that of plutonium metal. Each of the SSC constituents has safety oriented purposes which are, in order:

1. Ten mole percent thoria - Thoria reduces solubility of plutonia in water, reduces fuel volatility at high temperature, and improves compatibility with container materials.

2. Fifteen volume percent molybdenum coating - A continuous layer of molybdenum improves thermal conductivity and provides higher impact resistance.

3. Five volume percent void - Void space permits movement of the helium generated in the plutonia to locations external to the fuel body and allows fuel swelling with minimal external growth both of which enhance long-term high temperature fuel stability.

4. Four volume percent molybdenum overcoating - An overall molybdenum coating provides enhanced reentry protection and also improved compatibility with container materials.

Pertinent quantitative properties of both the SSC (Reference B-1) and plutonia molybdenum (PMC) cermet (Reference B-2) are listed in Table 4-1. It is apparent that the SSC shows only a minor loss in power density in comparison with the PMC and also provides enhanced fuel stability as a result of the small thoria addition. Both thermal conductivity and thermal expansion are functions of fabrication technique thus both are considered to be comparable for the two fuel forms. Minimal oxidation of the SSC occurs up to 400°C such that fuel bodies are readily handleable with little or no heat sinking. Short term stability has been demonstrated to 1500°C. Arc-tunnel tests to ~108 BTU/$ft^{1.5}$ have not caused excessive damage. Impact tests up to 378 fps have resulted in less than 2% of the material being less than 10 microns in diameter. Sea water solubility studies indicate typical dissolution rates of less than 10^{-10} g $^{238}Pu/mm^2$-day.

Safety of the solid solution cermet has been demonstrated in current technology programs for all potential hazardous conditions. Use of SSC fuel limits maximum power density of the fuel itself to 3.2 w_t/cm^3 and thereby limits the effective power density of a power source to a somewhat lower value because of the requirements of manufacturing tolerances and containment. Relative loss in effective power density is a function of size (large capsules lose less) and shape (spherical capsules may lose more). Minor changes in SSC composition including increasing the $^{238}Pu/^{total}Pu$ ratio from 0.8 to 0.9 could conceivably increase power density by ~15%. However, this will not occur within the next several years and therefore the current technology upper limit appears to be a thermal power density of 3.2 w_t/cm^3 for the BOL fuel body.

PLUTONIA-MOLYBDENUM CERMET

A decision was made by the AEC in August 1970 to switch from the plutonia solid solution cermet fuel form to a plutonia-molybdenum cermet fuel form for upcoming aerospace missions. The major reason for the change was the developmental problems in obtaining crack-free discs of SSC. Current technology is such that PMC shapes can be made readily while SSC shapes cannot. Limited process development on SSC continues at LASL with that fuel form possibly returning to use for future systems.

Original development of the PMC fuel form was conducted at Battelle Memorial Institute's Columbus Laboratories. Technology has been transferred to both Monsanto Research Corporation's Mound Laboratory and Los Alamos Scientific Laboratory. Both are producing satisfactory PMC shapes.

The PMC can be described as particles of plutonia (either microspheres or shards) coated with a layer of approximately 20 volume-percent molybdenum which is hot pressed to 93 ±2.5% of theoretical density and this shape is then over-coated with 2 mils of molybdenum. Therefore for a 50 w_t cylinder the composition would be

98.8 v/o (93 v/o (80 v/o PuO_2-20 v/o Mo)-7 v/o void)-1.2 v/o Mo

Current processing procedure results in a fuel form having somewhat less oxygen than stoichiometric $PuO_{2.0}$. This factor is an advantage for use in refractory metal systems which are degraded by the presence of oxygen. It may be an advantage or a disadvantage in systems containing noble metals (Pt, Rh, I_r) depending on container configuration.

REFERENCES

B-1. J. Leary. Passout for Isotope Fuels and Materials Committee Meeting, Oak Ridge National Laboratory, February 25-26, 1970.

B-2. W. M. Pardue, et al. Final Report for the Program to Develop Composite Fuel Forms of $Pu^{238}O_2$. BMI-1869, September 1969.

Appendix C

DETERMINATION OF MAXIMUM FUEL LOAD FOR AN UNVENTED SPHERE

Instead of determining directly the maximum permissible fuel load for an alpha-emitting fuel placed inside a non-vented sphere, with wall thickness as an added parameter, a complementary problem is adapted for computer solution. This problem is: given a fuel load Q and surface area A for a sphere, determine the minimum permissible wall thickness. This problem is, in principle, amenable to an analytic solution, but an iterative approach was chosen.

THEORY

Assuming for the moment that the amount of fuel Q will indeed fit within a sphere of surface area A, the pressure of the helium gas can be determined from the volume available to the gas and the temperature. The stress within the sphere wall is then calculable, and can be compared to the yield stress of the wall material. For walls of thickness approaching zero, the stress approaches infinity. As wall thickness increases the stress initially decreases; however, finally, the wall encroaches on the gas volume, and the pressure increa The stress reaches a minimum value as a result of the interaction of these two tendencies, and then rises, again approaching infinity as the gas volume goes to zero.

A curve showing this general behavior is shown as Figure C-1. Two alternatives are shown: either the minimum stress is below the wall allowable stress, or at all times the stress exceeds the allowable. In the first case, there are two solution points at which the wall stress equals the allowable; the one with the lower wall thickness is the appropriate choice, as it is lighter. In the other case, there is no solution; that is, the chosen Q cannot be fitted within a sphere of area A.

Figure C-2 shows the geometry used. The sphere is actually a double-walled container. The area used in the area of the inner sphere (the emitter);

70-2191

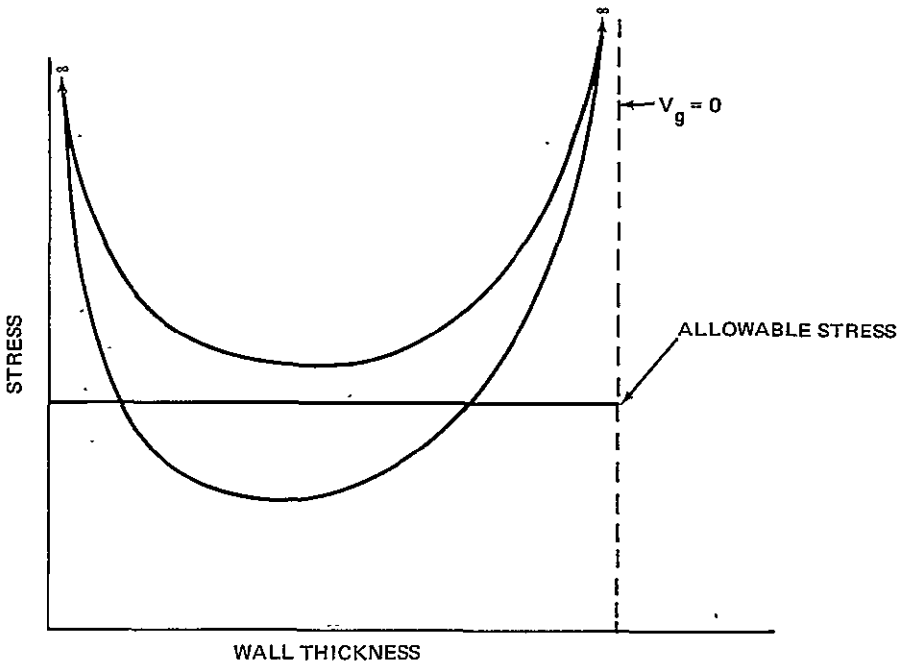

Figure C-1. Wall Stress vs Wall Thickness at Constant Area

70-2192

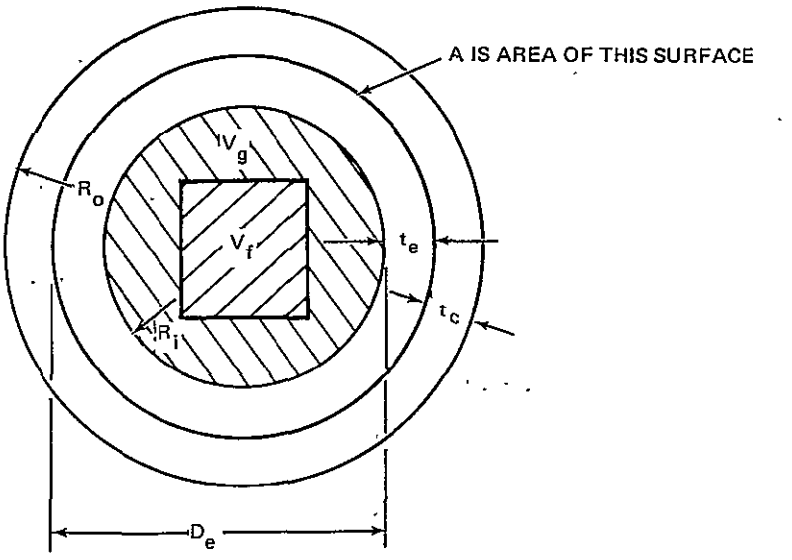

Figure C-2. Double-Wall Spherical Geometry

under stress, however, the emitter will yield until it is in contact with the outer sphere (the collector), and thus the combined thickness is available to withstand the internal pressure. The slight increase in gas volume due to yielding of the emitter is neglected in the calculations.

Given the emitter area, the diameter of the emitter is calculated as

$$D_e = \sqrt{A/\pi} \tag{C-1}$$

The inside radius of the inner sphere, which determines the volume within the sphere, is

$$R_i = 1/2\, D_e - t_e \tag{C-2}$$

and the internal volume becomes

$$V_t = \frac{4}{3} \pi R_i^3 \tag{C-3}$$

The volume occupied by the fuel material is

$$V_f = \frac{Q}{\sigma(1-D)} \tag{C-4}$$

with σ = fuel specific power (watts/cm^3)
D = diluent ratio (cm^3 diluent/cm^3 fuel)

The gas volume (V_g) is then $V_t - V_f$ and the void-to-fuel ratio is

$$R = (V_t - V_f) / (Q/\sigma) \tag{C-5}$$

The gas pressure is calculated from the ideal gas law, rewritten in terms of R and density:

$$P = \frac{Y\rho R_g \left(1.0 - e^{-\lambda L}\right) T_g}{WR} \tag{C-6}$$

where Y = isotopic purity of fuel

ρ = fuel density

R_g = gas constant

λ = fuel half-life

L = time since encapsulation

T_g = gas temperature

W = fuel atomic weight

The wall stress then becomes

$$\sigma = \frac{P R_o}{2 t_w} \quad , \quad \frac{R_o}{t_w} \geq 10 \qquad \text{(C-7)}$$

$$\sigma = \frac{P (2R_i^3 - R_o^3)}{2 (R_o^3 - R_i^3)} \quad , \quad \frac{R_o}{t_w} < 10 \qquad \text{(C-8)}$$

with R_o = outside radius of sphere

t_w = total wall thickness

then $t_w = t_e + t_c$

and $R_o = R_i + t_e + t_c$

COMPUTER CODE

The computer code uses an iterative method to find the minimum t_e which will satisfy the requirement that wall allowable stress equals wall stress. First a test is made for each Q and A pair to assure that the given Q will fit physically within a sphere of surface area A. A minimum emitter wall thickness may be specified, in which case it is used to calculate the volume for this check. If this test is passed, a first guess at the thickness is made, using one-tenth the value for which the total volume equals the fuel volume. Steps of this size are taken initially, with the wall thickness being increased until the allowable stress exceeds the wall stress. The step size is reduced by a factor of 10 and the process is repeated. A further factor of 10 is used on the step size before convergence is assumed.

A check is made for the no-solution case. If the minimum stress is above the allowable, a message to this effect is printed out. Messages are also printed if the fuel will not fit within the sphere, or if the solution thickness is less than the specified minimum, but at the latter thickness the wall stress exceeds the allowable.

The emitter temperature is, in general, a function of the heat flux for vacuum-mode thermionic converters of the type reported. Accordingly, the gas temperature is calculated by the computer from an input table of temperature vs heat flux. Another table, of stress vs temperature, is used by the

computer to determine the allowable stress.

Additional input is the minimum total wall thickness and the (fixed) collector wall thickness; the minimum emitter wall thickness is obtained by subtraction.

Table C-1 summarizes temperature vs flux and stress vs temperature data used in the calculations. The T vs Q/A table is for Ta-O-Cs surfaces, while the σ vs T data is the yield stress for annealed T-111

Table C-1

SUMMARY OF DATA USED
FOR UNVENTED CAPSULE DESIGN

Flux (w/cm^2)	Temperature (°K)	Stress σ (psi)
0.2	1090	34000
0.5	1200	32000
1.0	1350	30000
2.0	1535	27500
2.4	1560	27000
2.8	1570	26800

MAXIMUM FUEL LOAD FOR AN UNVENTED CYLINDER

A similar approach was used for the unvented cylinder. Stress is calculated at several points over the shell of a flat-ended thin shell cylinder of L/D = 1, and the maximum stress is used for comparison with allowable stress. Stress equations are taken from References C-1 and C-2.

REFERENCES

C-1. ASME Boiler and Pressure Vessel Code, Section III (with Addenda), 1965.

C-2. R. J. Rourk. Formulas for Stress and Strain. 4th Ed., N. Y., McGraw-Hill, 1965.

Appendix D
GENERATOR AND CONVERTER RELIABILITY

GENERATOR REDUNDANCY AND RELIABILITY

A generator is composed of a relatively large number of cells, each of which has rather high but less than 100% reliability. Converters are assumed to fail in either short-circuit or open-circuit modes. (The possibility of slow performance degradation is not considered; thus, each cell either works perfectly or fails completely). In order to determine generator reliability generator failure must be defined; generators meeting a pre-set criterion are good, those which do not meet it are failed, and there are no intermediate conditions. In general, the criteria will be stated as a minimum output power and voltage which must be present.

A series-parallel electrical interconnection of the cells can usually be arranged which will meet the performance criteria. Figure D-1 shows a flat network of cells, composed of "c" columns and "r" rows. The purpose of using such a network can be readily determined by examining the two extremes; a simple series arrangement (1 column), and a simple parallel arrangement (1 row).

With the assumption that the required number of cells are connected in series, and that the electrical load has been matched to the cells, a short-circuit failure will cause a reduction in voltage approximately equal to the output voltage of one cell, while the power loss will be somewhat greater than the power of one cell, because of the resulting mismatch. For example, with 10 cells in series, loss of one cell by short-circuit failure will drop the power to 89.75% of its initial value. For a given power requirement, 11.4% excess power will allow for one failure. Unfortunately, a single open-circuit failure will cause a complete generator failure. A simple series arrangement, then, although excellent with respect to short-circuit failure, is highly susceptible to open-circuit failure.

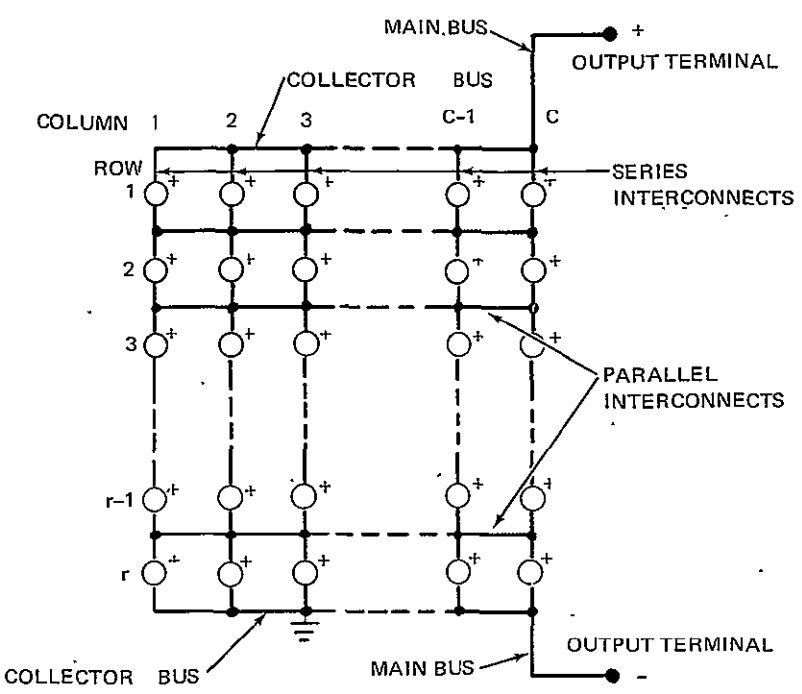

Figure D-1. Generator Electrical Network

Next a 10-cell parallel array is considered, again with a matched load. In this case, an open-circuit failure will result in a drop in power to 89.75% of initial, for a margin requirement of 11.4%. Now, unfortunately, a single short-circuit failure will result in total generator failure. A simple parallel circuit will, then, give excellent protection against open-circuit failure, but with extreme vulnerability to short circuits.

A series-parallel array as shown will give the advantages of both series and parallel connections. No single failure, either open-circuit or short-circuit, will cause complete generator failure. This advantage is, however, bought at the expense of losing a larger fraction of the total power as a result of single cell failure. For example, with 2 columns and 5 rows, a single open-circuit failure reduces the output power to 82.6% of the full 10 cells, while a short-circuit failure drops the power to 79.0%.

The equations for determining the power and voltage output of an array such as shown in Figure D-1 are quite simple. The assumptions are:

1. All interconnections have zero impedance
2. The converter current-voltage relationship is linear
3. All converters are identical
4. Failure is sudden and complete
5. The load is matched to the array with no failures.

Under these assumptions an equivalent circuit may be constructed as in Figure D-2. With no loss in generality, the equations are developed with a converter open-circuit emf of 1 volt and internal resistance of 1 ohm. The equivalent resistance for one row is, for "c" columns,

$$R_1 = 1/c \qquad \text{(D-1)}$$

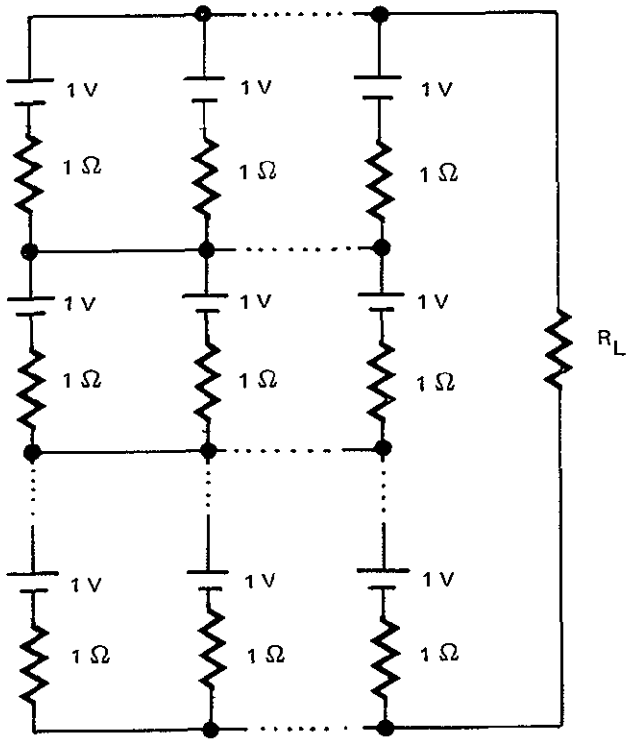

Figure D-2. Equivalent Electrical Circuit for Interconnected Array

If there are "r" rows, the array equivalent resistance becomes

$$R_a = r/c \tag{D-2}$$

For a matched load the load resistance equals the array equivalent resistance; thus

$$R_L = r/c \tag{D-3}$$

and the total circuit resistance is

$$R = 2r/c \tag{D-4}$$

Since the voltage output of the array is r, the total current is

$$I_a = \frac{V}{R} = \frac{r}{2r/c} = \frac{c}{2} \tag{D-5}$$

and the power delivered to the load becomes

$$P_L = I_a^2 R_L = \left(\frac{c}{2}\right)^2 \left(\frac{r}{c}\right) = \frac{rc}{4} \tag{D-6}$$

Finally, the voltage across the load is determined from

$$V_L = I_a R_L = \left(\frac{c}{2}\right)\left(\frac{r}{c}\right) = \frac{r}{2} \tag{D-7}$$

In a similar manner, the power delivered to the load and the voltage across it can be determined for an array with any number of open-and short-circuit failures. The equivalent resistance for a single row is

$$R_i = \frac{1}{c - n_i} \tag{D-8}$$

where n_i is the number of open-circuit cells in the row; a single short-circuited cell results in $R_i = 0$. The array resistance is

$$R = \sum_{i=1}^{r} R_i \tag{D-9}$$

and the array voltage is

$$V = r - s \tag{D-10}$$

where s is the number of rows containing at least one short circuit. Because R_L remains constant

$$I = \frac{r - s}{\sum_{i=1}^{r} R_i + \frac{r}{c}} \qquad \text{(D-11)}$$

The delivered power is obtained, as before, from

$$P = I^2 R_L \qquad \text{(D-12)}$$

and the voltage across the load from

$$V = I R_L \qquad \text{(D-13)}$$

The power and voltage can be expressed as fractions of the no-failure power and voltage; for power

$$\frac{P}{P_a} = \frac{I^2 R_L}{I_a^2 R_L} = \left[\frac{r - s}{\sum_{i=1}^{r} R_i + \frac{r}{c}}\right]^2 \Big/ \left[\frac{c}{2}\right]^2 \qquad \text{(D-14)}$$

Because voltage and power are related by

$$P = V^2/R_L \qquad \text{(D-15)}$$

The voltage fraction can be expressed as

$$\frac{V}{V_a} = \frac{\sqrt{P \cdot R_L}}{\sqrt{P_a \cdot R_L}} = \sqrt{\frac{P}{P_a}} \qquad \text{(D-16)}$$

If the number of cells to be interconnected is small, a completely deterministic solution is feasible. For example, for a 2 x 2 array, in which

o = probability of open-circuit failure
s = probability of short-circuit failure
g = probability of no failure

then,

$$g + s + o = 1.0 \tag{D-17}$$

with four cells, the probability of any combination of failures can be established by the expansion of

$$1.0 = (g + s + o)^4 \tag{D-18}$$

$$= g^4 + 4g^3o + 4g^3s + 6g^2o^2 + 12g^2os + 6g^2s^2$$

$$+ 4go^3 + 12go^2s + 12gos^2 + 4gs^3 + 4o^3$$

$$+ 6o^2s^2 + 4os^3 + s^4$$

The first term, g^4, represents the probability of all 4 cells operating, with a resulting normal power output. The second term, $4g^3o$, gives the probability of one open-circuit failure, with a resulting power output of 64% of normal. The third term yields the likelihood of one short-circuit failure, resulting in 44% of normal power.

Continuing, $6g^2o^2$ signifies two open-circuit failures. Of these, 1/3 of the time both failures will be in one row, with a resulting power of zero, while the other 2/3 have one failure in each row, with a power output of 44% of normal. The remaining terms can also be analyzed in the same fashion; obviously, this method rapidly becomes cumbersome. Because of the difficulties, a probabilistic computer code, written in a related IRAD effort, was used.

Certain assumptions are implicit in the code. First, failure of any cell is assumed to be completely random in nature; in other words, failure of one cell has no effect on any others. Second, all cells have identical open-circuit failure probabilities, and all cells have identical short-circuit probability; these two probabilities need not be the same, however. Third, the current-voltage characteristic of the cells is assumed linear. Fourth, the electrical load is assumed matched to the full array.

The computer code uses a probabilistic or Monte Carlo technique. The array is examined, cell by cell. For each cell a random number between

0 and 1 is generated; this number is used to determine whether the cell is good, open, or shorted. If the number is between 0 and s, the cell has short-circuited; between s and s + o, the cell is open-circuited; above s + o, the cell is good. After every cell in a row is examined the resistance and voltage of the row is determined and stored. The process continues, one row at a time, until the entire array has been examined. The equivalent resistance, voltage, current, and power are calculated in order, and the power recorded.

The process is repeated as many times as desired (usually several hundred or thousand times) and the tabulated results are interpreted to yield the probability of obtaining any given power or voltage. Since voltage across the load is proportional to the square root of the power, the power results can be used to find the probability of obtaining a given voltage. The 90% of full power curve also represents 94.9% of full voltage, for instance.

As an example of the reliability of the method, the 2 x 2 array partially analyzed above was examined by the Monte Carlo code, using o = 2% and s = 8%, and the output compared with analytical calculations. Table D-1 lists the results for 2500 histories. As can be seen, the results are quite acceptable.

Table D-1
COMPARISON OF MONTE CARLO AND ANALYTIC RESULTS
2 x 2 Array, 90% Reliability

Power	Exact	Monte Carlo
1	0.6561	0.6592
0.64	0.0583	0.0524
0.444	0.2501	0.2528
0.25	0.0111	0.0112
0	0.0244	0.0244
	Failures	
Type	Exact	Monte Carlo
Shorts	0.08	0.0808
Opens	0.02	0.0191
Total	0.10	0.0999

With any statistical method, the question of uncertainty arises. Generally, the uncertainty decreases as the number of cells and number of calculated arrays increases. Results for 1000 and 6000 histories are shown, for two different arrays, in Table D-2. The discrepancy is in no case more than 1%, indicating that, for scoping work, the use of 1000 histories is probably adequate, and that 4000 histories should yield results reliable to ± 0.5% or better.

CONVERTER RELIABILITY DEMONSTRATION

Before discussing the problem of demonstrating or determining the reliability of an individual thermionic battery, it is necessary to clarify some of the terminology used in reliability engineering; specifically, the difference between "reliability" and "confidence" or "confidence level" must be defined. The matter is clearly discussed in Reference D-1.

Table D-2

COMPARISON OF RESULTS FOR 1000 AND 6000 HISTORIES

Percent of Full Power	1000 Histories	6000 Histories	Percentage Discrepancy(1)
	2 x 10 Array		
71	91.80	92.57	0.83
70	93.80	94.43	0.67
67	97.90	97.88	0.02
63	98.30	98.23	0.07
	2 x 15 Array		
75	94.40	93.92	0.51
73	96.50	95.78	0.75
71	97.90	97.67	0.24
68	98.50	98.18	0.33
66	99.10	98.92	0.18

(1) Based on results of 6000 histories.

Reliability is the probability that an individual item will work properly; confidence is the probability that the stated reliability, taken from tests on a small sample, is representative of all the items.

There are many possible causes for equipment failure. Failures may occur from wear-out, the equipment may be intrinsically defective, environmental factors may increase in severity, failure of one item may throw an increased load on others resulting in their failure, and so on.

A very common assumption is that failures are strictly random in nature, occuring at some average rate which is essentially constant in time. If there is a fixed number of items under consideration, with no replacement possible (as is true for the multicell generator), the combination of a fixed failure rate per item and a continually decreasing number of non-failed items leads to the so-called exponential distribution,

$$f(t) = \frac{1}{\theta} e^{-t/\theta} \qquad \text{(D-19)}$$

where

$f(t)$ = failure rate in time

θ = average lifetime

t = time

Once the assumption of the exponential distribution is made, the probability of survival for any given time can be readily obtained. This probability of survival is, by definition, the reliability of the device. The pertinent equation is

$$R(t) = e^{-t/\theta} . \qquad \text{(D-20)}$$

where

$R(t)$ = reliability at any time t

The average lifetime θ must be determined by life testing. As with any other type of testing, the calculated mean life obtained from a small number of tests may not be representative of the true mean life; accordingly, a confidence level is attached to the results. Tables showing the number of

tests required to determine the mean life at confidence levels of 90% and 95%, as a function of the ratio of test time to mean life and also the number of failures during the test are presented in Reference D-1. A portion of these is presented as Table D-3.

Table D-3

MINIMUM SIZE OF SAMPLE TO BE TESTED FOR A TIME "t" TO ASSURE A MEAN LIFE OF AT LEAST "θ" WHEN "f" IS THE NUMBER OF FAILURES

Confidence = 90%

	t/θ				
f	0.2	0.1	0.05	0.02	0.01
0	12	24	47	116	231
1	20	40	79	195	390
2	28	55	109	266	533
3	35	69	137	333	668
4	42	83	164	398	798

Confidence = 95%

	t/θ				
f	0.2	0.1	0.05	0.02	0.01
0	15	31	60	149	298
1	25	49	97	236	473
2	33	65	129	314	630
3	41	80	159	386	775
4	48	95	189	456	914

REFERENCE

D-1. N. H. Roberts. Mathematical Methods in Reliability Engineering. McGraw-Hill Book Co., 1964.

Appendix E
AEROSHELL DESIGN CALCULATIONS

This appendix contains details of the design analysis for the flared-cylinder aeroshell configuration discussed in Section 6.

WEIGHT AND IMPACT VELOCITY

A weight and impact velocity analysis is made in terms of the vehicle ballistic coefficient. The component and total weights are characterized for a specific design with a fixed ballistic coefficient. Extrapolation to other ballistic coefficients is then performed by simultaneous solution of the component and total weight equations and the ballistic coefficient definition equation. The relevant equations for the example of a 100-w_e generator composed of 5-w_e converters in a 5-row, 4-column array are

$$W_{tot} = W_c + W_{cells} + W_f = \frac{\beta}{144}\,\frac{\pi}{4}\,D_f^2 \quad \text{(ballistic coeff. definition)} \tag{E-1}$$

$$W_c = 1.274 + W_{gc} \quad \text{(weight of cylinder = shell + graphite weights)} \tag{E-2}$$

$$W_{gc} = 2.768\sqrt{\frac{\beta}{30}} \quad \text{(graphite weight scaling eq.)} \tag{E-3}$$

$$W_f = \left[2.728\sqrt{\frac{\beta}{30}} + 1.828\right]\left(\frac{D_f}{12.15}\right)^2 \quad \text{(flare weight scaling eq.)} \tag{E-4}$$

$$W_{cells} = 15.4 \text{ lb} \quad \text{(weight of all 20 modules)}$$

Solution of these equations for selected values of β results in the total weight curve shown in Figure E-1. An absolute minimum weight occurs when $\beta \approx 55$ lb/ft^2. However, the curve is relatively flat for β between 30 and 80 lb/ft^2. Thus, to minimize the impact velocity, a ballistic coefficient of 30 lb/ft^2 occurring near the knee of the curve, is selected for the reference generator.

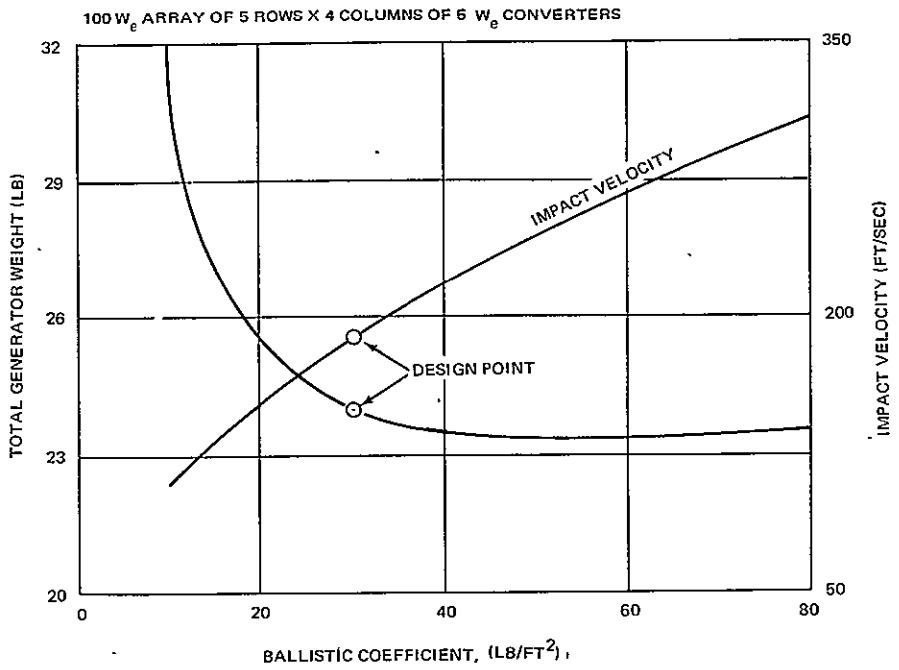

Figure E-1. Generator Weight and Impact Velocity Variation vs Ballistic Coefficient

The corresponding impact velocity curve given by the equation

$$V_r = 30.89\sqrt{\frac{\beta}{0.8}} \text{ fps} \qquad \text{(E-5)}$$

is shown also in Figure E-1. The drag at subsonic terminal velocity is estimated at 0.8 and the constant 30.89 derives from air properties for average annual temperatures at an impact altitude 2500 ft above sea level.

COMPLETE BURIAL AEROSHELL TEMPERATURE

In the low probability case of complete burial in sand or soil, the surface temperature T_s is given by the equation

$$\int_{T = T_\infty}^{T_s} k \, dT = \frac{Q}{2\pi L} \ell n \left(L/D + \sqrt{1 + (L/D)^2}\right) \qquad \text{(E-6)}$$

For the reference generator (100 w_e, 5-row, 4-column converter array), solution of the Equation E-6 for coastal plains clay, one of the lowest conducting soils, yields a generator surface temperature of 2200°K which is above soil melting temperature and is borderline for long term fuel containment. For partial burial, the temperatures will be much lower because of air convection at the surface and melting will not occur.

ABLATOR MATERIAL CHARACTERISTICS

Physical and thermal property data for POCO graphite are presented in Table E-1.

Table E-1
POCO GRAPHITE PROPERTY DATA VS TEMPERATURE

	Grade AXF-50		
	75°F	1500°F	3000°F
Density range (gms/cm^3)	1.80 - 1.88	N/A	N/A
Tensile strength (psi)	10,000	11,000	12,000
Compressive strength (psi)	20,000	N/A	N/A
Flexural strength (psi)	10,500	10,900	12,300
Modulus of elasticity (psi x 10^6)	1.68	1.84	2.08
Strain to failure (% elongation)	0.95	0.90	1.00
Poisson's ratio	0.15	0.18	0.22
Hardness (Rockwell B)	120	N/A	N/A
Thermal conductivity (Btu/ft-hr°F)	65	28	17
Coefficient of thermal expansion (in./in./°F x 10^{-6})	4.8	4.3	4.9
Specific heat (Btu/lb-°F)	0.20	0.42	0.50
Purity (average total ash-ppm)	200	N/A	N/A

A detailed comparison of POCO with ATJ-S (Reference E-1) indicated potential theoretical thermal stress advantages of ATJ-S (properties are similar). Thus, ATJ-S can be considered as an alternate or future replacement ablator material, pending further study.

The overall properties of 2D laminates, such as Pyro-Carb 406 used on the SNAP-27 capsule, do not offer any significant advantages over the fine-grain graphites (Reference E-1). The 3D filament wound composites and RPG composites are only in the development stage and insufficient property data are available to design heat shields with high reliability. Phenolic charring ablator materials such as Narmco 4028 and microballon-glassy composites such as Avcoat 5026-39, the Apollo Command Module Ablator, have attractive low densities and heats of ablation approaching that of graphite. However, long-term degradation at generator operating temperature, radiation levels and thermal stress, and mechanical erosion problems on steep angle reentry rule against their selection.

INSULATOR MATERIAL CHARACTERISTICS

Potential aeroshell insulators are characterized in Table E-2. Densities and thermal conductivities are compared for high temperature super insulators and insulation suitable for the radiator area on the cylindrical sides.

For insulation on the cylindrical sides, the magnitude of the thermal conductivity is not as important as the ratio of conductivities at operating and reentry temperatures because only moderate reentry insulation is needed. As-deposited pyrographite is the prime choice and has the benefits of reinforcing the heat-treated pyrographite. The artificial thermal switch of silver impregnated silica foam has the disadvantage of irreversibility. A temperature transient above 1227°K destroys the good thermal contact with the radiator area upon resumption of normal operation. The alumina offers low density and protection against high temperature oxidation, for example under launch pad abort conditions. However, its positive-slope conductivity curve results in high converter temperatures on reentry. Reinforced pyrographite appears to be an attractive alternative for future consideration as a low weight combination insulator/ablator heat shield on the cylindrical sides.

Table E-2

GENERATOR INSULATOR CHARACTERISTICS

	Density lb/ft^3	Thermal Conductivity, Btu/ft-hr °F 900°F	2000°F	3000°F	4000°F	Comments
High Temperature Super Insulators						
Heat-treated PG	121	0.20	0.05	0.08	0.12	Very anisotropic, backup ablator
UCAR Carbon PVB	50	0.10	0.13	0.16	0.20	Strong, resilient material
Expanded PG	60	0.30	0.09	0.10	.12	Anisotropic, compressible
UCC zirconia felt	20	0.07	0.11	0.18	-	Soft, low density material
ORNL fibrous carbon	7	0.05	0.10	0.22	-	Very low density
Moderate Insulators						
As-deposited PG	121	1.2	0.4	0.32	0.30	Backup ablation protection
Reinforced PG	50	1.7	1.3	1.0	-	Possible combined ablator/ insulator
Alumina 3400	35	0.28	0.30	0.42	-	Launch abort protection
Sb impregnated silica foam	50	1.0	0.24	0.64	1.0	Thermal switch.

If the number of columns is c, then the ellipsoidal-ended aeroshell cylinder has an internal diameter of

$$D_i = d\left(1 + \operatorname{cosec} \frac{180°}{c}\right) \tag{E-7}$$

where d is the Isomite diameter, including outer electrical insulation, if any. For the length, a gap of 0.5 in. is allowed between rows to accommodate the venting stems.

The dimension-dependent weights of the components in the cylindrical section are based on detailed calculations for a specific design (100-w_e generator with 5 rows and 4 columns of 5-w_e modules) and scaled for the code calculated dimensions. Aeroshell and heat shield thicknesses are identical to those for the reference design.

For the flare, in the shape of a frustum of a right cone with 45° half angle, the hypersonic drag coefficient based on base area is, according to Newtonion theory,

$$C_D = 2 \sin^2 (45°) = 1 \tag{E-8}$$

The drag on the nose section is also approximately unity (0.92 for a hemisphere but slightly higher as a blunter shape is reached with stagnation point ablation). Therefore, the base diameter D_f may be calculated from the condition of constant ballistic coefficient of 30 lb/ft^2.

$$\frac{W_{tot}}{C_D A} \equiv \frac{W_{tot}}{\frac{\pi}{4} D_f^2} = 30 \text{ lb/ft}^2 \tag{E-9}$$

Here, W_{tot} is the total weight of the cylindrical plus flare sections. Thus, an iterative calculation of flare diameter and weight is necessary. For the flare, the actual surface area is given by

$$A_f = \frac{\pi}{2\sqrt{2}} (D_f^2 - D_o^2) \tag{E-10}$$

where D_o is the outer diameter of the cylindrical section. The flare weight is based on this area and the thicknesses of ablator, insulation, and structure layers. The computer code iterates by calculating the weight of the cylindrical section for the given cell dimensions and stacking arrangement, guessing the weight of the flare, and calculating the flare diameter using equation (E-9). The total weight based on this diameter is recalculated and the process iterated.

REFERENCE

E-1. S. E. Bramer, H. Lurie, T. H. Smith. Reentry Protection for Radioisotope Heat Sources. Presented at 16th Annual American Nuclear Society Meeting, June 28-July 2, 1970, Los Angeles, California.

Appendix F

PRESSURE DISTRIBUTION ON AEROSHELL NOSE

Ablation distributions around the generator nose are dependent on the pressure and aeroheating distributions.

$$P = (P_s - P_\infty) \cos^2 \theta + P_\infty \qquad \text{(F-1)}$$

where θ is the ray angle, the subscript "s" indicates stagnation point and ∞ indicates free stream conditions. Neglecting P_∞ as small compared to P_s (Figure 8-5)

$$P/P_s \approx \cos^2 \theta \qquad \text{(F-2)}$$

For graphite oxidation in the diffusion-controlled regime, the ablation rate is proportional to the square root of the pressure. Therefore, the oxidation contribution to graphite ablation away from the stagnation point can be related to stagnation point oxidation times the cos θ. Graphite sublimation is mainly a function of the heating rate.

HELIUM PRESSURE IN AEROSHELL

At L years from beginning of life, the pressure within the aeroshell, assuming all generated helium is released from the fuel, is given by

$$P = \frac{0.8 \ \rho_t \ R \ T \ (1 - e^{-\lambda L})}{M \qquad VF} \qquad \text{(F-3)}$$

where ρ_t = fuel density (100% TD) = 11.46 g/cm^3

R = gas constant

M = molecular weight of PuO_2 = 270

VF = void-to-fuel ratio

λ = ln 2/half life = 0.000793 yr^{-1}

Here, the fuel purity is taken to be 0.8. Inside the aeroshell, the void-to-fuel ratio for the reference design is 2.24. Assuming reentry to occur at a maximum design life of 12 years, the pressure attained is

$$P\ (\text{atm}) = 0.113\ T°K \tag{F-4}$$

The equivalent stress in the cylindrical walls caused by this pressure is approximately

$$\sigma_e = \frac{P_r}{t} = 45.02\ T°K\ (\text{psi}) \tag{F-5}$$

ELECTRICAL INTERCONNECTOR POWER LOSS

The electrical connectors are sized to minimize generator weight. The power loss in a connector (P_L) is given by

$$P_L = I^2 \frac{\rho L}{A} \tag{F-6}$$

where I = current
ρ = resistivity
= 4.2 $\mu\Omega$-cm(OFHC copper at 800°K)
L = connector length
A = connector cross-sectional area

The connector weight (W_c) is given by

$$W_c = wL\,A \tag{F-7}$$

where w = connector material density
= 559 lb/ft^3 (copper)

using Equation (F-7) to eliminate connector length in (F-6) yields

$$P_L = \left(\frac{I}{A}\right)^2 \frac{\rho W_c}{w} \tag{F-8}$$

Differentiating the power loss with respect to weight and setting the result equal to the generator system power-to-weight ratio (R_{pw}):

$$\frac{d}{dWc}(P_L) = \left(\frac{I}{A}\right)^2 \frac{\rho}{w} \qquad (F\text{-}9)$$

$$= R_{pw}$$

Solving for the required cross-sectional area yields,

$$A = I\sqrt{\frac{\rho}{w\, R_{pw}}} \qquad (F\text{-}10)$$

Substituting in Equation (F-7) yields the connector weight per unit length.

$$\frac{Wc}{L} = I\sqrt{\frac{\rho\, w}{R_{pw}}} \qquad (F\text{-}11)$$

Equations (F-10) and (F-11) were used to prepare Figure 8-13 in this report.

Generator power output (P_G) is related to voltage (V_G) and current (I_G) as follows:

$$P_G = V_G I_G \qquad (F\text{-}12)$$

Solving for current yields

$$I_G = \frac{P_G}{V_G} \qquad (F\text{-}13)$$

Substituting in Equation (F-11) yields the connector specific weight

$$\frac{Wc}{P_G} = \frac{L}{V_G}\sqrt{\frac{\rho\, w}{R_{pw}}} \qquad (F\text{-}14)$$

Multiplying by the generator power-to-weight ratio yields the connector power loss as a percent of generator output

$$\%\ \text{connector power loss} = \frac{L}{V_G}\sqrt{\rho w\, R_{pw}} \times 100\% \qquad (F\text{-}15)$$

Equations (F-14) and (F-15) were used to prepare Figure 8-14 using an effective connector length of one foot.